The Pennsylvania State University

The Graduate School

Department of Meteorology

INTRODUCING THE CONCEPT OF POTENTIAL AEROSOL MASS (PAM)

A Thesis in

Meteorology

by

Eunha Kang

Submitted in Partial Fulfillment
of the Requirements
for the Degree of

Doctor of Philosophy

December 2007

The thesis of Eunha Kang was reviewed and approved* by the following:

William H. Brune
Professor of Meteorology
Head of the Department of Meteorology
Thesis Advisor
Chair of Committee

Dennis Lamb
Professor of Meteorology

Jerry Harrington
Associate Professor of Meteorology

James Freihaut
Associate Professor of Architectural Engineering

*Signatures are on file in the Graduate School

ABSTRACT

Potential Aerosol Mass (PAM) can be defined as the maximum aerosol mass that the oxidation of precursor gases produces. In the measurement, all precursor gases are rapidly oxidized with extreme amounts of oxidants to low volatility compounds, resulting in the aerosol formation. Oxidation occurs in a small, simple, flow-through chamber that has a short residence time and is irradiated with ultraviolet light. The amount of the oxidants ozone (O_3), hydroxyl (OH), and hydroperoxyl (HO_2) were measured directly and can be controlled by varying the intensity of UV light and the relative humidity. Maximum values were 40 ppmv for O_3, 900 pptv for OH, and 4 ppbv for HO_2. The oxidant amounts are 100 to 1000 times tropospheric values, but the ratios OH/O_3 and HO_2/OH are similar to troposphere values. The aerosol production mechanism and the aerosol mass yield were studied for several controlling variables, such as temperature, relative humidity, oxidant concentration, presence of nitrogen oxides (NO_x), precursor gas composition and amount, and the presence of acidic seed aerosol. The measured secondary organic aerosol (SOA) yield of several natural and anthropogenic volatile organic compounds and a mixture of hydrocarbons in the PAM chamber were similar to those obtained in large, batch-style environmental chambers. The similarity of the mass spectra for SOA in the PAM chamber to the large environmental chambers provides evidence that the highly oxidizing environment of the PAM chamber has the same oxidation processes that occur at ambient oxidant levels. The dependence of the formation and aging of SOA on precursor organic amount and more importantly on OH were studied by the measurement of evolution of chemical composition and size distribution of SOA in PAM. This PAM method is being developed for measuring potential aerosol mass in the atmosphere, but it is also useful for examining SOA processes in the laboratory and in environmental chambers.

TABLE OF CONTENTS

LIST OF FIGURES

LIST OF TABLES

ACKNOWLEDGEMENTS

I would like to sincerely thank God for giving me an opportunity to pursue my Ph.D. study and helping me complete this dissertation through the help of several people.

I am grateful to my academic advisor, Dr. William H. Brune, for his sincere guidance in many ways, especially with helping me find meaningful results from my experiments and apply theory to understand the practical results, and also with improving my scientific writing and presentation skills. I also thank the other committee members, Dr. Dennis Lamb, Dr. James Freihaut, and Dr. Jerry Harrington for serving on my committee.

I would like to thank Dr. Darin Toohey in University of Colorado at Boulder for his help about AMS and UHSAS measurement and data analysis.

I also would like to thank my colleagues in department of Meteorology for their time to help with my experiment, listen to my thoughts and to share our knowledge. My special thanks go to Margaret Root, Robert Lesher, Xinrong Ren, Xingqiu Mao, and Zhong Chen in our group.

I would like to thank my mother in heaven, my father, sister, and parents-in-law for their love and support. Finally I am grateful to my husband and my son for providing a real rest, understanding, encouragement, and trust during my long time with work and life.

Chapter 1

Introduction

1.1 Background

Secondary aerosol particles are produced by oxidizing gaseous emissions, forming low volatility compounds that either nucleate or partition on the existing aerosol particles. Secondary aerosol particles are a significant fraction of all fine particles less than 2.5 μm in diameter, called PM 2.5 (IPCC, 2001). These small atmospheric aerosol particles have significant effects on human health by intensifying bronchial and cardiopulmonary diseases in the human lung (Krewski et al., 2000; Lall et al., 2004). They also play an important role in the global radiative balance, directly by changing light scattering and indirectly by changing cloud characteristics such as the reflectivity, size distribution, concentration, and albedo (IPCC, 2001; Seinfeld and Pandis, 1139-1143, 1998). Understanding the origins and formation of the secondary aerosol particles is essential for understanding and predicting the impact of secondary aerosol on health and climate.

A growing body of evidence shows that organic compounds comprise a large fraction of most secondary aerosol particles (Murphy et al., 1998; Huebert et al., 2004; Drewnick et al., 2004b; Salcedo et al., 2006; Lanz et al., 2007). The sources of particulate organics, especially those of biogenic origins, are numerous and uncertain, (Kamens and Jaoui, 2001), unlike the sources for sulfate and nitrate, which are known to within an

uncertainty of 20-30% (IPCC, 2001). Quantifying the particulate organic component from precursor gases is further complicated by other factors, such as the type and concentration of the oxidants, the atmospheric humidity and temperature, the presence of nitrogen oxides (NO_x), and the presence of pre-existing acidic aerosol (for example, Seinfeld et al., 2001; Griffin et al., 1999; Presto et al., 2005; Northcross and Jang, 2006.). These and other recent studies have begun probing the aerosol properties resulting from the oxidation of different organic precursor gases. The goal is to understand the complexities and commonalities in order to understand the mechanisms and environmental conditions that control the formation and aging of secondary organic aerosol (SOA) particles.

Inorganic secondary aerosol from sulfur dioxide (SO_2) photo-oxidation by hydroxyl (OH), in contrast to SOA formation, has been well studied experimentally and theoretically. In particular, the binary nucleation of sulfate aerosols has been studied widely to determine the nucleation rate and the particle number concentration in ideal conditions (Jaecker-Voirol and Mirabel 1988; Vehkamaki et al., 2002). The interactions of sulfate aerosol particles with nitric acid, ammonia, and organics can affect the chemical composition, mass, and volatility of the secondary aerosol particle.

Secondary organic aerosol production has been studied in environmental chambers. In these controlled experiments, measurements of gas-phase and aerosol chemical composition, aerosol size distributions, and aerosol yield are compared to results from chemical models (for example, Kamens et al 1999; Jang et al. 2002; Gao et al., 2004). The typical environmental chambers are large batch-style Teflon bags with volumes up to 30 m^3 and residence times of several hours. These chambers are designed

to simulate the timescales of SOA formation and further oxidation in the atmosphere. The large size makes this simulation possible, although wall effects remain significant and a concern (Cocker III et al., 2001). In these environmental chamber experiments, the amounts of oxidants are usually similar to those encountered in the atmosphere, with ozone being as much as several hundred ppbv and OH in the range of 10^6-10^7molecules cm^{-3}. Recently a continuous laminar flow chamber with small volume of 9.5 L was developed that uses about 1 ppmv of ozone with a residence time of a few hours to study SOA formation (Jonsson et al., 2006). Wall effects and limited residence time remain as significant issues that may affect the fidelity of the chamber simulations to the atmosphere.

The chemical composition of SOA produced in the environmental chambers has been studied with an Aerosol Mass Spectrometer (Bahreini et al., 2006; Alfarra et al., 2006). The mass spectrum of SOA in the environmental chamber showed signs of an SOA aging process affected by the UV radiation or oxidants OH or hydorperoxyl (HO_2). However their oxidation reaction was too slow to detect the aging of SOA. The effect of OH/HO_2 reactions on SOA aging was not easily investigated because OH and HO_2 were not measured in the environmental chamber (Kroll et al., 2006; Alfarra et al., 2006)

A simple, conceptual kinetic model can capture the processes of secondary organic aerosol formation and aging (Chan et al., 2007), as illustrated in the schematic in Figure **1**. The model is based on the concept that semi-volatile organic species partition between the gas-phase and the particle phase as a function of its atmospheric concentration and the total organic particle mass (Odum et al., 1996; Donahue et al., 2005; Chan et al., 2007). In this model, the precursor gas, hydrocarbon (HC), is oxidized

to a semi-volatile product. This semi-volatile product rapidly partitions between the gas-phase ($\alpha_1 A_1^g$) and the particle-phase (A_1^p) according to a gas-to-particle partitioning equilibrium. However, the semi-volatile product in the gas-phase can be further oxidized to stable gas product (A_2^g) by OH or HO_2. As the semi-volatile product's gas-phase concentration decreases, its particle phase concentration decreases to stay in equilibrium. The semi-volatile product in the particle phase can also be oxidized to a stable particle-phase product (B_1^p). If a stable particle-phase product is formed, then some organic aerosol mass will remain even when all the semi-volatile product is removed from the gas-phase.

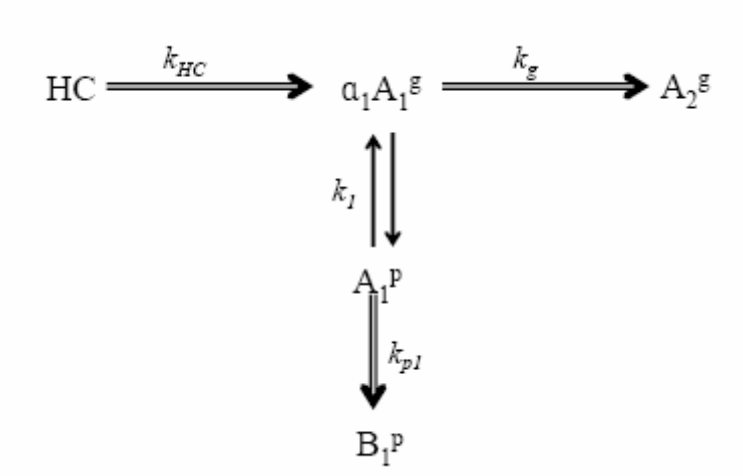

Figure **1**: Concept of the kinetic model from Chan et al., (2007). HC is the precursor hydrocarbon; k_{HC} is the gas phase oxidation rate constant; $\alpha_1 A_1$ is the unstable gas phase product; α_1 is the mass-based stoichiometric coefficient of semivolatile product i; A_2^g is the stable gas product; k_g is the oxidation constant; k_1 is the gas-to-particle partitioning equilibrium constant; A_1^p is the unstable particle product; k_{p1} is the constant to produce stable particle; and B_1^p is the stable particle product.

SOA formation is initiated by OH or O_3, but the production of semi-volatile products can require reactions with OH, O_2, HO_2 RO_2 (R = CH_3, $C2H_5$ …), nitric oxide (NO), or nitrogen dioxide (NO_2). SOA aging can result from reactions with OH, O_3, HO_2, ,RO_2, NO, or NO_2 or by chemical decomposition by ultraviolet light (UV). If, for instance, k_{HC}, k_g, and k_{pl} are all dependent on OH, then the proportion of stable gas and particle products will be the same no matter the OH concentration. If other oxidants or UV are involved in the formation of the stable gas product or stable particle product, then the SOA mass and chemical composition can depend on the ratios of these oxidants (Chan et al., 2007). While various schemes for SOA formation and aging have been proposed, studies from environmental chambers have not had sufficient control of the oxidant concentrations to confirm these schemes.

In the atmosphere, attempts have been made to measure all the SOA precursor gases, and then, using the yield data from environmental chambers, model the aerosol mass that results from the measured abundances of known aerosol precursor gases. Generally, the measured SOA mass has greatly exceeded the modeled SOA mass (Volkamer et al., 2006). Modeling the SOA mass is uncertain because not all the precursor gases may have been measured and their yields and the heterogeneous chemistry for the sampled environments may not be known. While the inorganic precursor gases SO_2 and NO_2 are routinely measured, the volatile organic compounds (VOCs) are much less commonly measured (Demerjian, 2000). The Photochemical Assessment Monitoring Stations in the United States of America measure some of the VOCs, but the high-molecular-weight VOCs that tend to produce secondary aerosol are

scarcely measured. Thus, modeling the aerosol mass that comes from atmospheric organic emissions is difficult and uncertain.

An alternate approach is the direct and fast measurement of aerosol forming potential of air masses in the atmosphere using networks of small, inexpensive chambers. Current environmental chambers are not designed to track the fast changes of precursor gases in the atmosphere; they are too large, have a long response time, and would be difficult to replicate into a network of chambers. A new concept and measurement method are required.

1.2 Definition of the concept of Potential Aerosol Mass (PAM)

We introduce a new concept: Potential Aerosol Mass (PAM). PAM can be defined as the maximum aerosol mass that the oxidation of precursor gases produces. All precursor gases are rapidly oxidized with extreme amounts of oxidants to low volatility compounds, resulting in the aerosol formation. For this approach to simulate the atmosphere, all of the processes, including oxidation of precursor gas, nucleation, and gas and particle partitioning, should occur as they do in the atmosphere, except that instead of taking hours, the processes should be complete in a few minutes. This fast secondary aerosol formation under highly oxidizing conditions should be able to simulate the processes that occur in either the batch-style environmental chambers or, more importantly, the real atmosphere. While defining such a quantity may seem difficult, considering all the factors that affect aerosol yield, our studies indicate that it may be possible.

The term, maximum aerosol yield, was introduced by Martín-Reviejo and Wirtz (2005). Their maximum aerosol yield is calculated by the slope of the increase of aerosol mass with decrease in precursor organic species in environmental chamber experiments. Martín-Reviejo and Wirtz (2005) observed higher value for maximum aerosol yield than for overall aerosol yield, but it was due to the use of threshold of reacted precursor organic in the calculation of overall aerosol yield. Their maximum aerosol yield can be calculated for only limited SOA with mass that increases linearly with the decrease of precursor organic species. The PAM concept applies to inorganic and organic secondary aerosol and it only depends on the consumed precursor gas amount and produced final particle product. Thus, the PAM concept is different from the concept of maximum aerosol yield.

1.3 Thesis research goal

In this research, we describe our initial efforts to develop the PAM concept. We provide results that indicate its feasibility and its applicability to SOA formation in the atmosphere. We describe a small, simple, flow-through chamber with a short residence time that is irradiated with ultraviolet (UV) light. In Chapter 3, tests for the feasibility of the PAM concept are described, including the following: (1) tests of an inorganic secondary aerosol, the sulfate aerosol; (2) tests of the aerosol formation mechanism and aerosol mass yield for several controlling variables, such as temperature, relative humidity, oxidant concentration, precursor gas composition and amount, presence of NO_x, and presence of acidic seed aerosol with α-pinene; and (3) the first field test. In

Chapter 4, the SOA results in PAM for several natural and anthropogenic volatile organic compounds are compared to others obtained in large, batch-style environmental chambers. In Chapter 5, the formation and aging of SOA in PAM is studied with aerosol mass spectra and particle number distribution. Also, the dependence of the aging of SOA on the precursor gas amount and OH and HO_2 is described.

Chapter 2

Experimental method

2.1 PAM chamber description

A prototype chamber was designed to examine the PAM concept. The basic requirements for the PAM chamber are the following: continuous flow with a long enough residence time that precursor gases will be fully oxidized to aerosol particles; sufficient flow to be compatible with a variety of aerosol particle sampling instruments; an air flow through the chamber that isolates particle sampling from potential wall effects; and the ability to vary the amount of UV radiation and amounts of water vapor, precursor gases, and oxidants. This prototype chamber generally meets these requirements, but is certainly not optimized.

The prototype PAM chamber is a cylinder made of Teflon FEP film (0.5 mm thick) with a volume of 19 L, a length of 60 cm, and a diameter of 20 cm (Figure **2**). Two ozone-producing UV grid lamps (BHK Inc.) are mounted one above the other on the wall of a larger, sealed housing in which the Teflon chamber is suspended. Each of these lamps is 15 cm × 15 cm and produces mainly 185 nm and 254 nm light. The volume inside the housing surrounding the Teflon chamber is purged with N_2 to prevent ozone formation outside of the chamber and to purge away any out-gassing from the Teflon chamber and the inside of the housing. Aerosol particles, gases, pressure, and temperature are sampled in the center at the bottom of the PAM chamber.

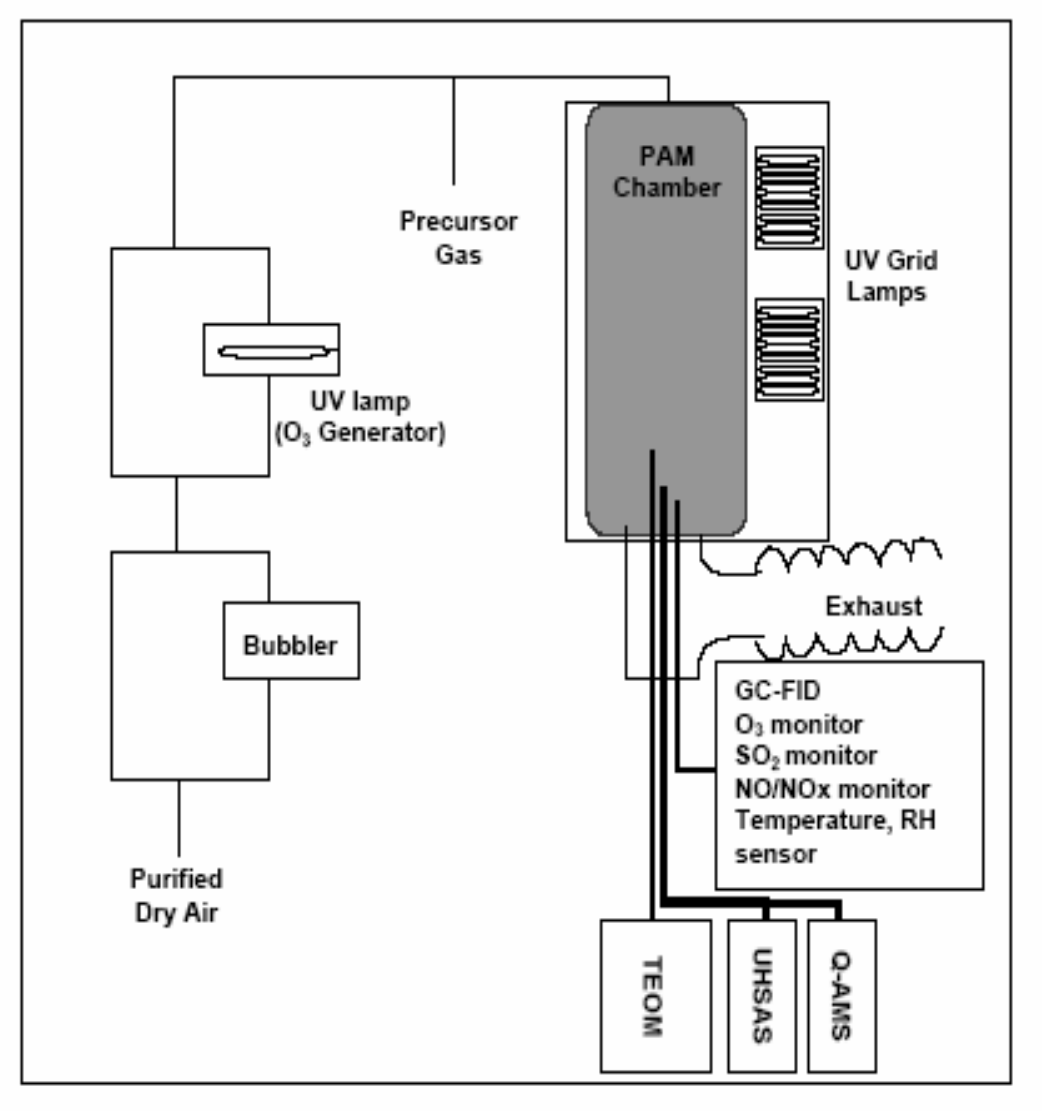

Figure **2**: Schematic diagram of the PAM chamber setup.

The sample air was continuously added to the chamber and released out through a large exhaust hose at the bottom. The chamber remained at ambient pressure. The volumetric air flow could be varied and was typically 5 to 20 $Lmin^{-1}$. At these flow rates, the air flow was calculated to be laminar with a Reynolds number less than 500. Two different methods were tried to bring the flow into the chamber: introducing the flow

through a system of perforated tubes at the top of the chamber in an effort to spread the flow across the chamber area, and introducing the air flow through a 1 cm diameter tube that protrudes a few cm into the chamber on its cylindrical axis. The results described in this feasibility study appear to be independent of the method of introducing the air into the chamber.

2.2 Determination of exposure time in the PAM chamber

We define the term, exposure time, to be the average time that the sample air is exposed to the oxidants in the chamber. In the continuous flow chamber, how much precursor gas is oxidized is determined by the oxidant concentration and the exposure time. The exposure time of the PAM chamber was determined by monitoring how fast SO_2 was changed from an initial value to a lower value after UV lights were turned on. At a flow rate of 5 $Lmin^{-1}$, the exposure time was 240 ± 36 s and at 10 $Lmin^{-1}$ was 180 ± 27 s. That the exposure times are not inversely proportional to the flow rates suggests that the air does not flow through the chamber with a uniform velocity across the chamber cross section.

2.3 Preparation of precursor gases

The purified dry air comes from room air that is compressed and then passed through a zero air generator (ZAG-75 Labgas Inc.) and a series of filters: Drierite, activated charcoal, hopcalite, and HEPA filter pack. The purified dry air was humidified

by passing it through a glass bubbler containing deionized water. The relative humidity was controlled by adjusting the fraction of the total air flow that passed through the bubbler. The total flow rate of the purified air was controlled by mass flow controllers (1179A, 1479A, MKS Inc.). The relative humidity in the chamber was measured by the relative humidity sensor (HUMICAP HMP 45A/D, Vaisala).

Other gases were added to the chamber by combining mixtures of these gases to the purified air upstream of the PAM chamber. Commercially prepared mixtures were used for SO_2 (10 ppmv, Scott Specialty Gases) and for NO (10 ppmv, Matheson-Trigas), both in ultra pure N_2 (99.999% pure, < 0.5 ppm THC, GTS). The flow rates of these mixtures and others were controlled by flow controllers (MKS Inc.) that were calibrated against a DryCal flow calibrator (BIOS).

For this feasibility study, nine hydrocarbons were used: three monoterpenes (α-pinene, β-pinene, Δ^3-carene), and six anthropogenic hydrocarbons (cyclohexene, m-xylene, p-xylene, 1,3,5-trimethylbenzene (1,3,5-TMB), toluene, and ethylbenzene). Three monoterpenes were chosen because they were main sources of biogenic VOCs emissions from forests. Six anthropogenic hydrocarbons were emitted from the combustion of fossil fuels representing SOA sources in urban area. The stated purities of parent hydrocarbons are as follows: α-pinene (Fluka, 99.0%), β-pinene (Fluka, 99.0 %), Δ^3-carene (Fluka, 98.5 %), cyclohexene (Fluka, 99.7%), m-xylene (Fluka, 99.5%), p-xylene (Fluka, 99.5%), 1,3,5-trimethylbenzene (1,3,5-TMB), (Aldrich, 100 mg of ampule), toluene (Fluka, 99.9%), and ethylbenzene (Fluka, 99.5%). The hydrocarbon gas mixtures were prepared in ultra pure N_2 (99.999% pure, <0.5 ppm THC, GTS) gas in the laboratory. To make a mixture, a hydrocarbon was added to a 6 L evacuated glass bulb and the pressure, P_{HC},

was measured (Baratron 390 HA, MKS Inc.). The bulb was then filled to a higher pressure with N_2, creating a mixture with a mixing ratio given by the following Eq. **1**:

$$Mixing \cdot ratio \cdot of \cdot a \cdot mixture(ppmv) = \frac{P_{HC} - P_0}{P_{Total} - P_0} \times 10^6 \quad \textbf{1}$$

where P_{HC} is the hydrocarbon partial pressure, P_0 is the minimum pressure achieved in evacuation (typically < 0.5 hPa), and P_{Total} is the final pressure of the mixture.

The reactive gases O_3, OH, and HO_2 were generated directly in the PAM chamber. Irradiating humid, purified air inside of the chamber with 185 nm UV light produced OH and HO_2 from H_2O and O_3 from O_2. For the studies of dark reactions with ozone, humid or dry purified air was passed through an external O_3 generator (AnaLamp low pressure Hg lamp, BHK Inc.) first and then added into the purified air before entering the chamber. OH and HO_2 were also generated in the external O_3 generator, but essentially all OH and HO_2 were reacted away before they reached to the chamber. Different O_3, OH, and HO_2 mixing ratios were generated by varying the power supplied to the UV lamps, using one or both UV lamps, and varying the humidity. The production of reactive gases could be rapidly terminated by turning off the UV lamps.

2.4 Gas measurement

Both gases and aerosol particles were sampled through inlets near the center of the lower end of the cylindrical PAM chamber (Figure **2**). Gaseous sample inlets were placed 5 cm above the bottom of the chamber. O_3, SO_2, and NO/NO_x in the chamber were continuously monitored by O_3 monitor (model 8810 ozone analyzer, Monitor Labs

Inc.), SO_2 monitor (43i-TLE SO_2 analyzer, Thermo Electron Corp.), and NO/NO_x monitor (42C Trace level $NO\text{-}NO_2\text{-}NO_y$ analyzer, Thermo Environmental Instruments). Initial and final hydrocarbon concentrations were measured by Gas Chromatography-Flame Ionization Detector (8610 C, SRI) before and after the UV light was turned on. Humidity and temperature was continuously monitored by a relative humidity and temperature sensor (HUMICAP HMP 45A/D, Vaisala).

2.5 Aerosol mass measurement by TEOM

Two aerosol sample inlets made of stainless steel and copper tubing were placed 12 cm above the bottom of the chamber. Aerosol mass was mainly detected with a real-time aerosol mass measurement instrument, Tapered Element Oscillating Microbalance (TEOM 1400A, R&P Co.). One other inlet was designed to connect additional aerosol measurement instruments such as Quadruple-Aerosol Mass Spectrometer (Q-AMS) or Ultra High Sensitivity Aerosol Spectrometer (UHSAS) (see the section 2.6).

TEOM is a real-time particle mass measuring instrument that operates by sampling ambient air through a filter at a constant flow rate, continuous weighing the particle collected filter and calculating mass concentration (TEOM series 1400a ambient particulate monitor manual, 2004). The mass loading of particle filter sitting at the end of the oscillating tapered element changes the frequency; this frequency change is calculated to aerosol mass concentration.

The raw frequency of the TEOM mass transducer was recorded every 10 s and aerosol mass was calculated and averaged for 2 min based on Eq. **2**:

$$\frac{\Delta M_{filter}}{\Delta t} = K_0\left(\frac{1}{f_{i+1}^2} - \frac{1}{f_i^2}\right),$$
$$MC(\mu g/m^3) = \frac{\Delta M_{filter}}{\Delta t} \times \frac{1}{flowrate(l/\min)} \quad \textbf{2}$$

where ΔM_{filter} is the collected particle mass of the TEOM filter at a given time, K_0 is a calibration constant of the mass transducer, f is frequency, t is time, MC is particle mass concentration, and *flow rate* is a sample flow rate through the TEOM. The mass concentration calculated by the raw frequency without the manufacturer's smoothing procedure enabled us to track rapid mass changes in the PAM chamber. The aerosol mass was obtained from the difference between produced aerosol mass and the background mass, which was the aerosol mass detected in purified air.

The TEOM temperature was set to 30°C to reduce the evaporation artifact of semi-volatile organic aerosol (TEOM 1400A, Technical note 4, 2004) instead of 50°C. The TEOM temperature setting of 30°C can result in increased noise due to humidity changes, but the additional noise was less than the acceptable uncertainty, 5 μg/m^3 for a 10-min average. The concern is that semi-volatile organics may be lost from the TEOM (Schwab et al., 2004; Long et al., 2005; Schwab et al., 2006; Wilson et al., 2006), even when operated at 30°C. If significant semi-volatile mass were being lost on the TEOM in the PAM measurements, then a large negative mass signal calculated by Eq. **2** would be observed after the UV lights were turned off. However, a negative mass of only at most a few percent of the measured mass was sometimes observed in the experiments or the preliminary field study. Furthermore, for experiments in which the PAM chamber was sampled with both the TEOM and an Aerosol Mass Spectrometer (AMS), the two

instruments measured the same mass to within 10%. Thus, for these studies, the TEOM does not appear to be losing a significant amount of semi-volatile organic mass.

2.6 Aerosol chemical composition measurement by Q-AMS

Quadruple-Aerosol Mass Spectrometer (Q-AMS, Aerodyne Research, Inc.) was used to measure chemical composition of SOA from α-pinene, m-xylene, p-xylene and a mixture of these three hydrocarbons. The Q-AMS was operated simultaneously with TEOM for continuous real-time measurement, and it averaged and stored mass spectrum every minute.

Q-AMS is an instrument to measure size-resolved chemical composition of aerosol in the atmosphere (Canagaratna et al., 2007; Jayne et al., 2000). The detailed description can be found elsewhere, and we introduce a brief description here (Jayne et al., 2000; Jimenez et al., 2003; Canagaratna et al., 2007). It has three parts; aerosol sampling inlet, particle sizing chamber, and chemical composition detection section (Figure **3**). Aerosol particles at atmospheric pressure are sampled in the particle inlet and are size-segregated and collimated while the sample is traveling through the aerodynamic lens. The collimated particle beam is chopped by the chopper wheel for the Time-Of-Flight (TOF) mode and Mass Spectrum (MS) mode alternatively. In the detection section, non-refractory components in particle beam are thermally vaporized and then ionized by electron impact. The positive ion fragments generated by the electron impact ionization are detected by the quadruple mass spectrometer to produce mass signals for mass-to-charge ratio (*m/z*) of the particle beam. In the MS mode, the chopper wheel blocks and

opens the particle beam to get particle mass for each chemical component regardless of particle size. In the TOF mode, the particle beam is chopped to get size-resolved mass spectrum for chemical components. Described data in Chapter 5 is the mass spectrum for chemical component regardless of particle size in the MS mode.

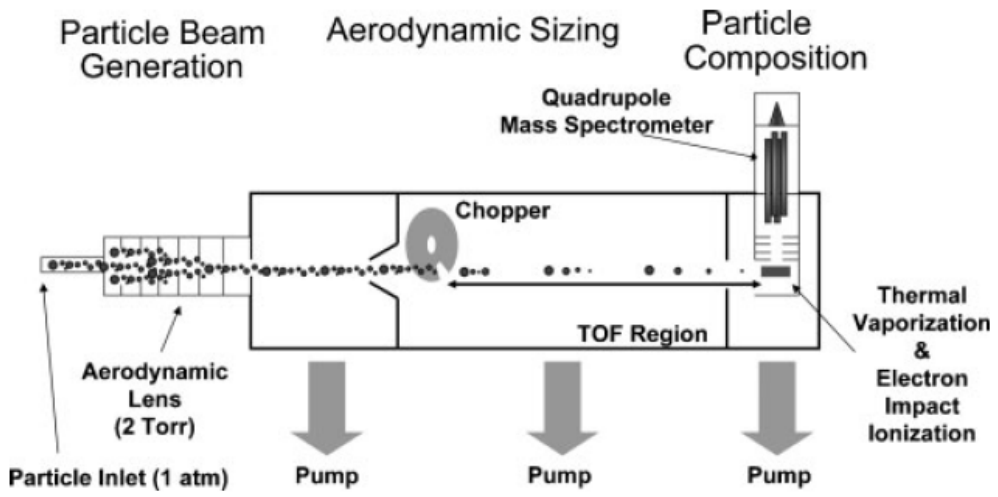

Figure **3**: A schematic of Quadruple-Aerosol Mass Spectrometer (taken from Canagaratna et al., 2007).

We measured particle number concentration of size distribution with Ultra High Sensitivity Aerosol Spectrometer (UHSAS, Droplet Measurement Technologies) for the supporting evidence of SOA aging in Chapter 5. The UHSAS is an optical-scattering, laser-based aerosol particle spectrometer system for accurately and precisely sizing particles in the range from 0.055 μm to 1.0 μm diameter (UHSAS manual). The UHSAS scans the size range every 10 s, and this short scanning time enabled us to observe the fast aerosol formation process in our PAM chamber.

2.7 The agreement of SOA mass in the Q-AMS and TEOM

Q-AMS is used to measure chemical composition of SOA in the PAM chamber. Its total aerosol mass concentration should be the same as the TEOM measurement. TEOM is a direct aerosol mass measurement instrument by weighing the particles collected on a filter. The total aerosol mass concentration in Q-AMS is calculated by summing the mass spectrum signal for the mass fragment range (mass to charge (*m/z*) 1 ~ 301). Figure **4** shows the peak and the stable mass measured in TEOM and in Q-AMS for various α-pinene amounts. As aerosol mass increases, the discrepancy between TEOM mass and Q-AMS mass increases. If the particle mass is too high, the detected signal in the Q-AMS detector can be saturated when the particles are vaporized, ionized, and detected. Therefore, the Q-AMS may need a non-linearity correction when the total mass exceeds 40-50 $\mu g/m^3$ (Toohey, Personal communication). The AMS presented here were not corrected for this factor. Moreover, the particles can be irregular in shape and a fraction of them may not reach the vaporizer or may bounce off the vaporizer surface before being totally vaporized, resulting the under-estimation of aerosol mass (Jayne et al., 2000; Alfarra, 2004). The minimum detectable size of particle in Q-AMS is 50 nm (Canagaratna et al., 2007), while TEOM can measure particles smaller than 10 nm in diameter. All of these factors tend to reduce the Q-AMS total particle mass measurement compare to the TEOM mass measurement. Thus it is not surprising that the ratio of TEOM mass to AMS mass is slightly greater than 1 in Figure **5**.

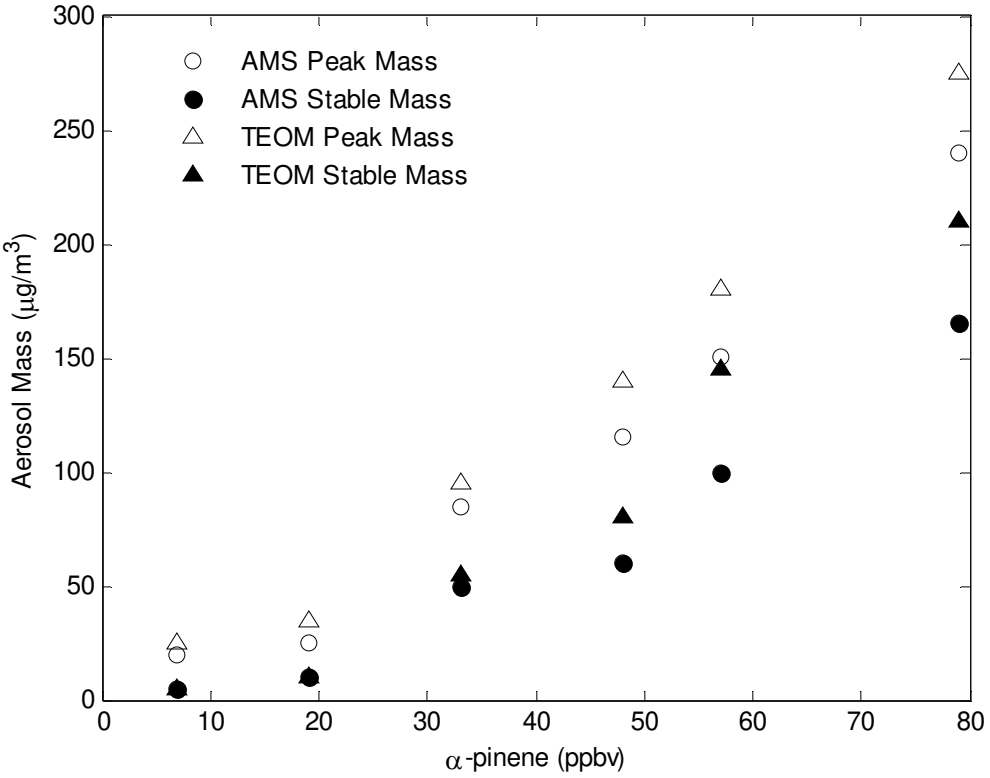

Figure **4**: Aerosol mass measured in AMS (○,●) and TEOM (Δ,▲). As aerosol mass increases, the discrepancy between AMS and TEOM increases for both of peak and stable mass.

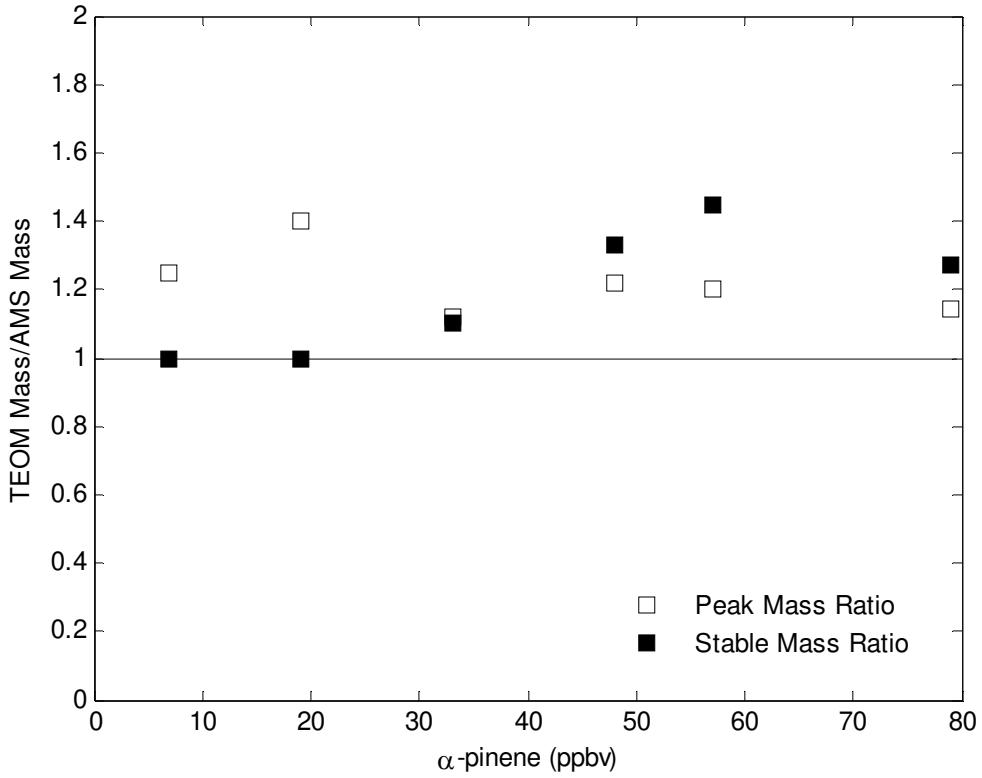

Figure **5**: The ratio of the TEOM measured aerosol mass over the AMS measured aerosol mass for various α-pinene mixing ratios. For peak and stable mass, TEOM mass is higher than AMS mass up to a factor of 1.4.

2.8 OH/HO_2 measurement by GTHOS

A unique feature of this PAM feasibility study is the direct quantification of OH and HO_2 in the PAM chamber for different conditions. The OH and HO_2 mixing ratios were measured separately by the Ground-based Tropospheric Hydrogen Oxides Sensor (GTHOS) (Root, 2007; Faloona et al., 2004). The TEOM inlet was replaced with the GTHOS inlet, which was at the same height in the PAM chamber that the TEOM inlet was. OH and HO_2 mixing ratios were measured for the range of relative humidity used in the feasibility studies.

The behavior of O_3, OH, and HO_2 are quite different as a function of relative humidity (Figure **6**). Ozone decreases about a factor of 2 with increasing relative humidity, unlike OH which increases over a factor of 10. The slight decrease in [O_3] at higher humidity is due to absorption of UV by the increased water vapor, and therefore the reduction of UV in the chamber, to the reactions with OH and HO_2, and to the photolysis of ozone and reaction with water vapor that results in the formation of OH. [O_3] could be varied from 0 to 40 ppmv. [OH] also depends on UV, but is roughly linearly dependent on water vapor. With the UV lamps on, [OH] could be generated over a wide range of mixing ratios, from ~7 pptv when RH was ~0% to 500 pptv when RH was ~45%. [HO_2] showed quite different behavior, changing non-linearly from 100 pptv when RH was ~0% to ~4.0 ppbv when RH was 15% or greater.

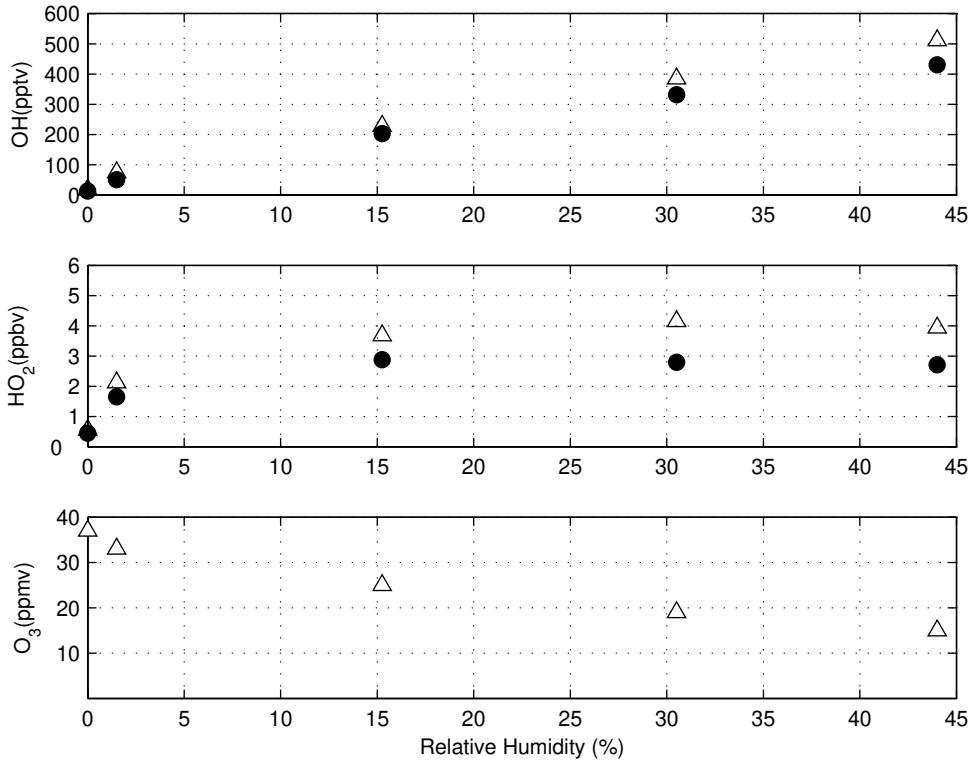

Figure **6**: OH and HO_2, measured directly by GTHOS, and O_3 in the PAM chamber as a function of relative humidity. Measurements were performed with one (filled circles) or two (open triangles) grid mercury lamps. This O_3 measurement is only with two grid mercury lamps. O_3 and OH were linearly changed with relative humidity while HO_2 were not.

This behavior of HO_2 and OH can be understood as follows. The concentrations of OH and HO_2 are so high that the lifetimes of OH and HO_2 are very short, much less than a second. The major loss of HO_2 is the reaction $HO_2+HO_2 \rightarrow HOOH+O_2$, and to a lesser extent the reaction $HO_2+OH \rightarrow H_2O+O_2$. $[HO_2]$ is at least 10 times larger than [OH], so that $[HO_x]$, the sum of [OH] + $[HO_2]$, is essentially equal to HO_2. Because the

HO_x loss is quadratic in HO_x, the HO_x concentration is nearly equal to the square root of the HO_x production (Eq. **3**):

$$[HO_2] = \sqrt{\frac{P_{HOx}}{2\,k_{HO2+HO2}}} \qquad \mathbf{3}$$

From Eq. **3**, an estimate of the HO_2 production rate is 3×10^{10} moleculescm^{-3}s^{-1}. On the other hand, the main loss for OH is reaction with HO_2, which is essentially constant above an RH of ~15%, while OH production continues to increase with increasing relative humidity. As a result, the OH mixing ratio continues to increase proportionally with increased OH production since the OH loss is fixed.

The ratios of O_3 to OH to HO_2 are similar to those encountered during midday in the lower atmosphere. Assuming typical atmospheric values, 50-100 ppbv for O_3, 20-80 pptv for HO_2, and 0.2-0.5 pptv for OH, typical O_3/OH ratios are 1×10^5-3×10^5 and typical HO_2/OH ratios are 10-100. These ratios are similar to the ratios in the PAM chamber: 2×10^5 for O_3/OH and ~15 for HO_2/OH. Thus, in terms of major oxidants, the PAM chamber can simulate atmospheric oxidation processes, but at greatly accelerated rates.

The OH and HO_2 mixing ratios were measured at the bottom of the PAM chamber. The OH mixing ratio derived from the change in $[SO_2]$ observed with and without the UV lights on agrees well within uncertainties with the [OH] measured directly by GTHOS (Root, 2007). This agreement between direct and indirect OH measurements suggests that the OH distribution in the chamber is fairly uniform. Furthermore, the directly measured OH and HO_2 mixing ratios allow the OH and HO_2 mixing ratios to be estimated from knowledge of only the UV light and the relative

humidity. Better control on these parameters will be built into the next version of the PAM measurement.

Chapter 3

Feasibility test of the PAM concept

The PAM concept is introduced and defined in the Introduction. In this chapter, the feasibility of the PAM concept is experimentally tested for secondary inorganic and organic aerosols in the PAM chamber and for atmosphere in the field test. Experiments with well known and widely studied secondary aerosols such as sulfate aerosol and SOA from α-pinene are essential tests of the PAM concept.

3.1 Inorganic secondary aerosol: SO_2 conversion to sulfate aerosol

3.1.1 Calculation of expected conversion ratio from SO_2 to sulfate aerosol

The quantitative conversion of SO_2 to inorganic sulfate aerosol was studied to demonstrate the PAM concept, even though the greatest value for PAM is improving the understanding of secondary organic aerosol. The oxidation pathways, nucleation process, sulfate mass per amount of SO_2, and unity yield are all well known in Eq. **4**:

$$SO_2 + OH\cdot + M \rightarrow HOSO_2\cdot + M$$
$$HOSO_2\cdot + O_2 \rightarrow HO_2\cdot + SO_3$$
$$SO_3 + H_2O + M \rightarrow H_2SO_4 + M \qquad \textbf{4}$$
$$H_2SO_4 + H_2O \xrightarrow{nucleation} \text{sulfate aerosol}$$

where $k_{OH+SO2} = 9.0\times10^{-13}$ molecule^{-1}cm^{3}s^{-1} at 298 K for the initial reaction of SO_2 with OH. Thus, simultaneous measurements of SO_2 and sulfate aerosol mass test both the rapid oxidation and nucleation of aerosol particles and the possible loss of sulfate aerosol particles to the walls.

The theoretical value of the maximum sulfate aerosol produced in the PAM chamber is calculated by,

$$The \cdot calculated \cdot conversion \cdot ratio = \chi(SO_2(1 \cdot ppbv)) \times \frac{mass \cdot of \cdot sulfur}{SO_2 volume} \times \frac{H_2SO_4 mass}{mass \cdot of \cdot sulfur} \times growth \cdot factor \quad \mathbf{5}$$

The growth factor is given by,

$$growth \cdot factor(f) = \frac{m_{H2SO4} + m_{H20}}{m_{H2SO4}} \quad \mathbf{6}$$

where m_{H2SO4} is the mass of sulfuric acid in particle phase; m_{H2O} is the mass of water uptake in particle phase. The sulfate aerosol produced by the SO_2 oxidation consists of sulfate and water molecules. The calculated conversion ratio is obtained by the SO_2 conversion to sulfate and a RH-dependent growth factor.

The calculation assumes that [OH] is in great excess in the chamber and that all of the oxidized SO_2 becomes sulfate aerosol. One ppbv of SO_2 produces 3.95 μgm^{-3} of H_2SO_4. A complication is the water uptake on the sulfate aerosol particles, which makes the aerosol particle mass dependent on relative humidity (RH). As a result, the conversion ratio from SO_2 to sulfate aerosol particle mass depends on a RH-dependent growth factor. The growth factor as a function of relative humidity is calculated by the theoretical model of Jaecker-Voirol et al. (1990) (Figure **7).** For example, at a relative

humidity of 28% and a TEOM temperature of 30°C, total conversion of 1 ppbv of SO_2 produces 5.8 μgm^{-3} of sulfate aerosol. The water uptake of the sulfate aerosol particles rapidly adjusts to equilibrium with the relative humidity, so that the relative humidity that is important in determining the aerosol particle mass is the relative humidity at the TEOM mass transducer.

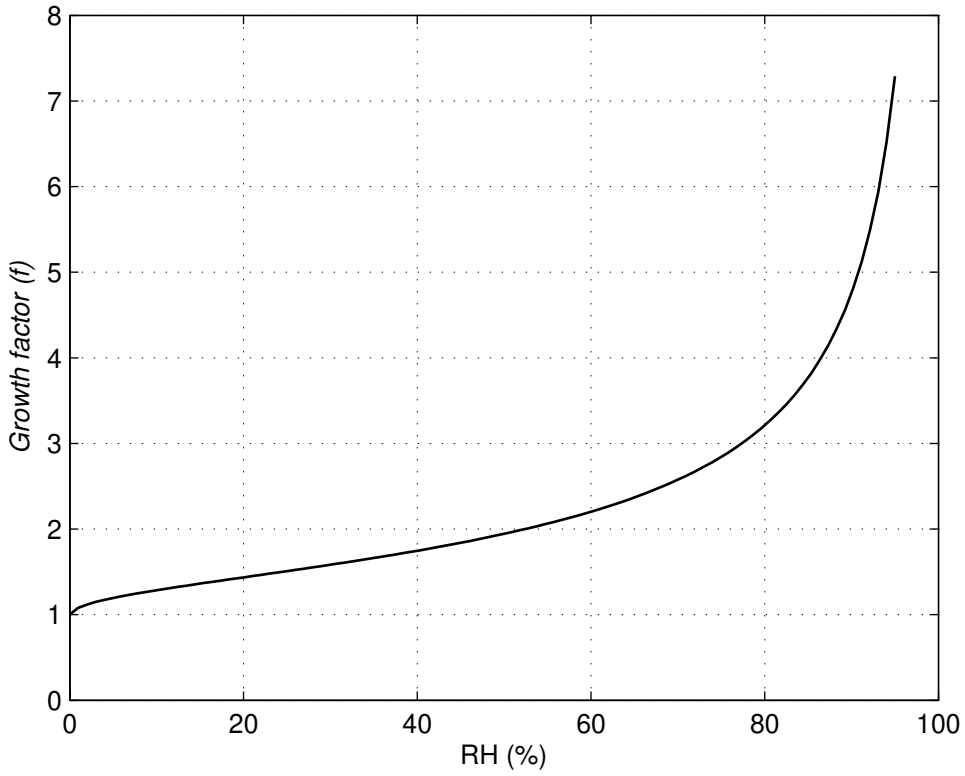

Figure 7: Growth factor ($growth \cdot factor(f) = \frac{m_{H2SO4} + m_{H20}}{m_{H2SO4}}$) of sulfate-water particle with respect to RH (%). The data are obtained from Jaecker-Voirol et al. (1990).

3.1.2 Experimental conversion ratio and comparison with expected conversion ratio

A range of SO_2 mixing ratios from 3 ppbv to 35 ppbv was added to the air flow in the chamber. For these experiments, the air flow rate was 5 $Lmin^{-1}$, the exposure time to the UV light was 240 ± 36 s, and the relative humidity was 40% in the chamber and 28% at the TEOM mass transducer. Both UV grid lamps were on, producing 450 pptv of OH in the chamber (See Figure **6**).

The unsmoothed TEOM mass was calculated from the raw frequency change measurements (Figure **8** (a)). For this graph, the SO_2 mixing ratios have been converted to sulfate mass using the calculated conversion ratio of 5.8 μgm^{-3} appropriate for the 28% relative humidity at the TEOM mass transducer. The aerosol mass quickly increased to the stable value simultaneously as SO_2 dropped down to background levels. The aerosol mass calculated from the raw frequency indicated that sulfate aerosol formation was completed in a few minutes in the PAM chamber. The slope in Figure **8** (b) represents the measured conversion ratio, 5.6 $\mu gm^{-3}(ppbv\ SO_2)^{-1}$, which agrees well with the expected conversion ratio of 5.8 $\mu gm^{-3}(ppbv\ SO_2)^{-1}$.

The effect of TEOM temperature on sulfate aerosol measurement was tested by changing TEOM temperature setting from 30°C to 50°C. The calculated and measured conversion ratios agree well for both of 30°C to 50°C. At a temperature of 50°C and relative humidity of 18% in the TEOM mass transducer, the measured conversion ratio was 4.69 $\mu gm^{-3}(ppbv\ SO_2)^{-1}$ and calculated conversion ratio was 4.98 $\mu gm^{-3}(ppbv\ SO_2)^{-1}$. Thus, the sulfate aerosol formation is not greatly affected by the TEOM temperature. For most

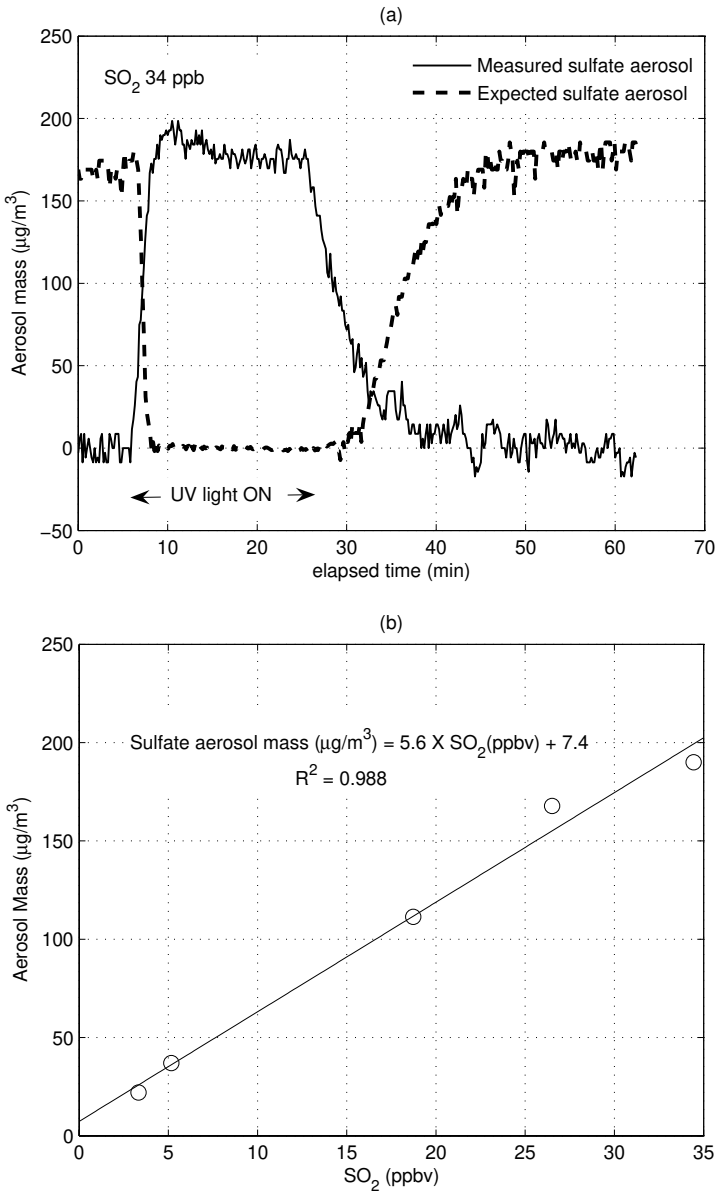

Figure **8**: (a) Measured and expected sulfate aerosol in the PAM chamber with 34 ppb of SO_2. The expected sulfate aerosol was obtained by the measured SO_2 mixing ratio multiplied by the calculated conversion ratio 5.8 $\mu gm^{-3}(ppbv\ SO_2)^{-1}$ for a TEOM temperature of 30°C and a relative humidity of 28%. (b) Measured sulfate aerosol mass versus SO_2. The least squares slope of 5.6 $\mu gm^{-3}(ppbv\ SO_2)^{-1}$ is well within measurement uncertainty of the calculated slope of 5.8 $\mu gm^{-3}(ppbv\ SO_2)^{-1}$.

of our studies of inorganic and organic secondary aerosol, the TEOM mass transducer temperature was kept at 30^{o}C.

The wall loss of precursor gases was tested by measuring the SO_2 mixing ratio in and out of the chamber. Less than 20% of SO_2 was lost on entrance into the chamber and on the Teflon chamber wall. This low wall loss rate is due in part to the relatively fast continuous flow in the PAM chamber. This small wall loss for SO_2 shows that other gases can be brought through the chamber with at most a small loss, but careful tests of inlet materials and heated and unheated inlets will be needed to minimize the loss of oxygenated VOCs and semi-volatile VOCs in the inlet lines and PAM chamber.

SO_2 conversion to sulfate aerosol was performed frequently to monitor the chamber's ability to reproduce the sulfate potential aerosol mass (PAM) quantitatively. For four SO_2 experiments, the measured conversion ratio was 92±4% of the calculated conversion ratio, well within the absolute uncertainty of ~13% and ~12% for the calculated conversion ratio and for the measured conversion ratio, respectively.

These experiments show that SO_2 can be completely converted to sulfate aerosol particles in the few minutes of exposure time in the PAM chamber and that at most a small amount of sulfate aerosol is being lost to the walls of the PAM chamber. In addition, the agreement between the measured and theoretical yields for different relative humidity values in the TEOM, which is different from the relative humidity values in the cooler PAM chamber, indicates that water on the sulfate particles rapidly comes into equilibrium with the water vapor at or on the TEOM filter. Thus, the PAM chamber gives quantitative measurements of the aerosol mass yield for SO_2.

The oxidation of SO_2 by OH is relatively slow compared to most hydrocarbon oxidation by OH, with $k_{OH+SO2} = 9.0\times10^{-13}$ molecule^{-1}cm^{3}s^{-1}. For example, α-pinene reacts with OH with a reaction rate coefficient of $k_{OH+\alpha\text{-pinene}} = 5.5\times10^{-11}$ molecule^{-1}cm^{3}s^{-1}. Essentially all SOA precursor gases react at least 3 times faster with OH than SO_2 does, so that these hydrocarbons should be completely oxidized in the PAM chamber (Table **1**).

This conclusion is supported by GC-FID measurements of the nine hydrocarbons that were studied. They were all depleted to below the detection limit in the PAM chamber after the UV lights were turned on.

Table **1**: The reaction rate coefficients with OH and O_3 for precursor

Precursor gas	**$k_{OH}\times10^{-12}$ (molecule^{-1}cm^{3}s^{-1})**	**$k_{O3}\times10^{-22}$ (molecule^{-1}cm^{3}s^{-1})**
SO_2	1.5	2.2
α-Pinene	50	820000
β-Pinene	70	230000
Δ3-Carene	91	590000
Cyclohexene	62	760000
M-Xylene	24	9.7
p-Xylene	14	15
1,3,5-TMB	57	29
Toluene	6.9	4.5
Ethylbenzene	7.0	-

3.2 Organic gas conversion to SOA with α-pinene

The feasibility of the PAM concept was checked by varying several parameters that might affect the SOA mass yield. The well-studied precursor gas, α-pinene, was

chosen for most of the tests. In the series of experiments, the goal was to determine the conditions for which the PAM chamber would produce the maximum SOA yield. The SOA yield was obtained by Eq. **7** (Seinfeld et al., 2001):

$$SOA \cdot Yield(Y) = \frac{M_O(produced \cdot organic \cdot aerosol \cdot mass)}{\Delta HC(reacted \cdot hydrocarbon \cdot mass)} \qquad \mathbf{7}$$

A typical procedure for these experiments was to first establish the flows of all the gases, then turn on the UV lights until the signal stabilized, and then turn off the UV lights again, as in Figure **8** (a). For the SO_2 experiments, the aerosol mass would quickly rise to near its peak value as the SO_2 value fell and then remain there. In most secondary organic aerosol experiments with sufficient oxidants in the PAM chamber, the aerosol mass would quickly rise to a peak within minutes, but would then decrease to a smaller stable value. It had no effect on the observed stable SOA properties, thus we will use the SOA mass observed after stabilization in the equation for aerosol mass yield for the feasibility study in this section, (Eq. **7**). This behavior will be discussed in Chapter 5 in detail.

3.2.1 SOA yield as a function of O_3

Ozone reacts with α-pinene, but at a rate that is slower than the reaction of OH with α-pinene (Table **1**). The yield from this reaction is a good test of the PAM concept because it is well studied and the SOA yields are known (Kamens et al., 1999; Odum et al., 1996; Pankow et al., 2001 and etc). The effect of ozone on the SOA yield from α-pinene was studied by varying the ozone mixing ratio in the chamber containing purified

dry air (RH < 1%) (Figure **9**). The initial α-pinene mixing ratio was 100 ppbv; the amount of α-pinene was enough to see the distinguishable SOA mass even with very low SOA yield. Ozone was varied by changing the flow rate through an external ozone generator, changing the UV lamp intensity with a controllable power supply, and covering a fraction of the UV lamps with an aluminum cover. [O_3] was produced in the range of 0.7 ppmv to 27 ppmv. [OH] was about 7 pptv and [HO_2] was 450 pptv in the dry, purified air. These [OH] and [HO_2] values were 10-50 times larger than observed in the troposphere, but ozone values were more than 100 times larger than observed in the troposphere.

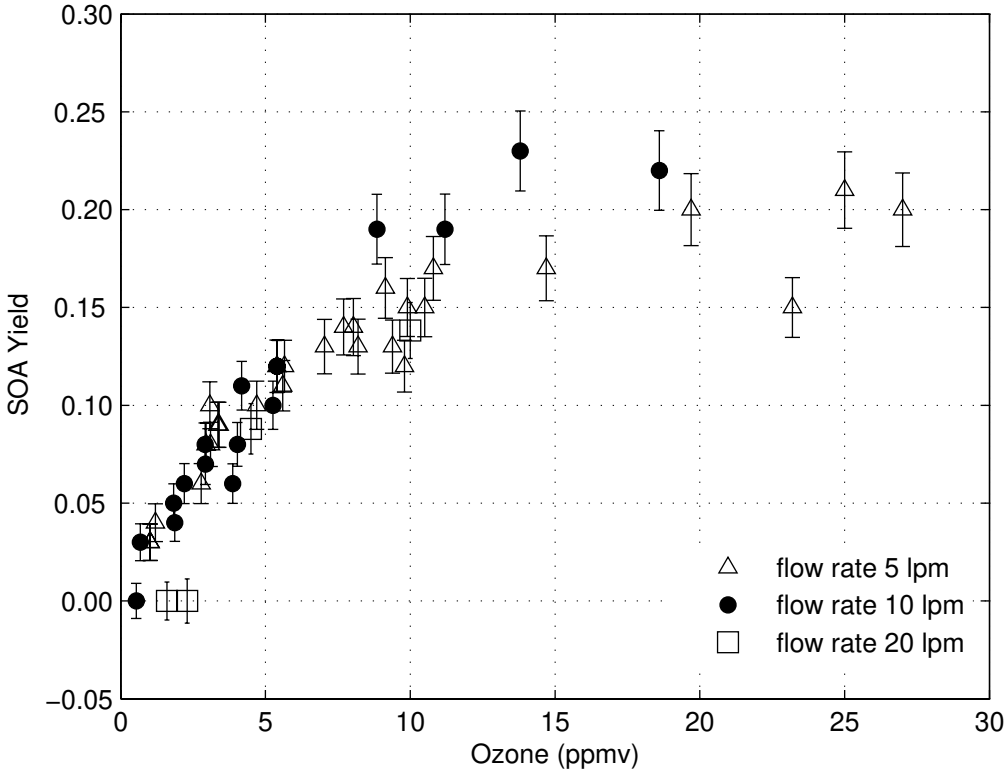

Figure **9**: The SOA yield as a function of chamber flow rate and [O_3] in the dry condition with 100 ppbv of α-pinene. The dominant oxidant in this study is ozone. Three different flow rates are used to change the residence time in the chamber. Error bars show the precision (1σ) for SOA yields.

The aerosol mass initially increased as ozone increased, but then reached a constant maximum stable value for ozone mixing ratio greater than ~12 ppmv. Thus, ozone levels greater than ~12 ppmv were sufficient to maximize the SOA yield. It is also important to note that higher levels of [O_3] do not reduce the aerosol yield, suggesting that O_3 does not react significantly with the α-pinene reaction products that influence the SOA yield. Additional ozone is not expected to reduce the SOA yield from α-pinene

because it has only one double carbon bond (Ng et al., 2006). This result demonstrates that the extreme oxidation in the PAM chamber is occurring as expected for this reaction.

3.2.2 SOA yield as a function of air flow rate in the chamber

The flow rate of air through the chamber affects primarily the exposure time in the PAM chamber. In order to achieve maximum aerosol mass, the exposure time in the chamber must be sufficient to allow for the oxidation of the precursor gas, the aerosol particle nucleation, the condensation of the low-volatility product, and any particle-phase or gas-phase reactions that occur. The higher the flow rate means the shorter the exposure time in the PAM chamber.

The SOA yield from ozonolysis of 100 ppbv of α-pinene in dry conditions was measured as a function of ozone for three flow rates: 5, 10, and 20 $Lmin^{-1}$ (Figure **9**). The behavior of SOA yield as a function of O_3 appears to be similar for flow rates of 5 and 10 $Lmin^{-1}$. The SOA yield for the 20 $Lmin^{-1}$ flow rate appears to be less than the other two, but not enough data could be obtained at higher ozone values to see if the aerosol yield leveled off at higher ozone values as it did for the slower flow rates. That the SOA yields at the 5 $Lmin^{-1}$ and 10 $Lmin^{-1}$ flow rates were similar indicates that the PAM chamber could be smaller than its present size and still achieve maximum SOA yields.

3.2.3 SOA yield as a function of OH

In the sunlit atmosphere, the reaction of OH with α-pinene is more important than the reaction of O_3 with α-pinene. This reaction is as well studied as the O_3 and α-pinene reaction is. In the PAM chamber, the SOA yield in UV irradiated chamber was about 5 times that in the dark chamber at same relative humidity and temperature (Figure **10**). This additional SOA yield likely comes from the reaction of OH with α-pinene. The rate coefficients of α-pinene with OH and with O_3 are 5.5×10^{-11}molecule^{-1}cm^{3}s^{-1} and 8.2×10^{-17}molecule^{-1}cm^{3}s^{-1} from 288K to 295K (NIST chemical kinetics database, 2000). Since 5 ppmv of O_3 and 300 pptv of OH were produced when the relative humidity was 30% and one UV light was on, the value of $k_{OH}[OH]$ was about 20 times greater than $k_{O3}[O_3]$. Thus, the photo-oxidation by OH was the most important reaction in the humid, UV-irradiated chamber. The oxidation pathways opened up by reactions with OH produce additional low volatility products for the particle phase (Kamens and Jaoui, 2001). The increased SOA yield in the PAM chamber when abundant OH is present is consistent with these additional pathways.

The OH mixing ratio was changed by varying the relative humidity while holding O_3 (5 ppmv) and UV light constant (Figure **11**). As OH increased, SOA yield increased but eventually leveled off for [OH] greater than 300 pptv. Thus, in this PAM chamber, 300 pptv of [OH] was sufficient to produce the maximum SOA yield for α-pinene.

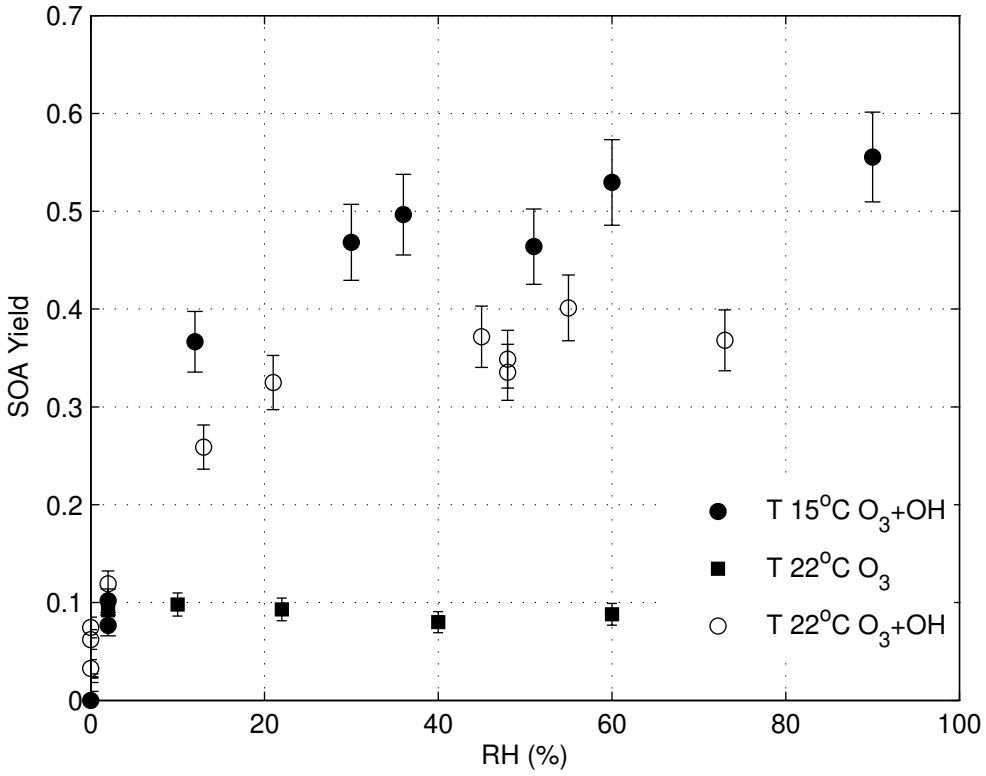

Figure **10**: SOA yield as a function of relative humidity in the UV-irradiated chamber with T=15°C (filled circles) and T=22°C (open circles) and in the dark chamber (filled squares). Ozone was constant at 5ppmv and α-pinene was initially 100ppbv. Error bars show the precision (1σ) for SOA yields.

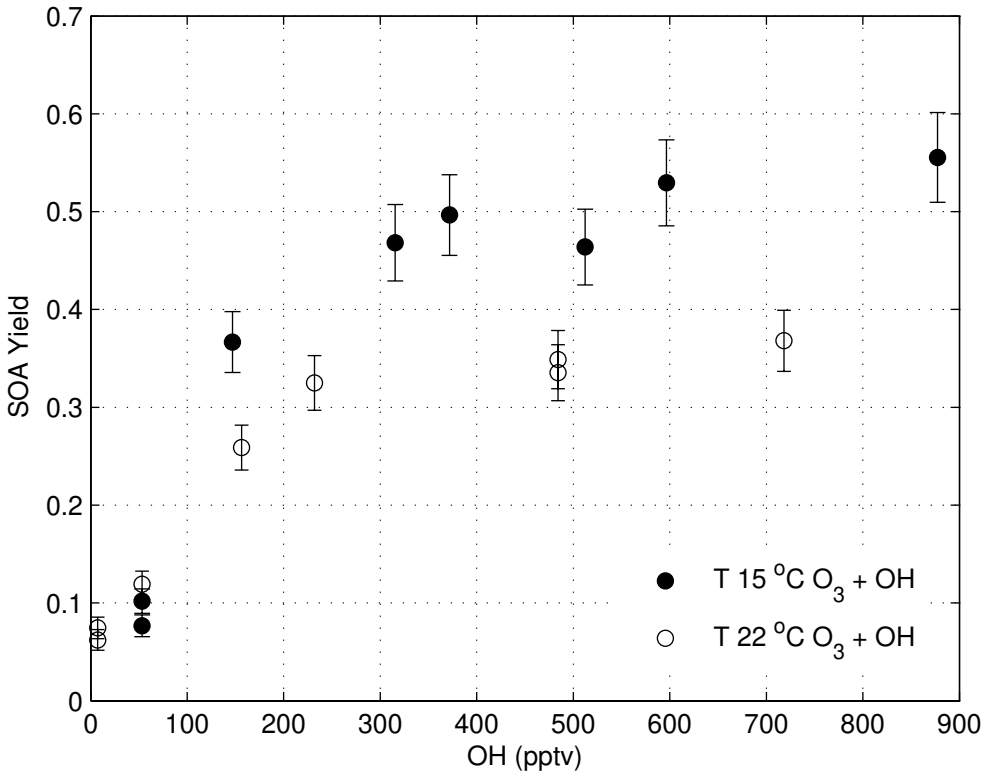

Figure **11**: SOA yield as a function of OH for T=15°C (open circles) and T=22°C (filled circles) in the UV-irradiated chamber for photo oxidation by OH and O_3. Ozone mixing ratio was constant at 5 ppmv; initial α-pinene mixing ratio was 100 ppbv. Error bars show the precision (1σ) for SOA yields.

3.2.4 SOA yield as a function of temperature and humidity

Temperature and humidity both affect aerosol mass yield (see for example Seinfeld and Pankow, 2003). Because most atmospheric organic aerosol particle constituents are semi-volatile, they partition between the gas phase and the particle phase. This partitioning is temperature dependent. The humidity can have two effects: adding mass by adding water to the SOA, or providing a liquid in which volatility-reducing

reactions can occur. Studying these effects is important for determining a definition for potential aerosol mass.

The effect of temperature on the SOA yield from α-pinene was tested by measuring the SOA yield with two different temperatures in the chamber, 22°C and 15°C. [O_3] was held constant at 5 ppmv while [OH] was varied by changing relative humidity. At low relative humidity (Figure **10**) and [OH] (Figure **11**), the SOA yields at 15°C and 22°C are comparable. However, the maximum stable SOA yield for 15°C is a factor of 1.4 greater than that at 22°C. The increased SOA yield at the lower temperature is consistent with the decrease in the partitioning of α-pinene products in the particle phase with increasing temperature (Pankow et.al., 2001). This temperature dependence applies to other organics as well. Therefore the definition of PAM may require that the measurement be made at a standard temperature or be made at several temperatures over a range of temperatures.

The effect of relative humidity on SOA yield was tested using oxidation primarily by ozone (Figure **10**). The relative humidity was varied from 2 to 60% in purified air, to which ozone and α-pinene were added before the air flowed into and through the dark chamber. In this case, the SOA yield did not change as relative humidity was increased, indicating that the relative humidity itself is not an important factor to change SOA yield for α-pinene ozonolysis. This result is consistent with a previous study of α-pinene ozonolysis, in which increasing the relative humidity from 0 to 40% increased the SOA mass only 10%, including the water mass in the aerosol particles (Cocker III et al., 2001).

3.2.5 SOA yield as a function of UV radiation

Extremely high UV actinic flux could possibly alter the SOA yields (Kamens and Jaoui, 2001; Presto et al., 2005). UV light can cause photo-reactions to occur on the SOA surface, producing species that have higher volatility and go into the gas phase. A test for this possibility with PAM is the comparison of the SOA yields that comes from adding ozone in the dark chamber to that from making the same amount of ozone in the chamber with UV radiation. The aerosol yield is compared for four cases: dark, dry chamber (externally generated ozone added to dry air (RH < 1%) in a dark chamber); UV-irradiated dry chamber (ozone generated by UV radiation in the chamber in dry air (RH < 1%), in order to minimize OH and HO_2 production); dark, humid chamber (with externally generated ozone added to air with RH=12% in a dark chamber); and UV-irradiated humid chamber (with ozone generated by UV radiation in the chamber in air with RH=12%). In all cases but the last case, [OH] was less than 15 pptv, about 10^{-6} times less than $[O_3]$, so that O_3 reactions with α-pinene dominate. In the case of the UV-irradiated humid chamber, the OH/O_3 ratio was at least 9×10^{-6} when $[O_3]$ was 15 ppmv and [OH] was 150 pptv; the OH reactions with α-pinene were much more significant.

The SOA yield for the dark, dry chamber and UV-irradiated, dry chamber are the same to within uncertainties for as much as 6 ppmv of ozone (Figure **12**). The external ozone generator could not produce more than 6 ppmv of ozone, so that above 6 ppmv, only yields from the UV irradiated chamber cases are shown. The yield for the case of the dark, humid chamber was slightly less than for the dry chamber cases. This effect needs further investigation. On the other hand, the yield for the case of the UV-irradiated humid

chamber is significantly greater than all the other cases, indicating the importance of OH in oxidizing α-pinene to SOA.

This agreement between the SOA yield in the dark, dry chamber and in the UV-irradiated dry chamber is inconsistent with the observations of Presto et al. (2005). They observed a 20-40% reduction in SOA yield between the case in which the chamber was UV-irradiated and the case in which ozone was added to a dark chamber. In both cases, they used cleaned air with RH < 10% and added up to 600 ppbv of ozone into the chamber. In order to remove OH in the chamber, they added 2-butanol and calculated that as much as 90% of the OH was removed.

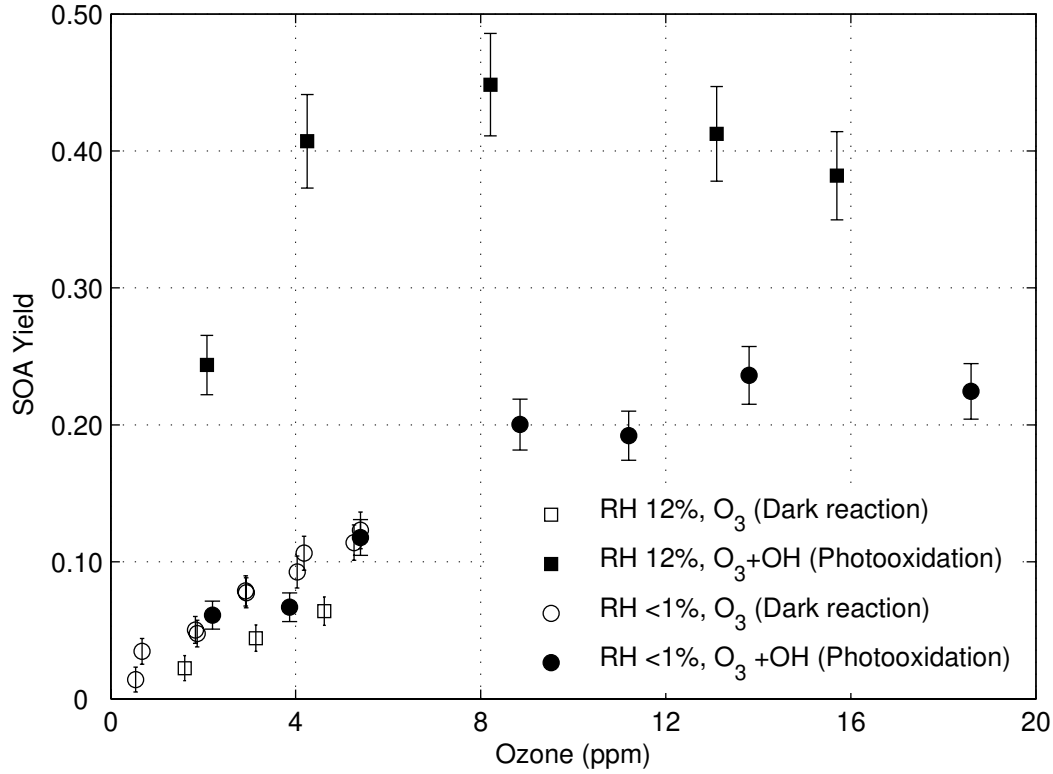

Figure **12**: SOA yield as a function of ozone for four chamber conditions: dark, humid chamber (open squares); and UV-irradiated humid chamber (filled squares), dark, dry chamber (open circles); UV-irradiated, dry chamber (filled circles). Initial α-pinene was 100ppbv. Error bars show the precision (1σ) for SOA yields.

The difference between the two observations could be explained by the 10 to 15 pptv of [OH] in the UV-irradiated, dry PAM chamber. This amount of OH was produced from the photolysis of a trace amount of H_2O that was in the dry air that entered the PAM chamber. This amount of OH will react with α-pinene about as fast as 6 ppmv of $[O_3]$. It is possible that a loss of SOA caused by UV radiation is balanced by an increase in SOA yield from this OH produced by UV in the chamber. This balance seems unlikely but will need to be tested by varying the humidity and thus OH for a fixed UV flux, to fix OH by

varying humidity and UV simultaneously and by adding a window in front of the UV lamps to block the OH-producing 185 nm radiation while passing the 254 nm radiation into the PAM chamber.

Ths difference between our result and that of Presto et al., (2005a) may also be due to the difference between our UV lamps, which have strong emissions at 185 nm and 254 nm, and their black lights, which have a broad spectral emission between 350 nm and 400 nm and no emissions at 185 nm and 254 nm. While it might be thought that the more energetic emissions at 185 nm and 254 nm would be more effective than the 350-400 nm emissions from the black light, we do not know the absorption cross sections for the photo-reactions that would reduce the SOA yield.

3.2.6 SOA yield as a function of acidic seed aerosol particles

Acidic seed aerosol particles have been shown to increase the aerosol yield under some circumstances (Jang et al., 2002; Northcross and Jang, 2006). Acid catalyzed reactions in the particle can result in lower-volatility products, thus shifting the partitioning of the reacting semi-volatile organic species toward the particle phase. The effect of acidic seed was tested with the addition of sulfate aerosol in a humid UV-irradiated chamber. SO_2 was added to the chamber; the acidic seed aerosol particles were formed by photo-oxidation of SO_2 initiated by reaction with OH. Once the measured sulfate aerosol mass was stabilized, α-pinene was added to the chamber. The SOA that resulted from the oxidation of the α-pinene by OH and O_3 was determined by subtracting

the aerosol mass obtained with just SO_2 added to the chamber from the aerosol mass obtained with both α-pinene and SO_2 in the chamber.

For all values of α-pinene from 50 ppbv to 270 ppbv, the SOA yield was up by a factor of 1.4 higher in the presence of the acidic seed aerosol than it is in the no-seed added experiments (Figure **13**). For this study, 5 ppbv of [SO_2] was added, producing 20 μgm^{-3} of acidic seed. This increase of yield is qualitatively consistent with the results of Northcross and Jang (2006), who observed a 60-70% increase in SOA yield for acidic seed condition compare to neutral seed condition from the α-pinene ozonolysis. Their conditions were quite different from ours; in the PAM chamber, both OH and O_3 oxidized α-pinene, while their chamber was dark and ozone was the only oxidant. It has been suggested that yield increases with the presence of the acidic seed aerosol because the acidic surface on the inorganic seed catalyzes the heterogeneous reaction of organic carbonyl species to increase SOA mass (Jang et al., 2002). The qualitative agreement between these two results suggests that the low-volatility products from both OH and O_3 reactions might interact with the acidic seed in similar ways to increase SOA yield.

As little as 15 μgm^{-3} of sulfate aerosol was able to increase the yield of 100 ppbv of α-pinene (Figure **14**). It is not possible for us to know the SOA yield in the presence of no acidic seed aerosol, since chambers exposed to SO_2 will from then on always generate a few acidic aerosol particles. Therefore, no seed in Figure **13** actually means that SO_2 is not added and the measured sulfate aerosol is less than 5 μgm^{-3} for 10 min average, the precision of TEOM. In the no seed case, the α-pinene SOA yield was about 60% of that observed with added SO_2. To within experimental uncertainty, the SOA yield

is independent of the acidic aerosol seed mass greater than 15 μgm^{-3}. The effect of acidic seed is also independent to within experimental uncertainty of three different O_3 values and two different relative humidity levels. These experiments suggest that the acidic seed effect is independent of both the OH and O_3 mixing ratios.

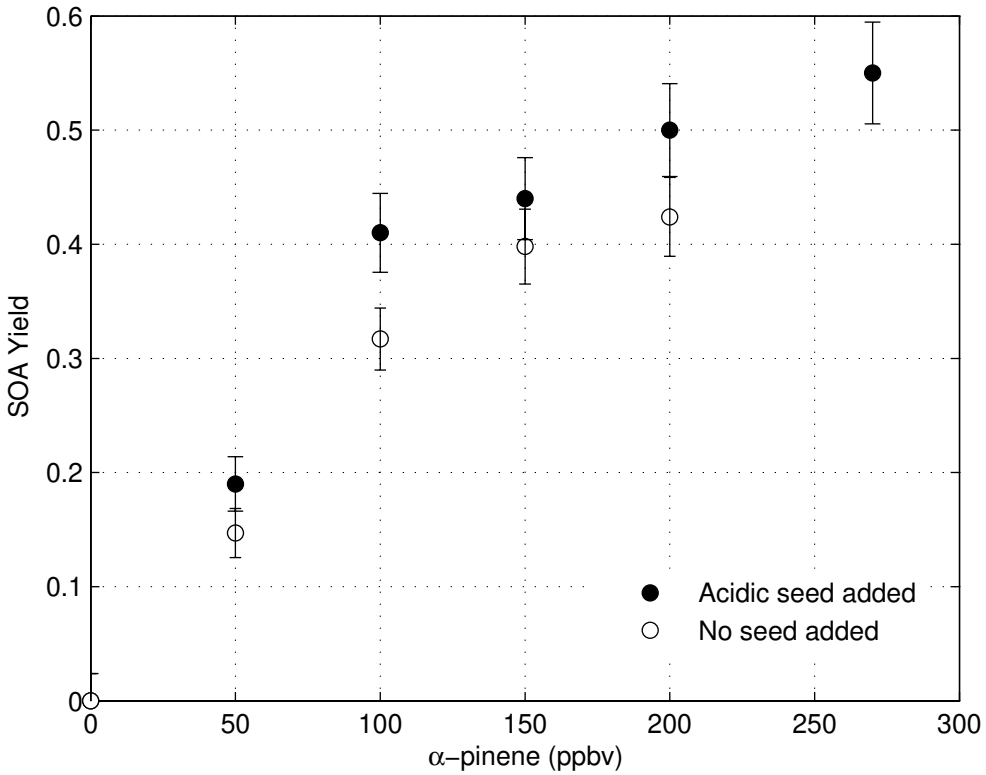

Figure **13**: Acidic seed effect on SOA yield for various α-pinene concentrations. Sulfate aerosol, roughly 50$\mu g\ m^{-3}$, from the oxidation of 10ppbv SO_2 is used as acidic seed. Error bars show the precision (1σ) for SOA yields.

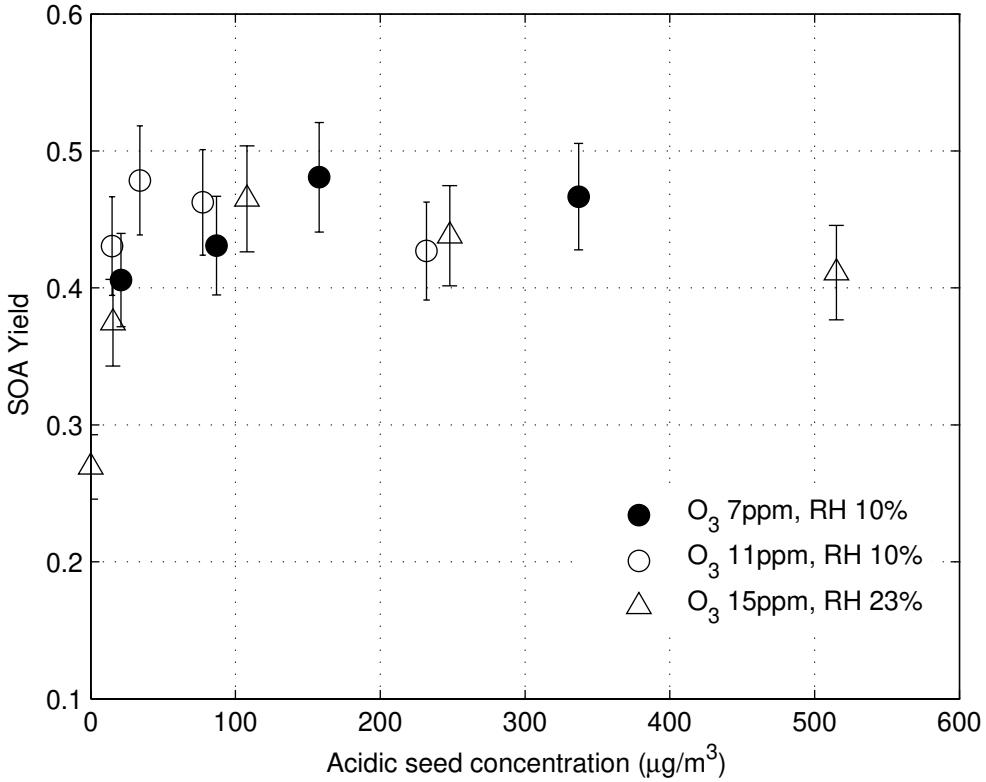

Figure **14**: Acidic seed effect on SOA yield for 100 ppbv of α-pinene for photo-oxidation of 100 ppbv of α-pinene by different amounts of O_3 and OH. SO_2 is added and the resulting sulfate aerosol was used as acidic seed. Note that the SOA yield at zero acidic seed is half all other values. Error bars show the precision (1σ) for SOA yields.

3.3 Results from a preliminary field study

A first field test of PAM was conducted in September, 2006. The PAM instrument was installed in the Nittany Atmospheric Trailer and Integrated Validation Experiment (NATIVE) trailer at the Pennsylvania State University campus at University Park, Pennsylvania. In the NATIVE trailer are measurements of SO_2, NO, NO_y, CO, O_3, UV radiation, relative humidity, temperature, pressure, and wind speed and direction. The

PAM chamber was placed inside of the trailer and the inlet was located 1.8 m above the trailer roof. The gas sampling inlet was at the same height as the PAM chamber sampling inlet. It is possible to sample either ambient air containing aerosol particles or air run through a HEPA aerosol particle filter. By turning the UV light in the chamber on and then off periodically for both ambient air and particle-filtered air, the aerosol mass, potential aerosol mass, and sum of the two can all be measured by the PAM chamber and the TEOM instrument. However, for this preliminary study, only particle-filtered air was sampled to see secondary aerosol formation clearly. The chamber was operated with a flow rate through the chamber of 10 $Lmin^{-1}$ and only one UV light, which produced 4 ppmv of [O_3] and about 400 pptv of [OH], with an ambient relative humidity of 38%. These conditions are more than sufficient to oxidize all of the hydrocarbons in the laboratory experiments, and were in fact chosen because they do optimize the yields for all hydrocarbons tested. But the test of SO_2 consumption with UV light shows that only 50% of the SO_2 was oxidized.

Examples of the PAM measurements come from two days, 6 September and 7 September (Figure **15**). The formation of secondary aerosol is shown in the shaded periods when the chamber was irradiated with UV. Increases in measured aerosol mass occur every time the chamber is irradiated with UV light. Typically the increase was 5-10 μgm^{-3}. This potential aerosol mass appears to come from sources other than either SO_2 or NO_y. Unfortunately for this preliminary study, no hydrocarbon measurements were made and the origins of the potential aerosol mass could not be ascertained.

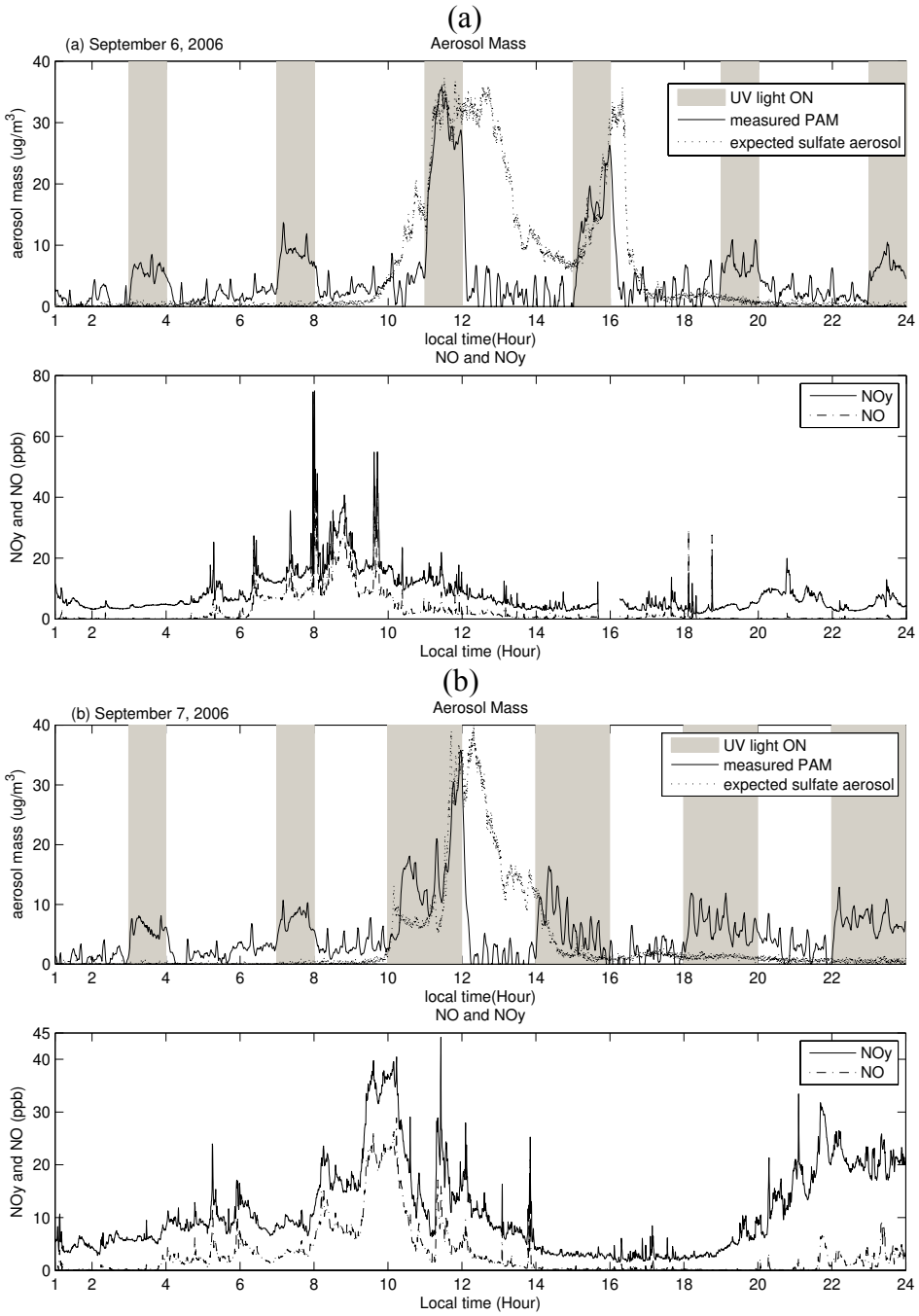

Figure **15**: PAM measurements in ambient aerosol-free air on September 6, 2006 (a) and on September 7, 2006 (b). For the two days the relative humidity was 38±3% and the temperature was 31±1°C in the chamber. The UV-irradiated chamber (gray bar) had 4 ppmv of [O_3] and ~400 pptv of [OH]. Calculated sulfate aerosol (dashed line) was obtained with the measured SO_2 multiplied by the SO_2 consumption ratio 0.5 and the calculated conversion factor 4.67μgm^{-3} (ppbv SO_2)$^{-1}$. Measured PAM (solid line) was the measured aerosol mass by TEOM. NO_y, NO and SO_2 were measured by NATIVE.

In some cases, a SO_2 plume was sampled. SO_2 tended to increase after 10 am and decrease before sunset. This behavior can be explained by considering the effects of meteorology and long-range transport of SO_2 from the power plants to the west and southwest of central Pennsylvania. During the night, the SO_2 is released in plumes that are transported above the nocturnal boundary layer. SO_2 in the nocturnal layer is lost to the surface. In the morning, convection causes the boundary layer to rise, mixing the air from above down to the surface. This process brings the air with enhanced SO_2 to down to the ground. In the evening, convection ceases and the boundary layer height decreases and the transported SO_2 stays at above the developing nocturnal boundary layer. This explanation is consistent with the behavior of SO_2 seen in Figure **15**.

The measured SO_2 mixing ratio can be converted into an expected sulfate aerosol mass by accounting for the partial 50% conversion of SO_2 to sulfate and using the calculated conversion ratio of 4.67 $\mu gm^{-3}(ppbv\ SO_2)^{-1}$, which is appropriate for the 30% relative humidity at the TEOM mass transducer. For 6 September, the measured and calculated potential aerosol mass agreed to well within experimental uncertainties, indicating that in these air samples, the potential aerosol mass consisted only of SO_2. However, on 7 September, the potential aerosol mass measurement was 5-10 μgm^{-3} greater than expected from SO_2, indicating that the air masses containing SO_2 on 7 September also contained other aerosol-forming gases. A comparison between the potential aerosol mass and NO_y suggests that the additional potential aerosol mass was not due to NO_y.

These results from this preliminary field test show the feasibility of the PAM concept for ambient air. The PAM chamber conditions, while sufficient for this

preliminary study, were not optimized. The many experiments that have been conducted since September 2006 provide insight into the PAM chamber operating conditions and protocols that will give much better and much more information that was obtained then.

Chapter 4

SOA yields for biogenic and anthropogenic hydrocarbons

A powerful test of the PAM concept is the comparison of hydrocarbon SOA yields obtained in the PAM chamber with those obtained in large environmental chambers. Similar yields for a number of hydrocarbons under similar conditions provide strong evidence that the aerosol masses obtained from the PAM chamber are the same as those obtained in large environmental chambers. If the large environmental chambers are reasonable simulations of the atmosphere, similar yields also suggest that the PAM measurements represent the potential aerosol mass in the atmosphere.

4.1 SOA yields for individual biogenic and anthropogenic hydrocarbons

The SOA yields were measured for three monoterpenes and six anthropogenic hydrocarbons that are commonly found in the lower atmosphere. The three monoterpenes were α-pinene, β-pinene, and Δ^3-carene; the six anthropogenic hydrocarbons were cyclohexene, m-xylene, p-xylene, 1,3,5-trimethylbenzne (1,3,5-TMB), toluene, and ethylbenzene. All experiments except some runs for α-pinene were performed at a constant temperature (297±1K), with UV irradiation, in purified air without added acidic seed. NO_x was added for some experiments to test for a NO_x effect. In all experiments, $[O_3]$ was greater than 10 ppmv and [OH] was greater than 300 pptv. Under these conditions, the hydrocarbons were reacted away; the remaining

hydrocarbons were measured to be less than the GC-FID detection limit. The complete list of experiments and the comparisons with previous studies is presented in Table **2**. The SOA yields of nine hydrocarbons are compared to those from larger environmental chamber studies that had similar initial precursor gas mixing ratios and chamber conditions.

The PAM yields are similar to the yields from previous studies for α-pinene, cyclohexene, m-xylene, p-xylene, 1,3,5-TMB, and toluene. If anything, the SOA yields in the PAM chamber are at the high end of the previously reported SOA yields. Two PAM yields - β-pinene and ethylbenzene – are significantly higher than from previous studies; one PAM yield for Δ^3-carene, is significantly lower. These differences will be discussed in more detail below.

For all hydrocarbons, we were unable to match exactly the experimental conditions such as temperature, relative humidity, NO_x mixing ratios, total organic aerosol mass (M_o), and types and amounts of oxidants that were used in the large environmental chamber studies. The values are similar, especially for precursor organic mixing ratios, but not exactly the same. However, despite these differences, the similarity of the PAM and previous yields provides evidence that the rapid oxidation in the PAM chamber simulates SOA formation in the large environmental chambers.

The NO_x in the PAM chamber is generally much lower than in the previous large environmental chamber studies. Background NO_x in the PAM chamber was ~ 3 ppbv and added NO_x in some runs was never more than 150 ppbv. The ratio of $[VOC]_0/[NO_x]_0$ (ppbC/ppb) in the chamber was always higher than 15 for both of background NO_x condition and added NO_x conditions. The low NO_x condition refers to $[VOC]_0/[NO_x]_0$

(ppbC/ppb) > 15; the high NO_x condition refers to $[VOC]_0/[NOx]_0$ (ppbC/ppb) < 15 (Presto et al., 2005; Song et al., 2005). Compared to the previous studies in other chambers, our PAM chamber was operated essentially in the low NO_x condition for all experiments.

Table **2**: SOA formation from photo oxidation

VOC	Temp (K)	RH (%)	ΔHC (ppb)	NOx (ppb)	HC/NOx (ppbC/ppb)	SOA Yield in PAM	Reference Yield
α-Pinene	298	<2	100 ± 12	N/M	N/M[1]	0.20 ± 0.03[2]	0.23[3] (O, 91,Presto et al., 2005)[4]
($C_{10}H_{12}$)	298	14-24	100 ± 12	N/M	N/M	0.40 ± 0.10	0.32 (P, 109, Lee et al. 2006)
β-Pinene	298	42	156 ± 19	<3	>500	0.49 ± 0.06	0.27 (P, 97, Griffin et al., 1999)
($C_{10}H_{12}$)	298	42	156 ± 19	43	36	0.48 ± 0.06	0.31 (P, 170, Lee et al., 2006)
							0.32 (P, 170, Varutbangkul et al. 2006)
Δ [3]-Carene	297	48	161 ± 18	<3	>500	0.07 ± 0.01	0.18 (P, 105, Griffin et al., 1999)
($C_{10}H_{16}$)	297	48	161 ± 18	89	18	0.13 ± 0.02	0.38 (P, 109, Lee et al., 2006)
Cyclohexene	298	40	266 ± 18	N/M	N/M	0.19 ± 0.01	0.12 (O, 151, Varutbangkul et al. 2006)
(C_6H_{10})							0.14 (O, 240, Keywood et al. 2004)
m-Xylene	298	55	324 ± 28	<3	>500	0.10 ± 0.01	0.13 (P, 322, Cocker III et al 2001)
(C_8H_{10})							0.06 (P, 355, Odum et al, 1997)
							0.08 (P,311, Song et al. 2005)
							0.39[5] (P, 60, Ng et al., 2007)
p-Xylene	297	40	170 ± 11	<3	>500	0.05 ± 0.01	0.03 (P, 199, Odum et al, 1997)
(C_8H_{10})	297	40	170 ± 11	107	13	0.07 ± 0.01	
1,3,5-TMB	298	< 2	682 ± 31	<3	>500	0.06 ± 0.01	0.07 (P, 543, Cocker III et al 2001)
(C_9H_{12})	298	55	556 ± 31	<3	>500	0.09 ± 0.01	0.03 (P, 210, Odum et al, 1997)
	298	40	394 ± 31	46	77	0.11 ± 0.01	
Toluene	297	30	231 ±61	<3	>500	0.09 ± 0.02	0.13 (P, 240, Takekawa et al., 2003)
(C_7H_8)	297	30	231 ± 61	51	32	0.12 ± 0.03	0.07 (P,245, Odum et al, 1997)
							0.30[6] (P, 64, Ng et al., 2007)
Ethylbenzene	297	35	197 ± 15	<3	>500	0.33 ± 0.02	0.09 (P, 230,Odum et al, 1997)
(C_8H_{10})	297	32	197 ± 15	130	12	0.35 ± 0.02	

Previous studies in large environmental chambers have examined the differences in SOA yields under high-NO_x and low-NO_x conditions. In most cases, the high NO_x condition reduced SOA yield for both biogenic hydrocarbons and anthropogenic hydrocarbons, whereas the SOA yield in low NO_x condition was the same regardless of the amount of NO_x (Song et al, 2005; Presto et al., 2005). For instance, α-pinene ozonolysis showed that the SOA yield was constant for $[VOC]_0/[NO_x]_0$ (ppbC/ppb) > 15 and decreased as $[VOC]_0/[NO_x]_0$ decreased (Presto et al., 2005). They suggested that as the $[VOC]_0/[NOx]_0$ ratio decreases, the volatile product formation increases, thereby reducing aerosol yield. For $[VOC]_0/[NOx]_0$ ratios between 3 and 10, they suggest that a greater amount of nitrate radical (NO_3) is available to react with α-pinene and that the product of α-pinene and NO_3 does not contribute aerosol phase.

Our results appear to be inconsistent with recent experiments that used neutral seed particles in the low NO_x condition (Ng et al., 2007). Ng et al. (2007) observed maximum SOA yield 0.39 and 0.30 for m-xylene and toluene respectively. These values contrast with our studies, in which the stable SOA yield is about 0.10 for both m-xylene and toluene. Part of this difference might be explained by the aerosol seed that was used in the Ng et al. (2007) experiments but not in ours.

The SOA yield was measured many times for 100 ppbv of α-pinene over the course of two years. The standard deviation of all these measurements is large, about 25% of the mean value of 0.40. During the two years, many changes were made to the PAM chamber and experimental method as we were learning and the PAM concept was being optimized. Thus, this variability should not be too surprising. None-the-less, the SOA yield for α-pinene from the PAM chamber agrees with those from other chambers.

The SOA yield for β-pinene is 0.48 in the PAM chamber. This yield is greater than the SOA yields of 0.27-0.32 found in the large environmental chambers. This difference cannot be attributed to a difference in the initial β-pinene mixing ratios for Lee et al. (2006) or Verutbangkul et al. (2006); the initial β-pinene was 156 ppbv in the PAM chamber and 170 ppbv for the others. The greater SOA yield from β-pinene measured in the PAM chamber may be due to its low-NO_x condition (Ng et al., 2006) or to some undetermined difference in environmental conditions (Lee et al., 2006; Griffin et al. 1999).

The SOA yields from α-pinene and β-pinene in the PAM chamber appear to be different. However, the SOA yield can be sensitive to the organic aerosol mass, M_o. When the SOA yield for 156 ppbv of β-pinene is compared to the SOA yield for 150 ppbv of α-pinene (Figure **16**), the two yields are the same, 0.49. This result appears to be consistent with that of Lee et al. (2006).

The SOA yield from ethylbenzene in the PAM chamber, which was 0.34, is significantly greater than the SOA yield reported in Odum et al. (1997), which was 0.09. The large environmental chamber used in the work of Odum et al. (1997) was operated at a temperature of ~ 34^{o}C. This temperature is 10^{o}C higher than the temperature in the PAM chamber. Our study of temperature effects show up to a 40% decrease in SOA yield for a 7^{o}C of temperature increase for α-pinene (Figure **11**). Theoretically, SOA yield should decrease at higher temperatures because the partitioning of the semi-volatile organic product shifts toward the gas-phase as the saturation vapor pressure of semi-volatile product increases with temperature (Pankow et al., 2001). Thus, the temperature difference may partially explain the higher SOA yield from ethylbenzene in our PAM

chamber experiments, although a series of experiments in the PAM chamber at different temperatures are required to quantify this temperature effect.

The SOA yield of 0.07 from Δ^3-carene with NO_x at chamber background levels was lower than the low end of yields from previous studies, 0.18 (Griffin et al., 1999; Lee et al., 2006). Lee et al. (2006) observed higher SOA yield for ozonolysis than photo-oxidation for Δ^3-carene. They observed a low caronaldehyde yield and a high SOA yield from ozonolysis, and a higher caronaldehyde yields and a lower SOA yield from the photo-oxidation. The major difference between ozonolysis and photo-oxidation is the presence of OH radical. If the OH or HO_2 radical are responsible for the reduction in SOA yield of Δ^3-carene by the formation of aldehydes, then the lower SOA yield in the PAM chamber may be due to higher OH/O_3 and HO_2/O_3 ratios in the PAM chamber experiments compared to the large environmental chamber experiments of Lee et al. (2006).

Another test of the feasibility of the PAM concept was to measure the potential aerosol mass of hydrocarbons that were added in known amounts to room air in the PAM chamber. If the SOA yields are additive, then the SOA yield calculated for the added hydrocarbon should equal the yield obtained by the addition of the same amount of hydrocarbon in purified air. Room air was obtained from the pressurized room air passing through air compressor and the coarse particle filter. The relative humidity in the chamber was 10-14% due to the high pressure in the air compressor, and the NO_x concentration varied day-to-day from 5 ppbv to 25 ppbv. All experiments were conducted in the low NO_x condition ($[VOC]_0/[NO_x]_0$ (ppbC/ppb) > 15).

The SOA yields in room air and purified air were similar for some hydrocarbons and different for others. The SOA yield of Δ^3-carene in room air was 0.26, which was 2 times greater than SOA yield 0.13 in purified clean air. The SOA yield of 1,3,5-TMB in room air was 0.19, which was also 1.7 times greater than SOA yield 0.11 in purified clean air. SOA yields of m-xylene and p-xylene in room air were 0.16 and 0.11, which were 1.6 times higher than SOA yields in purified air, 0.10 and 0.07, respectively. For other hydrocarbons, SOA yield in room air was similar to or only slightly higher than the SOA yield in purified clean air. For example, SOA yield of β-pinene in room air was 0.50, which was close to SOA yield in purified air, 0.48. SOA yields of cyclohexene and toluene in room air was 0.19 and 0.13, and their SOA yields in purified air were 0.20 and 0.12 respectively. The total potential aerosol mass from room air without the added hydrocarbons did not exceed 10 μgm^{-3}, a value much smaller than typically observed from the added hydrocarbons.

A significant difference between room air and purified clean air could be the presence of other precursor gases in room air that form seed aerosols. Different hydrocarbons were studied on different days. If the amount of gases that form seed aerosols were different from day-to-day, those differences could explain these results.

4.2 SOA yields from a hydrocarbon mixture of α-pinene, m-xylene, and p-xylene

A recent study suggests that the large number of co-condensing semi-volatile gases results in the formation of aerosol mass much greater than the expected sum of the yields of individual hydrocarbons (Volkamer et al. 2006). If this enhancement is due to

an increase in SOA yields in any common mixture of atmospheric hydrocarbons, then it would be possible to test this enhancement with experiments in the PAM chamber. For this experiment, the SOA yield of a hydrocarbon mixture of α-pinene, m-xylene, and p-xylene in a 1.00:1.25:1.25 ratio was measured and compared with the sum of the individual SOA yields.

To calculate the sum of the yields of the individual hydrocarbons, the yield of each individual hydrocarbon was measured as a function of total organic aerosol mass, M_o, for the individual hydrocarbon (Eq. **1**):

$$\Delta HC_i \times Y_i(M_O) = M_i$$
$$\sum M_i = M_O \qquad \textbf{1}$$

where ΔHC_i is consumed precursor hydrocarbon amount; Y_i is the SOA yield of each hydrocarbon; M_o is the measured SOA mass from the hydrocarbon mixture.

We assume that the yield of any individual hydrocarbon depends on the total organic aerosol mass, M_o, regardless of the origin of organic aerosol. This assumption is based on the argument of Seinfeld and Pankow (2003), that the SOA yields is only dependent on the organic mass concentration, and organic aerosols do not interact with each other in a mixture. Thus, to get the estimated SOA mass of individual hydrocarbon species (M_i), the SOA yield value of each hydrocarbon corresponding to the total SOA mass in the mixture, $Y_i(M_o)$, was obtained from the individual yield curve in the Figure **16**, and multiplied by the reacted hydrocarbon concentration (ΔHC_i). The calculated mass, M_i, for all three hydrocarbons were then summed up to give the expected SOA mass, ΣM_i, which could then be compared with M_o, the total SOA mass measured in the mixture (Eq. **1**).

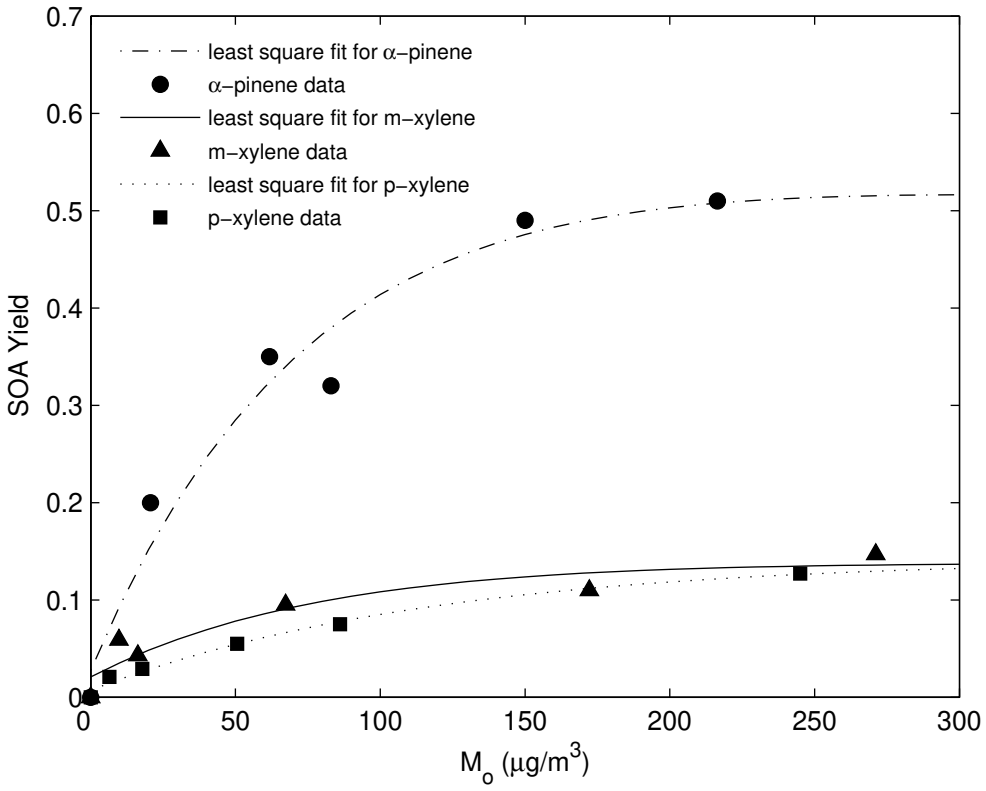

Figure **16**: SOA Yield curve for α-Pinene, m-Xylene, and p-Xylene at 20% RH and greater than 10 ppmv of ozone and 300 pptv of OH. The least-squares fitted lines are used to determine the yield of individual hydrocarbon in a mixture.

Four different hydrocarbon mixing ratios were used, although the mixture of the three hydrocarbons was constant (Table **3**). In all four experiments, M_o was similar to $\sum M_i$ within a factor of 1.3 or better. Thus, this mixture does not exhibit an enhancement in the SOA over what is expected from the individual hydrocarbon.

Table **3**: A photo oxidation experiment for a hydrocarbon mixture with α-pinene, m-xylene and p-xylene

No.	α-pinene			m-xylene			p-xylene			ΔMo (μg/m³)	∑M$_i$ (μg/m³)
	ΔHC (ppb)	Y	M$_i$ (μg/m³)	ΔHC (ppb)	Y	M$_i$ (μg/m³)	ΔHC (ppb)	Y	M$_i$ (μg/m³)		
1	10	0.16	8.90	13	0.05	2.79	13	0.02	1.29	10.0	13.0
2	26	0.34	48.1	33	0.09	12.3	33	0.07	9.60	70	69.9
3	33	0.44	78.4	41	0.11	20.4	41	0.09	16.6	117	115
4	66	0.51	165	75	0.13	42.0	76	0.12	38.7	200	246

This conclusion is the same as reported by Odum et al. (1997). They observed good agreement of M_o and $\sum M_i$ for anthropogenic mixture containing toluene, m-xylene, m-ethyltoluene, n-propylbenzene, 1,2,4-trimethylbenzene. Their experiments were performed in large environmental chamber using sunlight. Typical sunlight can produce up to 100 ppbv of O_3, 0.2 pptv of OH, and 20 pptv of HO_2 daytime in urban area (Ren et al., 2006). Our PAM chamber is operated in highly oxidizing condition with more than 10 ppmv of O_3, 300 pptv of OH, and 3 ppbv of HO_2. While the oxidant mixing ratios were 100 times larger than in either the large environmental chamber or the atmosphere, the ratios of the oxidants were similar. Thus, the result obtained in the PAM chamber likely applies to the atmosphere.

This agreement also supports that the assumption based on the argument of Seinfeld and Pankow (2003) is valid. However, the greater SOA yield observed when acidic inorganic seed was present in a smog chamber indicates that the organics are interacting with the inorganic acid to increase the SOA yield (Jang et al., 2002). More

mixtures that include both inorganic and organic precursor gases will need to be tested in the PAM chamber to examine this synergistic effect on SOA yield.

This agreement is, however, inconsistent with Robinson et al. (2007). They tested diluted diesel exhaust and observed higher SOA mass than expected from a model that used known SOA yields from VOCs. They suggest that many IVOC (Intermediate Volatility Organic Carbons) were in the diesel exhaust, resulting in the higher SOA mass than expected. It may be that some simple mixtures, such as the ones used by Odum et al. (1997), and us, contain fewer and less IVOCs.

The comparison of $\sum M_i$ to M_o suggests that simultaneous measurements of PAM and all known volatile organic compounds can be used to test for unmeasured VOCs that can be oxidized to form SOA in the atmosphere during field studies. $\sum M_i$ might be less than M_o for four possible reasons: unmeasured SOA-precursor VOCs; errors in the measurements of SOA-precursor VOCs; SOA yield values that are either incorrect or not applicable to the atmospheric environment; and synergetic enhancement of SOA by co-condensing gases, such as the SOA yield increase on acidic seed aerosol. Examining these issues will require the simultaneous deployment of the PAM chamber, aerosol mass and chemical measurements, and measurement of all known precursor inorganic and organic atmospheric constituents in a field study.

Chapter 5

The formation and aging of SOA in the highly oxidizing environment

As stated in the Introduction, SOA formation is initiated by OH or O_3, but the production of semi-volatile products can require reactions with OH, O_2, HO_2, RO_2 (R = CH_3, $C2H_5$ …), NO, or NO_2. The aging can be defined as the change of aerosol properties by the exposure on oxidant (OH, O_3, UV, and etc) of particle surface (Rudich et al., 2007). The aging process can cause the shift in the gas and particle partitioning equilibrium by the further oxidation of the gaseous product, heterogeneous oxidation of the organic layer in the particle, and the reactions that lead to oligomer formation (Rudich et al., 2007). Therefore, the aging of SOA can result from reactions with OH, O_3, HO_2, RO_2, NO, or NO_2 or by chemical decomposition by ultraviolet light (UV) (Kroll et al., 2006; Surratt et al., 2006). These processes can be examined by monitoring the peak and stable mass from the TEOM, chemical composition from the Quadruple-Aerosol Mass spectrometer (Q-AMS) and the particle number concentrations from the Ultra High Sensitivity Aerosol Spectrometer (UHSAS). Emphasis is given to the dependence of these quantities on the initial amounts of precursor gas mixing ratio and on the amount of OH and HO_2.

5.1. Characteristics of SOA formation and aging

5.1.1 Mass spectra of SOA in the PAM chamber

Mass spectra were measured for SOA formed from the photo-oxidation of α-pinene, m-xylene, p-xylene and a mixture of these three hydrocarbons in the PAM chamber (Figure **17**). The mass spectrum is obtained from the Q-AMS measurement. While the mass spectra consist of fragments of the initial chemicals in the SOA, work by several researchers has found that the mass fragments can be used to identify chemical species of SOA, as listed in Table **3**. The mass fragment *m/z* 43 represents oxidized, carbonyl containing compounds such as aldehydes and ketones (Alfarra et al., 2006; Canagaratna et al., 2007). The mass fragment *m/z* 44 represents CO_2^+ fragment or highly oxidized compounds such as fulvic acid, decarboxylation of oxo- and di-carboxylic acids (Alfarra et al., 2006). The mass fragment *m/z* 18, 28, 45, … and the mass fragment *m/z* 27, 29, 41, 55, 57, 69, 71, …are also identified to oxygenated organics and hydrocarbons, respectively. The mass fragments to represent inorganic like ammonium, nitrate and sulfate are very different from the mass fragments of organics except *m/z* 18 (Table **4**), so they are not examined here. The mass fragments *m/z* 18 can be identified with oxygenated organics or water. The interference of water on the organic signal can be empirically corrected (Alfarra et al., 2006). These other masses are not used in this study.

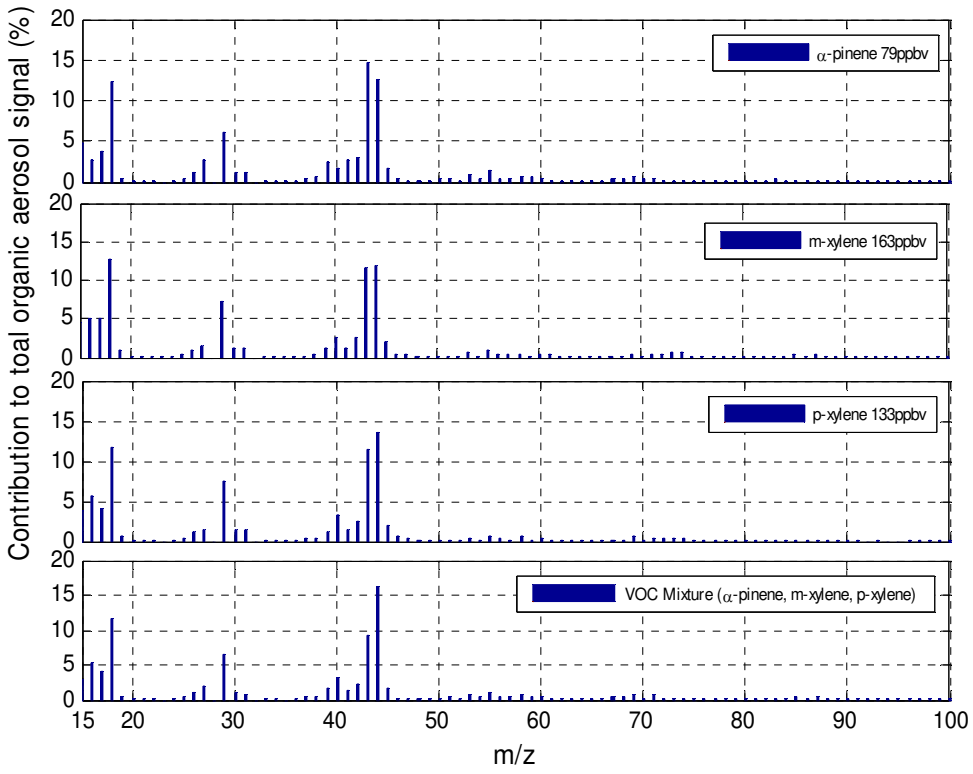

Figure **17**: Mass spectra for the stable SOA mass of α-pinene, m-xylene, p-xylene, and a VOC mixture of 37 ppbv of α-pinene, 46 ppbv of m-xylene, 47 ppbv of p-xylene formed under photooxidation. The contribution to total organic aerosol signal is the percentage of the aerosol mass of each *m/z* divided by the total organic aerosol mass. For all runs, OH is 260 ± 10 pptv.

Table **4**: The list of mass fragments to identify aerosol species in the AMS mass spectrum (Cited from Canagaratna et al., (2007))

Group	**Molecule/Species**	**Ion fragments**	**Mass fragments (*m/z*)**
Water	H_2O	H_2O^+, HO^+, O^+	18, 17, 16
Ammonium	NH_3	NH_3^+, NH_2^+, NH^+	17,16,15
Nitrate	NO_3	HNO_3^+, NO_2^+, NO^+	63,46,30
Sulfate	H_2SO_4	$H_2SO_4^+$, HSO_3^+, SO_3^+, SO_2^+, SO^+	98,81,80,64,48
Organic (Oxygenate)	$C_nH_mO_y$	H_2O^+, CO^+, CO_2^+, $H_3C_2O^+$, HCO_2^+, $C_nH_m^+$	18,28,44,43,45, …
Organic (hydrocarbon)	C_nH_m	$C_nH_m^+$	27,29,41,43,55,57,69, 71, …

The dominant organic mass products are the mass fragments *m/z* 29, 43 and 44 for all four cases (Figure **17**). The mass fragment 43 signal can be compared to the total mass signal. The fraction of the total mass that is mass fragment 43 is 15% for α-pinene, 12% for m-xylene and p-xylene, and 9% for the mixture. The mass spectrum for α-pinene has higher *m/z* 43 than *m/z* 44, which is different from the mass spectra of m- and p-xylene and the mixture. The mixture has the highest fraction of *m/z* 44, 16%, much higher than *m/z* 43. Additionally *m/z* 41, 42, 55, 57, and 69 are observed, although their contribution to total SOA mass is small. The mass fragment *m/z* 18 was similar for all cases, 12 to 13%. This result can be explained by the constant relative humidity condition for all cases. Although all four mass spectra have many of the same peaks, the contribution of each mass fragment to the total organic mass differs, especially for α-pinene.

A crucial test of the PAM concept is the comparison of the chemical composition of the SOA formed in the PAM chamber to the SOA formed in large environmental chambers. The mass spectrum of SOA for α-pinene and m-xylene in the PAM chamber are compared with those taken in large environmental chambers (Figure **18**). SOA mass spectra for α-pinene are compared that from Bahreini et al., (2006) in (a) and with that from Alfarra et al., (2006) in (b).

While mass spectra from Bahreini et al. (2006) and the PAM chamber have the same peaks, the relative values are somewhat different. This difference is significant for *m/z* 43 and 44. However, the environmental conditions were quite different between the two studies. In the PAM chamber, the SOA came from the photo-oxidation of 79 ppbv of α-pinene, while in the environmental chamber used by Bahreini et al., (2006), the SOA came from the ozonolysis of 189 ppbv of α-pinene. Our studies show quite clearly that the amount of precursor gas affects the relative values of signals at different masses. For instance, the mass ratio of *m/z* 43 to *m/z* 44 is greater for a greater precursor gas amount, as will be explained in detail in section 5.2.2. The mass spectrum of Alfarra et al., (2006) in Figure **18** (b) is from the photo-oxidation of 160 ppbv of α-pinene. Alfarra et al., (2006)'s mass spectrum is somewhat different from that of Bahreini et al. (2006) as well as from the mass spectrum in the PAM chamber. However, the contribution of *m/z* 43 and 44 to SOA mass is greater in the PAM chamber than that in either Bahreini et al., (2006) or Alfarra et al., (2006). At the same time, the contribution of larger organics, such as *m/z* 55 and 69, is less than that in either Bahreini et al., (2006) or Alfarra et al., (2006). This difference suggests that the SOA produced in the PAM chamber is more highly oxidized than in their environmental chambers.

(a)

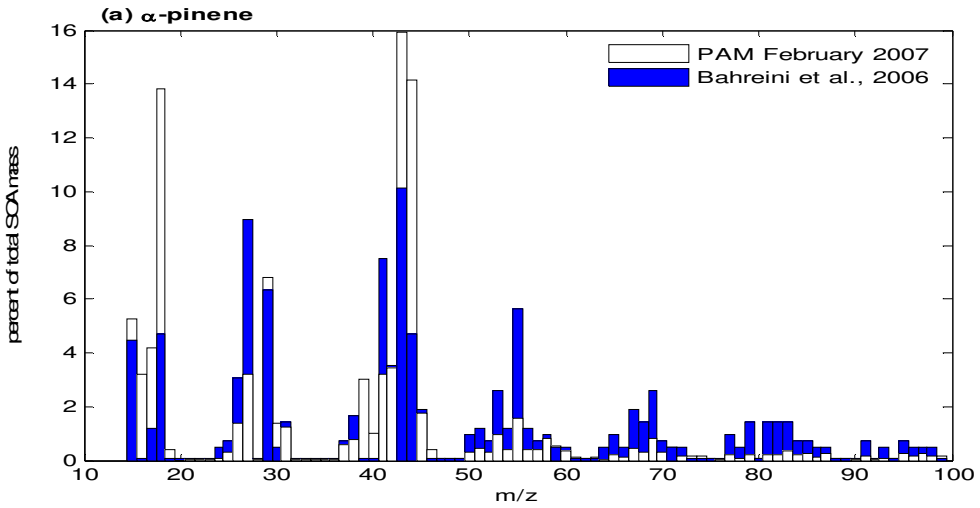

(b)

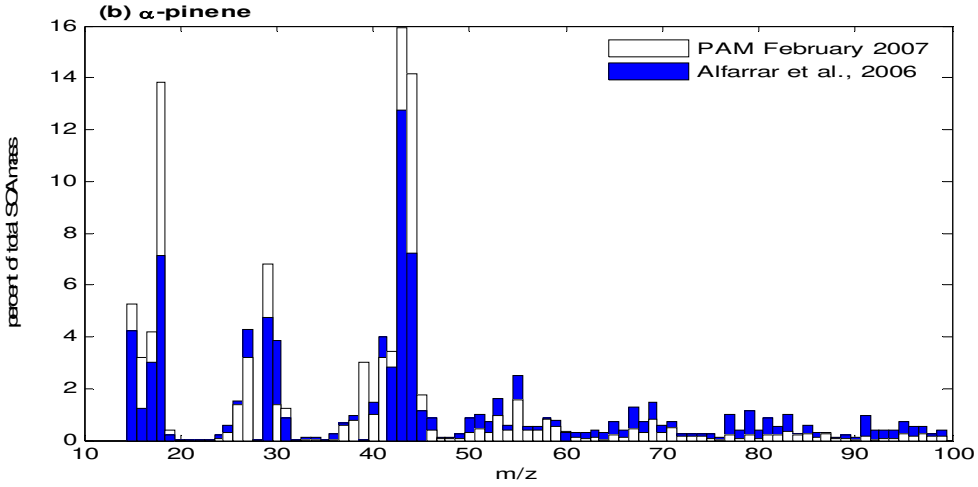

Figure **18**: **(a)** Percent SOA signal versus mass for α-pinene for PAM and Bahreini et al. (2006). White is from the stable SOA from photo-oxidation of 79 ppbv of α-pinene in the PAM chamber, 16 February 2007; Blue is from Bahreini et al. (2006)'s ozonolysis of 186 ppbv of α-pinene. The smaller percent fraction from PAM or the large chamber study is plotted in front of the larger percent fraction.

(b) Percent SOA signal versus mass for α-pinene for PAM and Alfarra et al. (2006). White is from the stable SOA from photo-oxidation of 79 ppbv of α-pinene in the PAM chamber, 16 February 2007; Blue is from Alfarra et al. (2006)'s photo-oxidation of 160 ppbv of α-pinene.

(c)

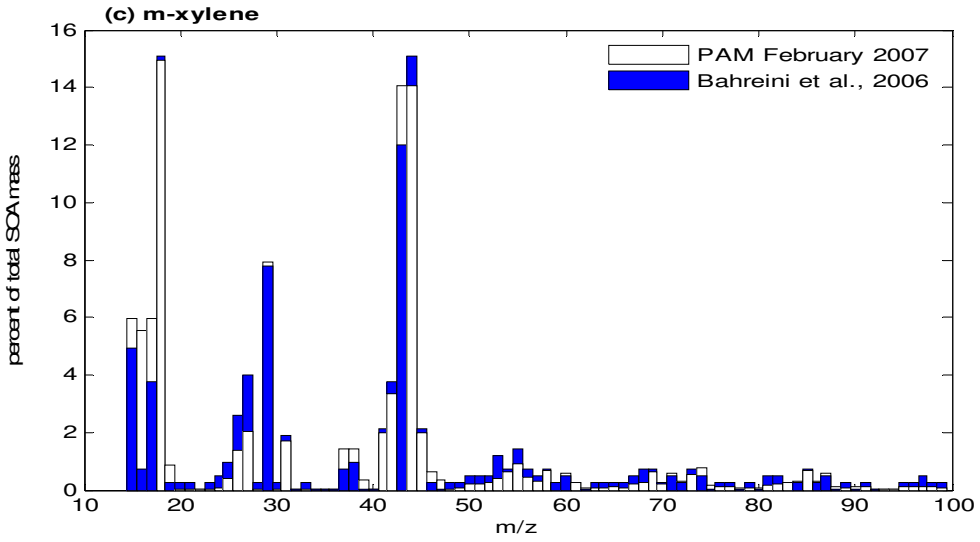

Figure **18**-continued: **(c)** Percent SOA signal versus mass for m-xylene for PAM and Bahreini et al. (2006). White is the stable SOA from photo-oxidation of 163 ppbv of m-xylene in the PAM chamber, 21 February 2007; Blue is from Bahreini et al. (2006)'s 143 ppbv of m-xylene photo-oxidation.

The percent of total SOA mass is obtained by the percentage of mass signal per *m/z* to the sum of mass signals. Because the AMS mass spectra were measured off Figure 14 in Bahreini et al. (2006), Figure 8 in Alfarra et al., (2006) and the jpg files of the time evolution of the PAM chamber mass spectra, some additional measurement error is possible.

The mass spectrum of m-xylene in the PAM chamber is in a good agreement with that in Bahreini et al., (2006) (Figure **18** (c)). The mass spectra are similar because they were obtained by photo-oxidation of similar amounts of m-xylene, 163 ppbv in our study and 143 ppbv in Bahreini et al., (2006). The ratio of *m/z* 43 to *m/z* 44 from the PAM chamber is about 1.0, while the ratio from Bahreini et al. (2005) is 0.8. This difference should not be surprising. The degree of oxidation depends on the total exposure to oxidants and on the initial precursor gas amount, which affects to total SOA mass. The

smaller precursor gas amount, the more oxidized the SOA particles will be for a given exposure to oxidants. The lower m-xylene amount in the Bahreini et al. (2005) experiment means that the SOA particles should be more aged and have a lower *m/z* 43 to *m/z* 44 ratio than the SOA particles in the PAM chamber, as is observed. Taking the difference in precursor gas amount into account explains most of the differences in the *m/z* 43 to *m/z* 44 ratio that were observed.

The difference between the percent of total SOA signal for m-xylene: Bahreini et al. (2006) – PAM in Figure **19** also shows a good agreement. The mass fragment 43 and 44 in the PAM study is about 20% different from Bahreini et al., (2006), but other larger mass fragments are similar. This good agreement provides evidence that the processes that are occurring in PAM are also occurring in the large environmental chamber.

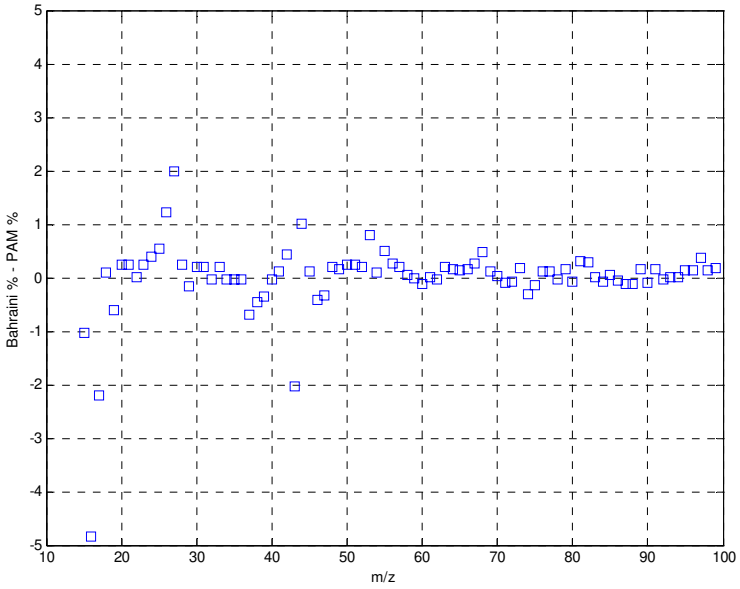

Figure **19**: The difference between the percent of total SOA signal for m-xylene: Bahreini et al. (2006) – PAM.

5.1.2 Peak and stable SOA yields in PAM

The formation and aging of SOA in a highly oxidized environment is studied by the observation of the SOA mass change and the SOA size distribution as a function of time. It is illustrated by the TEOM mass and the number concentration in the size distribution by UHSAS from m-xylene photo-oxidation in Figure **20**. Figure **20** shows that when the UV light was turned on, SOA formed and grew immediately to reach a peak value before decreasing to a smaller stable value. When SOA mass reached a stable value, the aerosol mass and chemical component distribution did not change anymore and were constant. It shows that the peak mass is associated with the large particles that are produced by the initial oxidation, while the stable mass is a result of the stable particle distributions.

The UHSAS could scan the particle size range from 55 nm to 1 μm in 10 s. Thus we could see the formation, growth, and aging of SOA once the particles became larger than 55 nm. The formation occurred on a timescale much shorter than the exposure time of the PAM chamber, which is about 3 min. However, the growth and aging occur on timescales much larger than the exposure time. Figure **21** shows the evolution of size distribution from 160 ppbv of m-xylene photo-oxidation by plotting the size distribution every 3 min. except for the first and the second size distributions. The elapsed time contains a 20-30 s delay due to the sampling flow rate of the UHSAS and the distance of sampling tubing from the chamber to the UHSAS. The rapid nucleation was observed within minutes. After the nucleation and the continuous growth, the appearance of two

distinct distributions was observed at 16 min. Eventually the size distribution became broad and no longer changed.

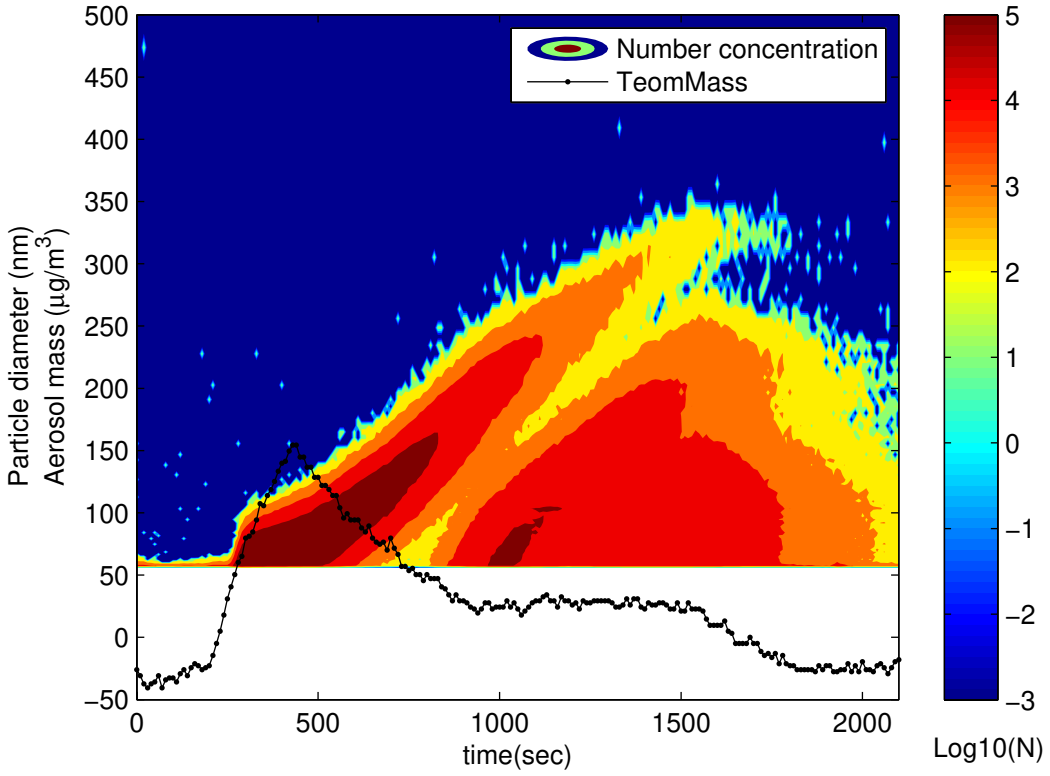

Figure **20**: The example of peak and stable mass of SOA measured by TEOM and the relationship with the particle size distribution by UHSAS. Black dotted line represents the SOA mass concentration measured from TEOM.

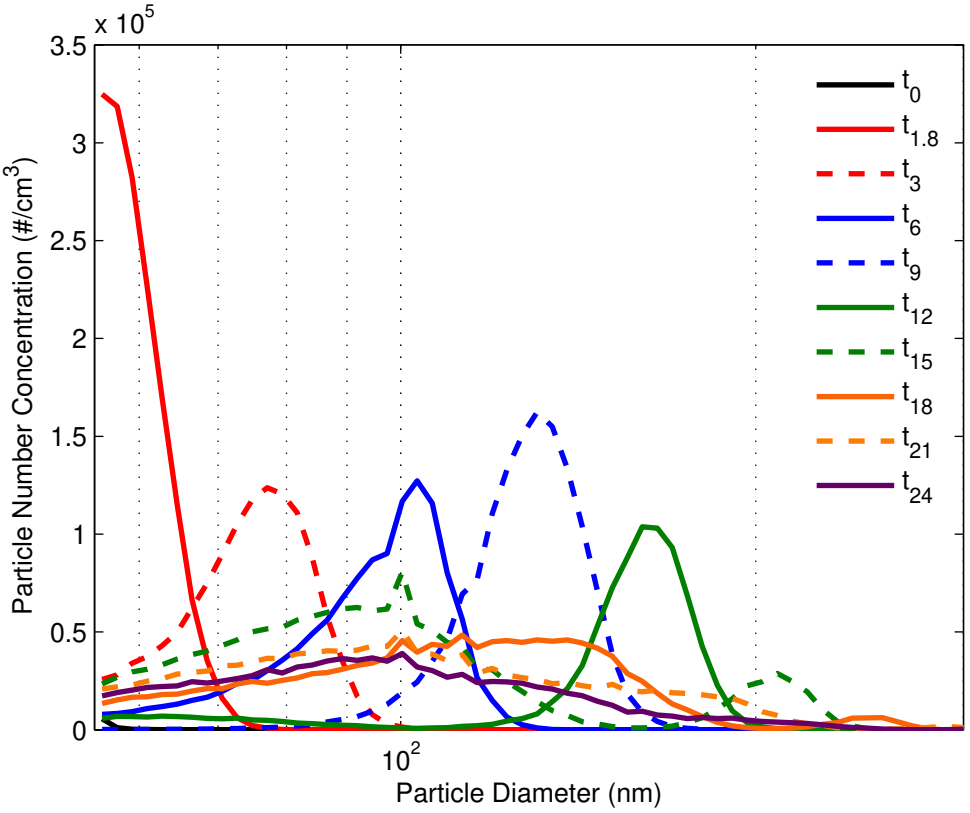

Figure **21**: Particle number distribution of SOA from 160 ppbv of m-xylene photo-oxidation. The number distribution change with time was plotted and the elapsed time (min) after the UV light on was denoted in the legend (i.e., t_6 means elapsed time = 6 minutes).

This behavior observed in the first few minutes is a transient phenomenon that is observed only in the PAM with the pure organics and a mixture of three organics when we turn on the UV light to initiate the oxidation. When we ran the chamber with the UV light on continuously for a stable oxidant level, and added precursor gas later, we did not observe the peak mass and the following stable mass. Interestingly, it is not observed in the atmosphere (Figure **15**). That it is not observed in the large environmental chamber

suggests that it is due to the extremely rapid initial particle formation in the highly oxidized environment in the PAM chamber.

The peak and stable mass was not observed in inorganic sulfate aerosol formation because inorganic sulfate aerosol has such a low saturation vapor pressure that it is completely non-volatile in the troposphere and cannot be further oxidized. In the ozonolysis of α-pinene in the dark chamber, the mass increased to a maximum, stable value without going through a peak. This difference suggests that the observed behavior of peak mass followed by a stable mass is a characteristic of SOA formed from the photo-oxidation in the PAM. Kroll et al., (2006) observed similar behavior of peak and stable aerosol mass from isoprene photo-oxidation in the low-NO_x condition in their large environmental chamber. They suggest that this peak and stable mass could be from the photochemical aging of SOA by OH or UV irradiation. However, they could not test their hypothesis due to the lack of information about OH in their chamber (Kroll et al., 2006; Surratt et al., 2006).

The degree of oxidation depends on the total exposure to oxidants and on the initial precursor gas amount, which affects to total mass. This observed behavior might be explained by the further oxidation of the semi-volatile organics produced by the oxidation of precursor organics. The partitioning of the semi-volatile organics is in equilibrium between the gas and particle phases (Odum et al., 1996). If these semi-volatile organics are further oxidized to stable gas-phase products, the amount of semi-volatile organics partitioned between the gas and particle phases decreases, thus decreasing the SOA mass.

5.2 Dependence of SOA formation and aging on precursor gas amount and organic aerosol mass (M_o)

The relative ratio of *m/z* 43 to *m/z* 44 in the ambient aerosol was used to indicate if the organic aerosol was fresh or aged. Alfarra et al. (2006), Zhang et al. (2005b), and Robinson et al. (2007) observed the larger *m/z* 44 value than *m/z* 43 ((*m/z* 44)/(*m/z* 43) >1) in aged air masses such as in rural or remote alpine locations, and the larger *m/z* 43 value than *m/z* 44 ((*m/z* 44)/(*m/z* 43) <1) in fresh organic aerosol containing air mass such as forest or urban locations (an example of Zhang et al., (2005b) in Figure **22**).

Mass fragment 43 and 44 are simply identified to be aldehyde and acid, respectively. The examination of relative amount of aldehyde and acid is a way to indicate how oxidized, or photo-chemically aged, the organic aerosol is. An example of the hydrocarbon oxidation step is shown in Eq.**9**. A hydrocarbon is oxidized to alcohol, to aldehyde, to acid, and finally to CO_2 and H_2O by the attack of an oxidant, such as O_3, OH or other radicals.

$$\underset{\text{Hydrocarbon}}{CH_4} \rightarrow \underset{\text{Alcohol}}{CH_3OH} \rightarrow \underset{\text{Aldehyde}}{H_2C{=}O} \rightarrow \underset{\text{Acid}}{HCOOH} \rightarrow \cdots\cdots\cdots \rightarrow \underset{\text{product of complete oxidation}}{H_2O + CO_2} \qquad \mathbf{2}$$

Many mass spectra of SOA for α-pinene, 1,3,5-TMB, and m-xylene in environmental chambers were observed to have larger *m/z* 43 than *m/z* 44. It has been suggested that SOA produced in environmental chambers represents relatively young organic aerosol, similar to that observed in forest or urban locations (Alfarra et al., 2006; Bahreini et al., 2006). However, Alfarra et al., (2006) also observed 25% and 50% increase of *m/z* 44 after 8 hours in the environmental chamber for α-pinene and 1,3,5-TMB, respectively. While Alfarra et al. (2006) proposed that OH or UV are possible

controlling factors for SOA aging, they were unable to determine the quantitative dependence of OH on SOA formation and aging. In Our PAM chamber, however, could study the oxidant effect on the formation and aging process, which is described in Section 5.3.

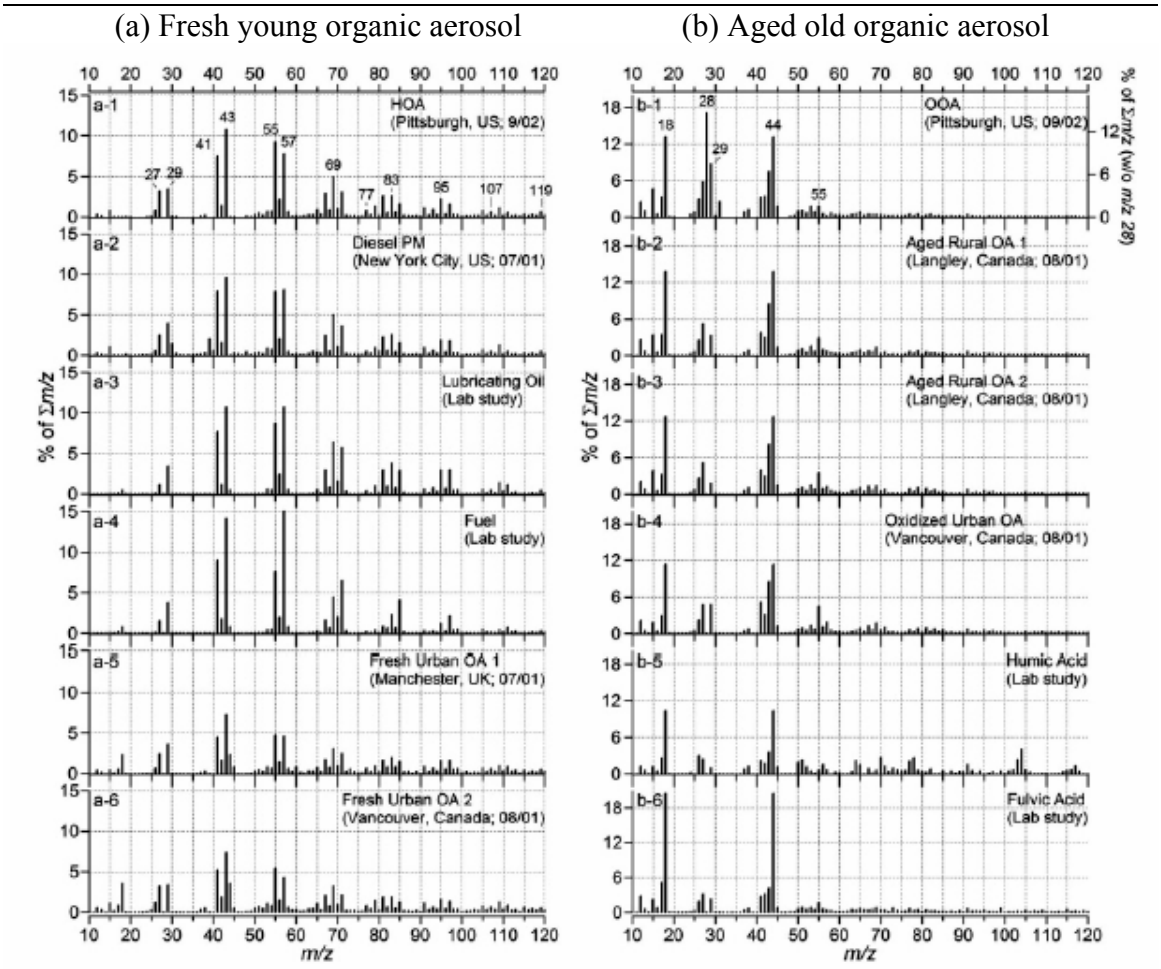

Figure **22**: Aerosol mass spectrum for various field and chamber measurements. (a) shows the greater *m/z* 43 than *m/z* 44 representing fresh organic aerosol. (b) shows the greater *m/z* 44 than *m/z* 43 representing aged old organic aerosol. The figure is cited from Figure 9 of Zhang et al., (2005b).

To examine the dependence of SOA formation and aging on precursor gas and organic aerosol mass produced from the precursor gas, ozone and OH were kept at 9 ppmv and at 300 pptv, respectively, in the PAM chamber for all experiments in this section.

5.2.1. Dependence of peak-to-stable SOA yield on precursor gas amount and organic aerosol mass (M_o)

The dependence of peak and stable mass yield of SOA on precursor gas and on the organic aerosol mass (M_o) were observed for α-pinene, m-xylene, and p-xylene (Figure **23**). As the precursor gas amount increased, both the peak and stable mass yields increase, but the difference between the peak and the stable mass decreased (Figure **23**(a)). The similar behavior was observed for the dependence on the organic aerosol mass (M_o) (Figure **23** (b)).

Figure **24** shows the dependence of the peak-to-stable SOA yield ratio on precursor gas amount and organic aerosol mass. The peak-to-stable SOA yield ratio is obtained by the equation: (peak mass yield – stable mass yield)/peak mass yield. The value, peak-to-stable SOA yield ratio is used to express how much freshly formed aerosol is further oxidized in the aging process (Recall the Section 5.1.2). As the precursor gas amount increases, the peak-to-stable SOA yield ratio decreases. This behavior is same for organic aerosol mass (M_o). As precursor gas amount and produced organic aerosol mass (M_o) increases, the stable mass increases and the peak-to-stable SOA yield ratio decreases. This phenomenon will be examined in more detail in the section 5.2.2.

SOA mass yield is dependent on total organic aerosol mass as well as precursor gas amount (Seinfeld and Pandis, 1997). Organic aerosol mass was generated by the direct oxidation of precursor gas without any seed particles, so that the dependence on precursor gas amount cannot be distinguished from the dependence on the total organic aerosol mass. Each experiment discussed in this section was conducted with only pure α-pinene, m-xylene, or p-xylene. Therefore the total organic aerosol mass is equal to the SOA yield times the precursor gas amount. Although the yield is somewhat dependent on M_o, the peak-to-stable SOA yield ratio has similar behavior for (a) and (b) in Figure **23** and in Figure **24**. In the next section 5.2.2, the dependence of the SOA aging only on organic aerosol mass will be considered.

The slope of peak-to-stable SOA yield ratio as a function of organic aerosol mass is different for α-pinene than it is for m-xylene and p-xylene. This difference comes from the chemical products that are formed in the photo-oxidation of α-pinene being different from those from the anthropogenic hydrocarbons, m-xylene and p-xylene.

(a) Dependence of precursor gas amount

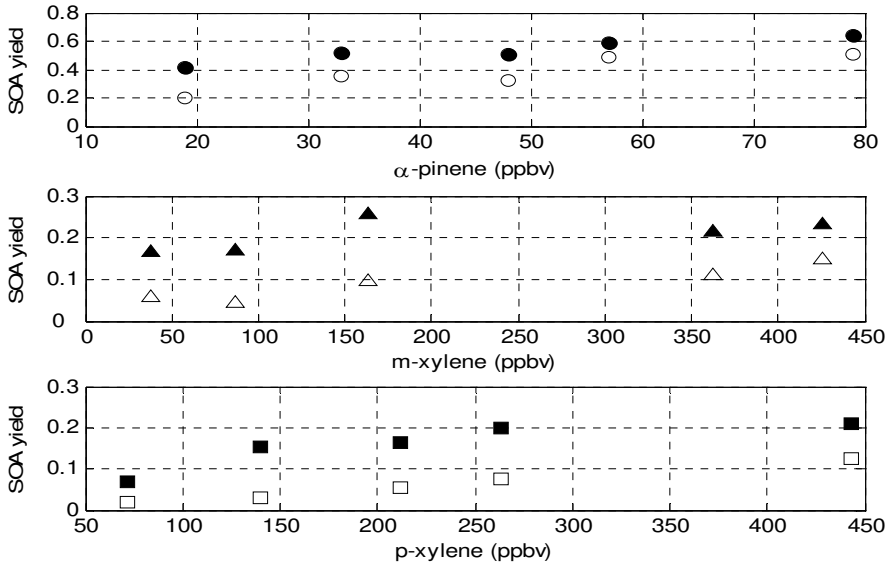

(b) Dependence of organic aerosol mass

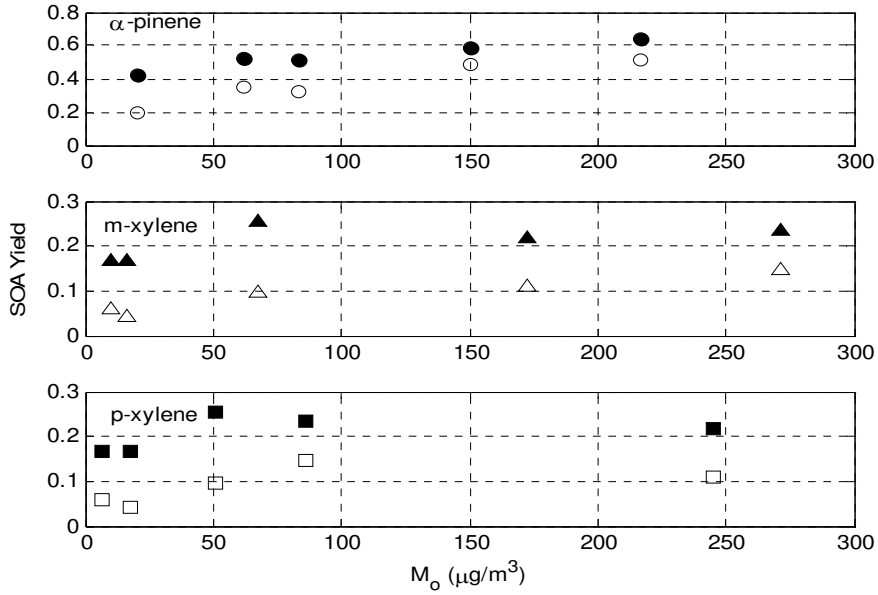

Figure **23**: The peak and stable SOA mass yield dependence on (a) precursor gas amount and (b) produced organic aerosol mass for α-pinene, m-xylene and p-xylene photooxidation. The filled symbols (●, ▲, ■) represent the SOA yield at the peak aerosol mass, and the opened symbols (○,Δ,□) represent the SOA yield at the stable aerosol mass.

(a) Dependence of precursor gas amount

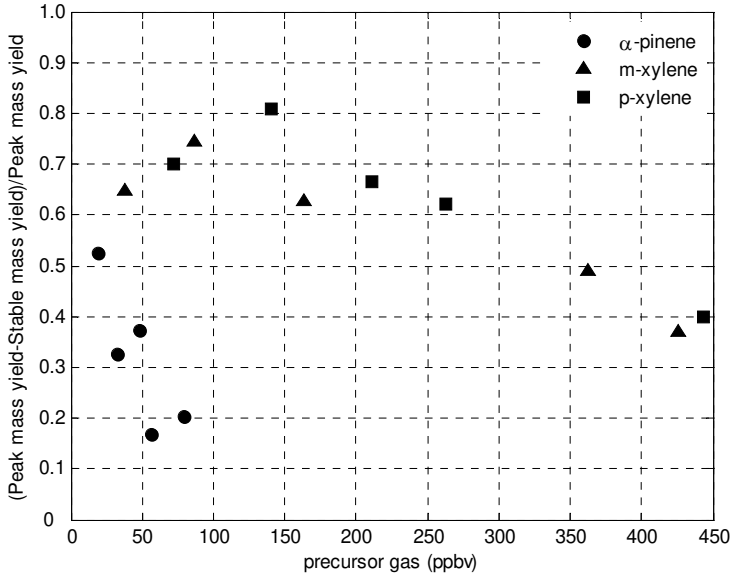

(b) Dependence of organic aerosol mass (M_o)

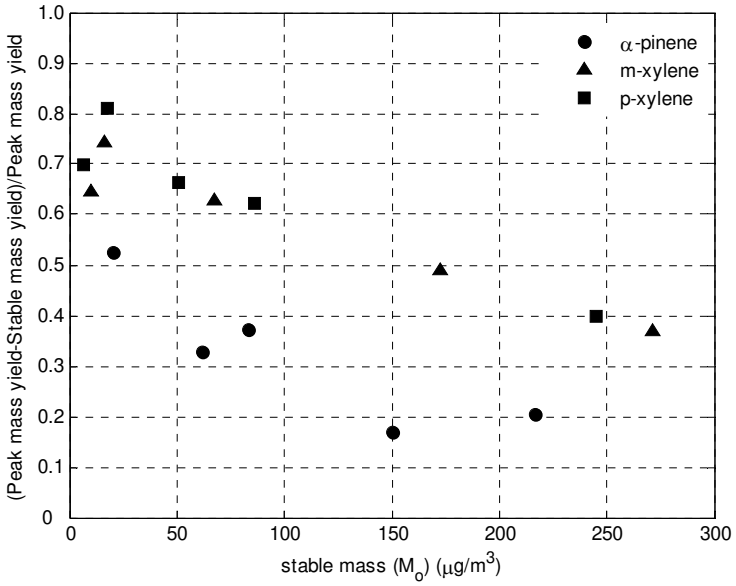

Figure **24**: Dependence of the peak-to-stable SOA yield ratio (1) on precursor gas amount, and (2) on organic aerosol mass amount (M_o). The peak-to-stable SOA yield ratio is obtained by the equation: (peak mass yield – stable mass yield) / peak mass yield.

5.2.2 Dependence of mass fragments 43 and 44 on organic aerosol mass (M_o)

The change of mass fragments 43 and 44 were observed for various organic aerosol masses (M_o). The examination of *m/z* 43 and 44 is used a way to examine how oxidized, or photo-chemically aged, the organic aerosol is, as discussed in Section 5.2 . In the PAM experiments, as organic aerosol mass was increased, the ratio of *m/z* 43 to *m/z* 44 increased (Figure **25**). The greater amounts of SOA mass produced from greater amounts of precursor gas was observed to be relatively younger than SOA produced from small amounts of precursor gas.

The reason of the higher ratio of *m/z* 43 to *m/z* 44 for higher organic aerosol mass can be found from Figure **26**. This figure shows the number distribution of SOA from m-xylene photo-oxidation measured by the UHSAS. The amounts of m-xylene were varied while the relative humidity was held constant. The UV light was periodically turned on and off, creating constant amounts of OH and O_3 when the light was on. For a greater amount of precursor gas, the total organic aerosol mass is greater and the particles tend to be larger. The aging of the SOA is assumed to be started by the attack of OH on the particle surface. In the PAM chamber, the oxidation occurs so fast that the oxidant has no chance to penetrate into the bulk volume of SOA. Bigger particles have a lower chance of being oxidized by OH than small particles because of the low surface-to-volume ratio. Thus the ratio of *m/z* 43 (an indicator of fresh particles) to *m/z* 44 (an indicator of aged particles) depends on total aerosol mass, as in Figure **25.**

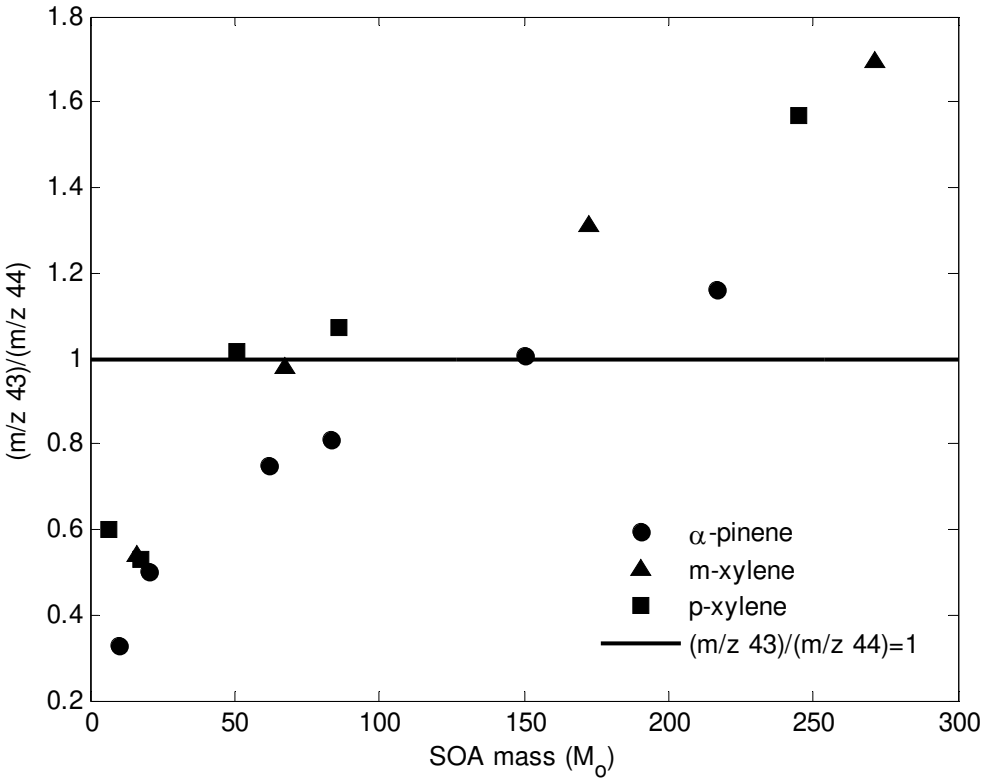

Figure **25**: The ratio of *m/z* 43 to *m/z* 44 to SOA mass for α-pinene, m-xylene and p-xylene with respect to M_o. The solid line is the indication of *m/z* 43 = *m/z* 44. OH for all runs is 260 ±10 pptv.

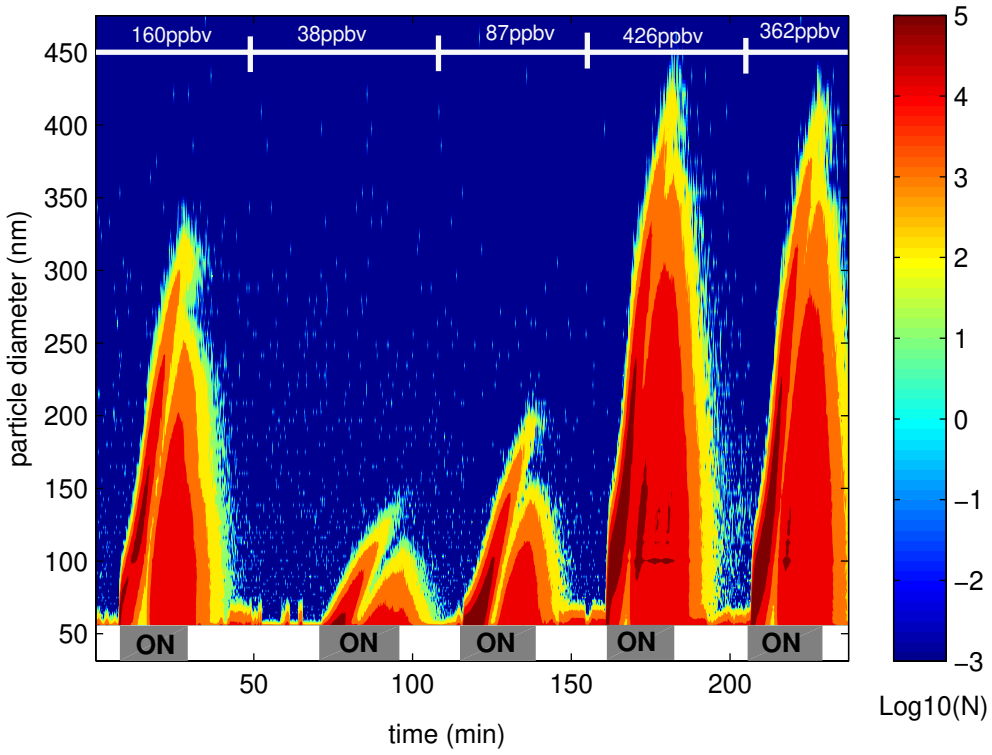

Figure **26**: Particle number distribution of SOA from m-xylene photo-oxidation from five experiments using different amounts of m-xylene. As m-xylene amount increases, more large particles are produced. Text box in top of the plot shows the m-xylene amount used. Added m-xylene concentrations were 160 ppbv, 38 ppbv, 87 ppbv, 428 ppbv, and 362 ppbv as indicated in the upper part of the figure. UV light irradiation was indicated with grey block with "ON" in bottom of the plot.

Evident in Figure **26** is the appearance of multiple distinct particle distributions in all the experiments. We suggest a scenario to explain the two distinct particle distributions here. The first mode comes from rapid nucleation and coagulation to form large particles that eventually leave the chamber. The second mode is a result of having many very small particles remain in the chamber after the initial nucleation so that the oxidized gases can then simply condense on them. The particles are only interacting

physically each other, resulting in a change of the number distribution but not the total aerosol mass concentration. The ratio of *m/z* 43 to *m/z* 44 and the stable aerosol mass appear to be quite constant in the second mode period. To understand this behavior will require modeling the chemistry and microphysics of SOA formation and aging in our highly oxidizing PAM chamber.

5.3 Dependence of SOA formation and aging on OH and HO_2

The measurement and the control of OH and HO_2 in PAM chamber enabled us to study the effect of OH and HO_2 on the SOA aging. We examined the role of OH and HO_2 on the formation and aging of SOA by varying the OH and HO_2 concentrations for different types and amounts of precursor gases.

5.3.1 Dependence of peak-to-stable SOA yield on OH and HO_2

The dependence of the peak-to-stable SOA yield on OH and HO_2 was studied with 30 to 500 pptv of OH and 230 to 1600 pptv of HO_2. The ozone was kept constant at 9 ppmv in the chamber. To study only the oxidant effect, precursor gas amounts were kept constant at 35 ppbv for α-pinene, 150 ppbv for m-xylene, and 133 ppbv for p-xylene for all studies discussed here.

Figure **27** shows the dependence of the peak and the stable yield of SOA on OH. The peak yield and stable yield are the SOA yield when aerosol mass was at the peak value and the stable value, respectively (please see the Section 5.1.2). With very low OH,

both of the peak yield and the stable yield were low and the peak-to-stable SOA yield ratio was also low. As [OH] increases, the peak yield and the stable yield increases and then eventually levels off above 400 pptv of [OH] (Figure **27**).

Figure **28** shows the dependence of the peak-to-stable SOA yield ratio for α-pinene, m-xylene, and p-xylene on OH. The peak-to-stable SOA yield ratio represents the contribution of unstable organic products that tend to evaporate during the SOA aging process. The peak-to-stable SOA yield ratio of α-pinene is observed to be less than those of m-xylene and p-xylene (Figure **28**). This result means that the photo-oxidation product of m-xylene and p-xylene is more unstable and semi-volatile than that of α-pinene. It is consistent with the observation of the higher SOA yield of α-pinene than m-xylene and p-xylene (Table **2**).

The same curve shape for the peak-to-stable SOA yield ratio of m-xylene and p-xylene is consistent with the chemical structures of m-xylene and p-xylene being similar. The peak-to-stable SOA yield ratio increases and then eventually levels off above 400 pptv of OH mixing ratio. It appears that 400 pptv of OH is enough to oxidize all of existing organic aerosols to well aged particles for 35 ppbv of α-pinene, 150 ppbv of m-xylene, and 133 ppbv of p-xylene. We already observed the dependence of SOA aging on total organic aerosol mass. If precursor organic amount of SOA mass were different from those in this case, then the curve in Figure **28** will be different.

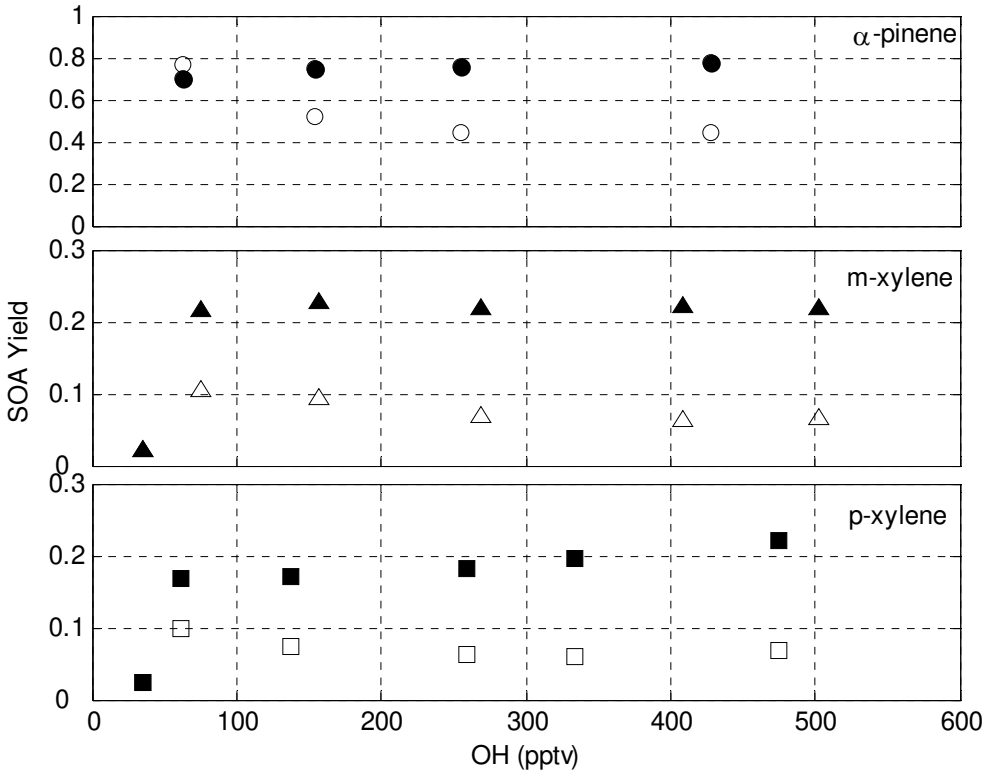

Figure **27**: The effect of OH on peak and stable mass of SOA. The filled symbols (●, ▲, ■) represent the SOA yield at the peak aerosol mass, and the opened symbols (○,Δ,□) represent the SOA yield at the stable aerosol mass.

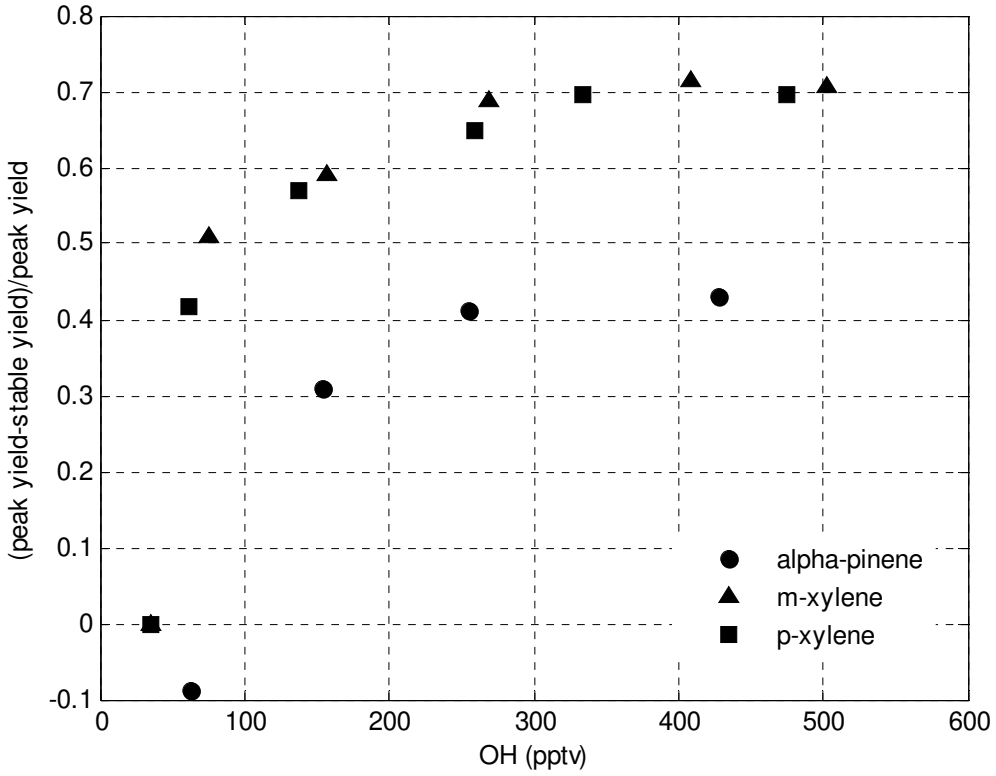

Figure **28**: The peak-to-stable SOA yield ratio with respect to OH mixing ratio. The peak-to-stable SOA yield ratio is obtained by (peak mass yield - stable mass yield)/peak mass yield. 35 ppbv of α-pinene, 150 ppbv of m-xylene, and 133 ppbv of p-xylene were used.

The effect of HO_2 on the peak-to-stable SOA yield ratio was also studied. Figure **29** and Figure **30** show the dependence of HO_2 on the peak and stable yield of SOA and on the peak-to-stable SOA yield ratio, respectively. The peak-to-stable SOA yield ratios for all three VOCs increase as HO_2 increases up to 1500 pptv and then continues to increase even when HO_2 is constant (Figure **30**). The increase for low HO_2 is a direct result of the simultaneous increase in OH, since OH and HO_2 are correlated at

lower values. Therefore, the aging is greater when OH is greater, but is not correlated to HO_2. The net result is that OH is involved in the oxidation of unstable organic aerosol for these organic precursor gases, but not HO_2. That conclusion seems to be consistent with the *m/z* 43 and 44 ratios that come next.

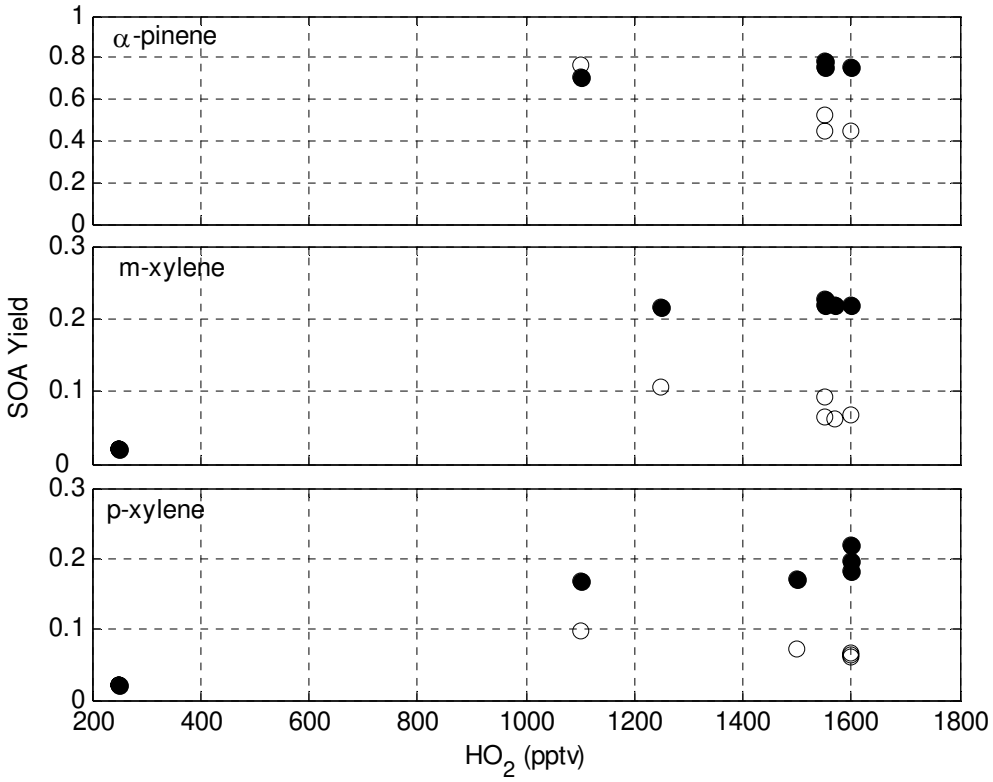

Figure **29**: The effect of HO_2 on peak and stable yield of SOA. The filled symbols (●, ▲, ■) represent the SOA yield at the peak aerosol mass, and the opened symbols (○,Δ,□) represent the SOA yield at the stable aerosol mass.

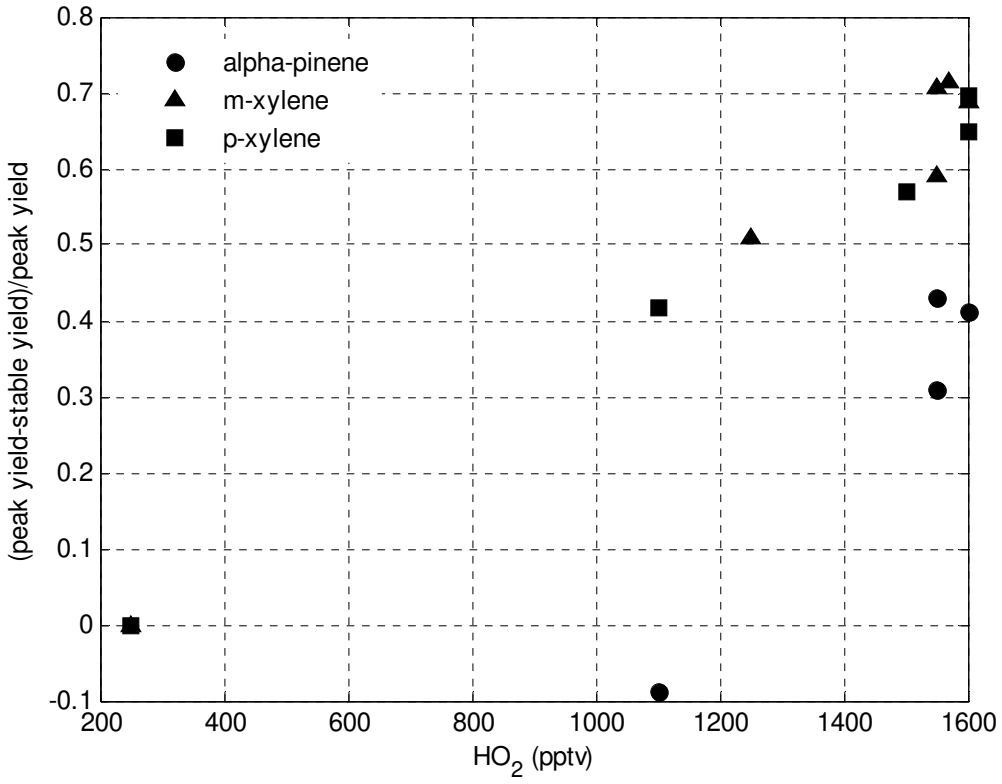

Figure **30**: The peak-to-stable SOA yield ratio with respect to HO_2 mixing ratio. The peak-to-stable SOA yield ratio is obtained by (peak mass yield - stable mass yield)/peak mass yield.

5.3.2 Dependence of chemical composition on OH and HO_2

To see the effect of OH and HO_2 on the SOA aging in a different way, we examined the change of SOA mass spectra with respect to OH and HO_2. Mass fragments 43 and 44 are dominant products of SOA; thus their ratio change is an indicator of aging (recall Section 5.2). The decrease in the ratio of *m/z* 43 to *m/z* 44 means the increase of highly oxidized acids compared to less oxidized aldehydes in the particle phase (Eq.**9**).

Figure **31** shows the dependence of the change of *m/z* 43 and *m/z* 44 on OH and HO_2. The percent of *m/z* 43's mass to total SOA mass is obtained by the equation: *m/z* 43 = 100×(measured aerosol mass of *m/z* 43)/(total organic aerosol mass). A similar equation is used for *m/z* 44. The percent of *m/z* 43's mass to total SOA is designated as *m/z* 43, and the same for other mass fragments.

The left panel in Figure **31** shows the OH dependence on *m/z* 44 and 43. Mass fragment 44 linearly increases as OH increases, while *m/z* 43 linearly decreases. The decreasing rate of *m/z* 43 is matched to the increasing rate of *m/z* 44 for all three VOC cases. It supports the hypothesis that aldehydes (*m/z* 43) are being converted to acids (*m/z* 44) as the SOA ages, although all of aldehydes appear to be converted to acid (Recall Eq. **9**). The right panel in Figure **31** shows the HO_2 dependence for *m/z* 43 and *m/z* 44, but the changes of *m/z* 43 and 44 are not correlated to HO_2. In other words, the change of *m/z* 43 and *m/z* 44 is strongly related to OH, not HO_2.

In some studies, *m/z* 57 is also used as an aging indicator (Zhang et al.,2005). Figure **32** shows that the behavior of *m/z* 57 is similar to that of *m/z* 43, and opposite to the behavior of *m/z* 44.

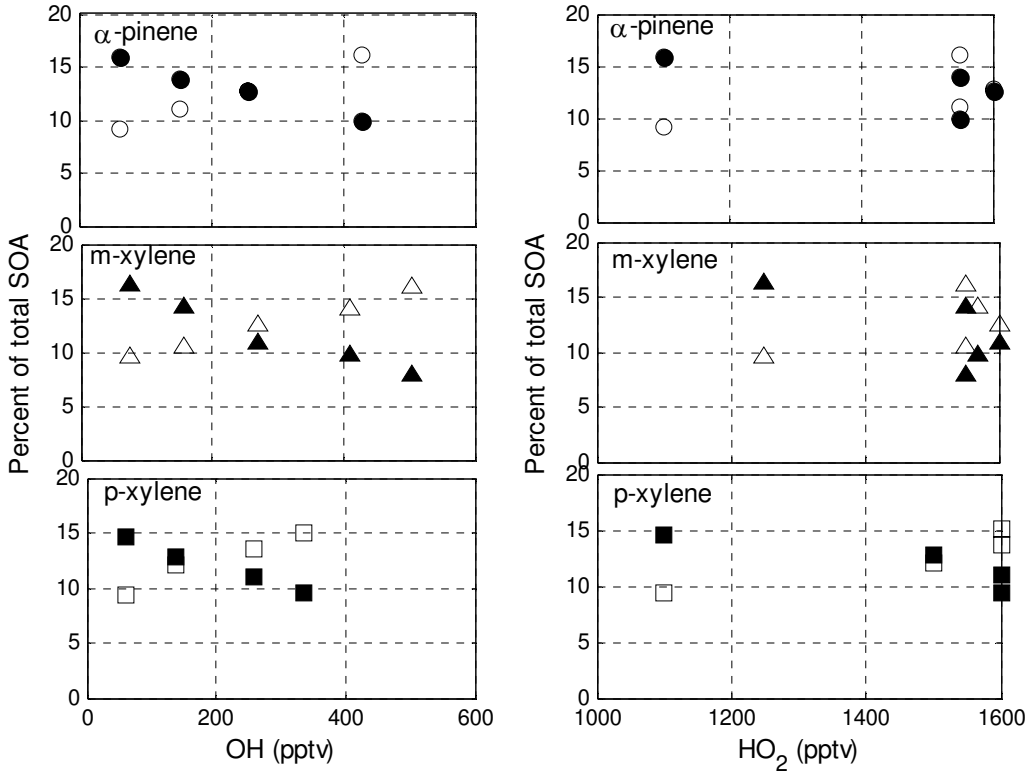

Figure **31**: The percentage of the total mass attributed to *m/z* 43 mass and *m/z* 43 mass. The percent of *m/z* 43 mass to total SOA mass = (mass concentration at *m/z* 43)/(the sum of organic particle mass concentration). Filled symbols (●, ▲, ■) represent the percent of total SOA of *m/z* 43 for α-pinene, m-xylene, and p-xylene. Opened symbols (○,Δ,□) represent the percent of total SOA of *m/z* 44 for α-pinene, m-xylene, and p-xylene.

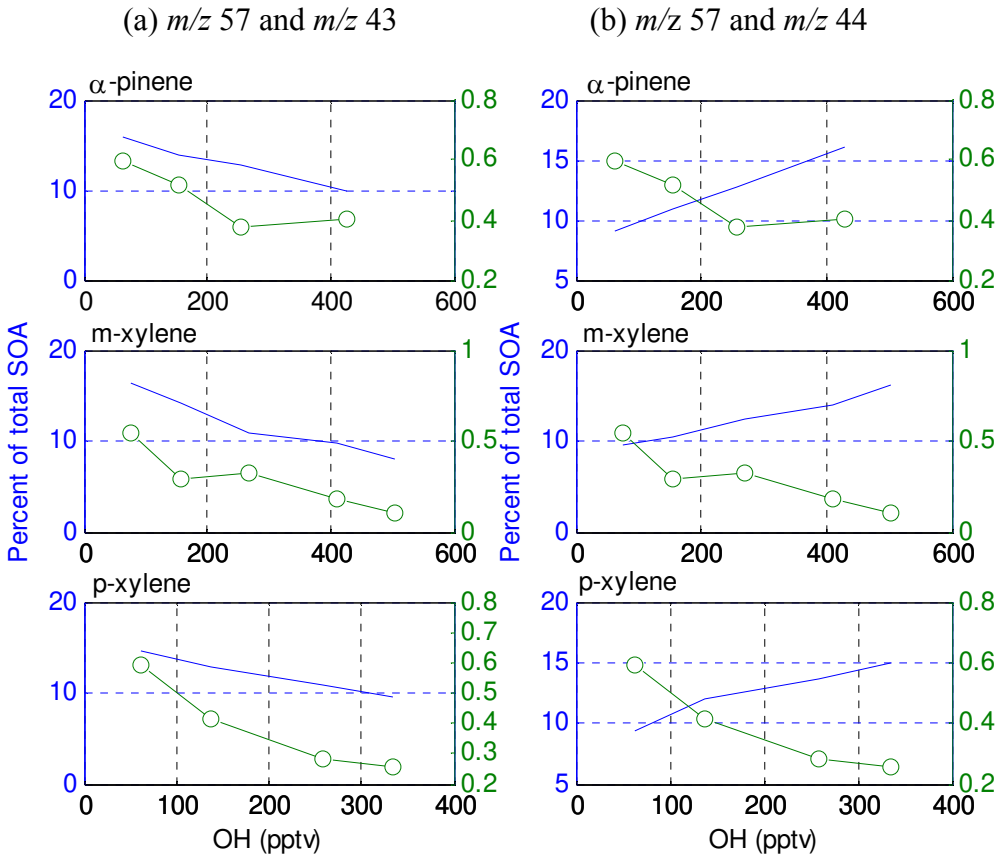

Figure **32**: Percent of *m/z* 57 mass to total SOA mass, percent of *m/z* 43 mass to total SOA mass, and the percent of *m/z* 44 mass to total SOA mass for various OH amounts. The green line with opened circles represents *m/z* 57 for (a) and (b). The blue line in (a) and (b) shows *m/z* 43 and *m/z* 44, respectively. Mass fragment 57 behaves similarly to *m/z* 43 and opposite to *m/z* 44.

The ratio of *m/z* 43 to *m/z* 44, which is expressed to (*m/z* 43)/(*m/z* 44), is another indicator of aging; the ratio's dependence on OH and HO_2 are shown in Figure **33** and Figure **34**, respectively. The ratio of *m/z* 43 to *m/z* 44 decreases linearly as OH increases for all three VOCs (Figure **33**), indicating oxidation by OH. Figure **34** shows the relationship between the ratio of *m/z* 43 to *m/z* 44 and the amount of HO_2, but the ratio of *m/z* 43 to *m/z* 44 is not dependent on HO_2. The ratio of *m/z* 43 to *m/z* 44 decreased as HO_2

increased, but it kept decreasing even when HO_2 became constant near 1500 pptv. Thus, the ratio of *m/z* 43 to *m/z* 44 provides more evidence that OH, and not HO_2, is responsible for the SOA aging.

The behavior of the ratio of *m/z* 43 to 44 is similar to the peak-to-stable SOA yield ratio for indicating SOA aging. The decrease of the ratio of *m/z* 43 to 44 in the mass spectrum indicates that the organic aerosol is more aged by larger amounts of OH for the same exposure time in the PAM chamber. In other words, the variable oxidant amount in PAM chamber enable us to observe fresh formed young SOA and aged old SOA with respect to OH, as is also shown in Figure **31**.

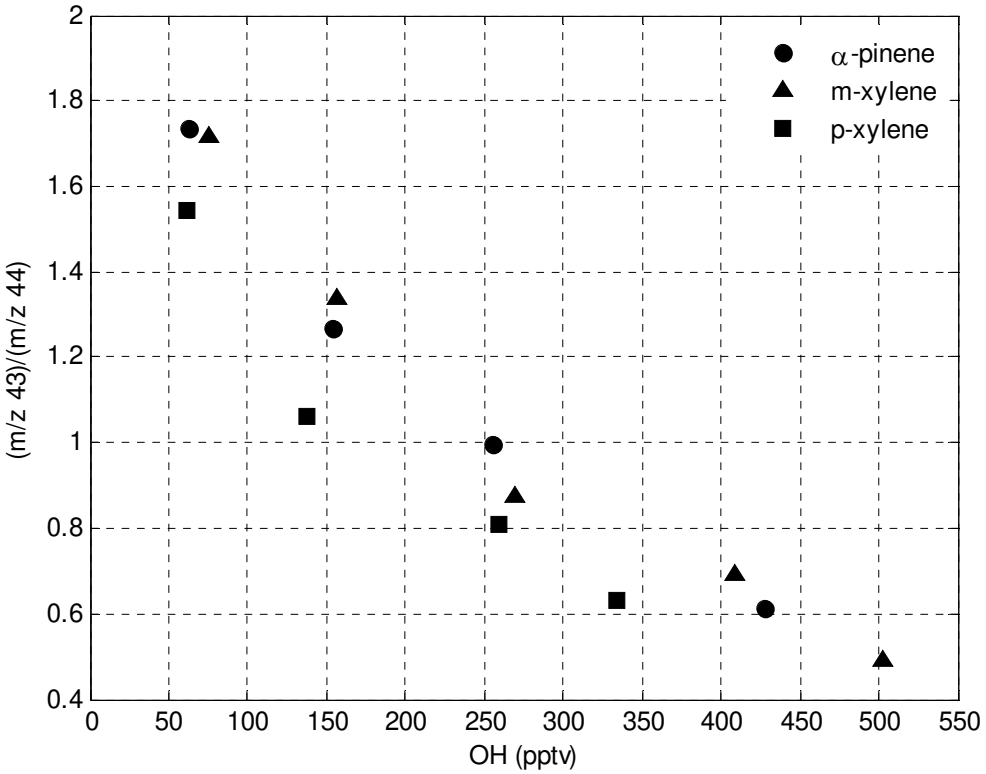

Figure **33**: Observation of the contribution of *m/z* 43 and *m/z* 44 to total organic aerosol mass with respect to OH mixing ratio.

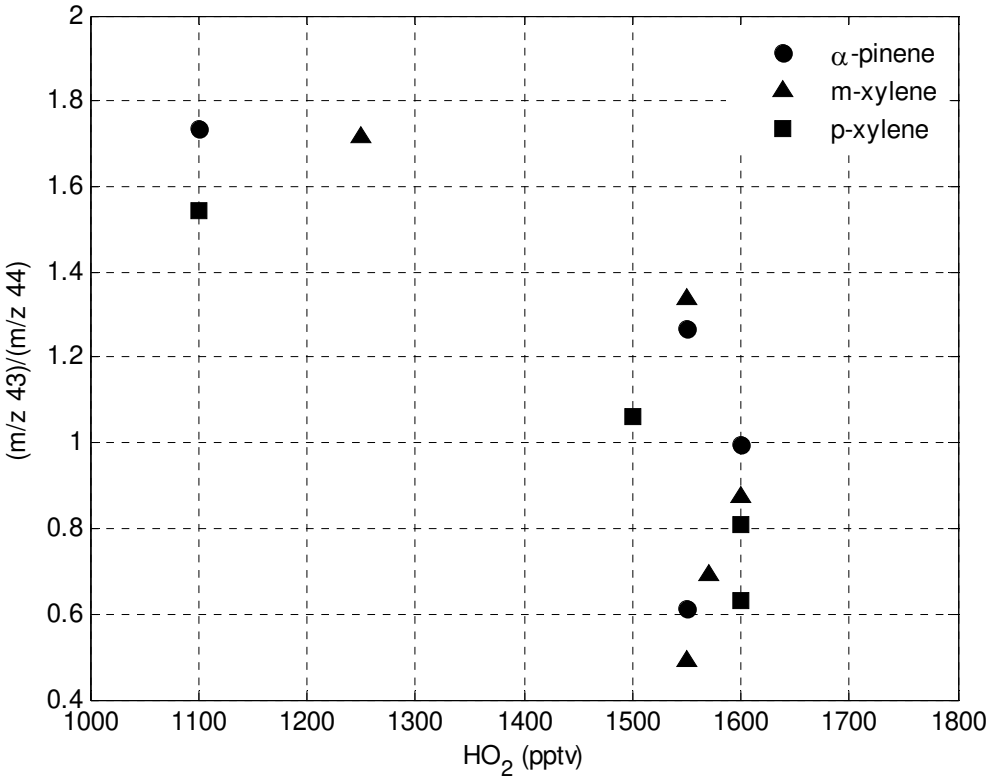

Figure **34**: Observation of the contribution of *m/z* 43 and *m/z* 44 to total organic aerosol mass with respect to HO_2 mixing ratio.

Understanding the detailed behavior of the peak and stable masses and the m/z 43 and m/z 44 mass spectra peaks will require much more work in the laboratory. However, several conclusions can be drawn from the experiments done here.

First, the mass spectra for SOA in the PAM chamber by Q-AMS measurement is similar to the mass spectra found in the large environmental chambers. This similarity provides evidence that the highly oxidizing environment of the PAM chamber has the same oxidation processes that occur at ambient oxidant levels. Studies in large

environmental chambers generally capture only relatively young SOA formation, studies in the PAM chamber provides observations of aged SOA from fresh SOA to old aged SOA by varying the OH mixing ratio.

Second, the two methods of examining the amount of aging, the peak-to-stable SOA yield ratio and the ratio of *m/z* 43 to *m/z* 44, lead to the same conclusions: (1) the sensitivity of the SOA aging to the precursor amount suggests that microphysical processes may be limiting the aging; (2) the major oxidant of the precursor gas and the further aging appears to be OH for these three precursor gases.

Third, as precursor gas amount increases, less aging of SOA is observed. As precursor gas amount (or organic aerosol mass) increases, the peak-to-stable SOA yield ratio decreases and the ratio of *m/z* 43 to *m/z* 44 is decreases. This behavior suggests that the relatively low surface-to-volume ratio of larger organic aerosol particle sizes (and thus mass) limits the oxidation to the SOA surface. However, it is not clear if the aging is occurring in the gas phase or the particle phase. Determining the gas and particle reactions and their relative importance will require a full mechanism of SOA formation and aging and information about the change in the concentrations of the gas phase products.

Fourth, the SOA is further aged for greater amounts of OH. As OH increases, the peak-to-stable SOA yield ratio increases and then appears to level off, while the ratio of *m/z* 43 to *m/z* 44 decreases and may level off for OH greater than 400 pptv. This observation suggests that the SOA aging is approaching completion and additional OH does not alter the aged SOA characteristics.

Chapter 6

Conclusions

We have introduced the concept of Potential Aerosol Mass (PAM) and have performed experiments with inorganic and organic precursor gases to test its feasibility. These experiments provide strong evidence that PAM is a viable concept. PAM measurements can be made with a small, simple, flow-through chamber with a few minutes of exposure time in a highly oxidizing environment. The PAM chamber has two advantages over larger environmental chambers: negligible wall effects and the ability to complete the experiments in minutes, not hours.

We have demonstrated that the sulfate yield agrees to within 6% of theory. This agreement shows that the conversion of SO_2 to sulfate can be completed even in a chamber with only a few minutes of residence time. It also shows that the wall loss of sulfate aerosol particles in the PAM chamber is negligible.

The behavior of the SOA yields as a function of variables, such as temperature, relative humidity, oxidant concentration, presence of NO_x, precursor gas composition and amount, and the presence of acidic seed aerosol were generally comparable to the results found in large environmental chambers. Differences remain, possibly due to our inability to closely match the conditions in the large environmental chambers. However, the SOA yields disagree for different environmental chambers and even for different years in the same chamber. Some of these differences are understood; some are not. Thus, the PAM SOA yields are validated by their general consistency with the SOA yields in the large

bulk-type environmental chambers. At the same time, these new results complement those found in the large environmental chambers.

A novel aspect of the PAM chamber experiments is the direct measurements of the oxidants O_3, OH, and HO_2 in the chamber. These direct measurements enabled the quantification of these oxidants as a function of UV light and relative humidity. As a result, the ratios can be varied by at least a factor of 10 in the range of oxidant ratios that are observed in the low-NO_x troposphere. This variability enables a careful examination of SOA formation and aging in both chambers and the atmosphere.

The measurements of the evolution of the SOA chemical composition and particle size distributions in the PAM chamber indicate that particle chemical composition and size distributions obtained in the PAM chamber experiments are comparable to those observed in large environmental chambers. Also, the chemical composition and size distribution of SOA enabled us to see evidence of SOA aging and the role of OH on aging process. OH initiates the precursor gas oxidation as well as produces organic aerosol aging. Thus for amounts of OH that are sufficient to oxidize all the precursor gas, additional OH increases the amount of SOA aging. This phenomenon will be studied in greater detail with more experiments in the laboratory and with modeling of the oxidation processes.

The focus of this research is on the definition of the PAM concept and the demonstration that SOA yields from PAM chamber experiments are comparable to those found in large environmental chambers. The goal of definitively defining Potential Aerosol Mass has not yet been achieved; only the feasibility of the PAM concept has been demonstrated. The PAM chamber still needs to be optimized and the operating

conditions still need to be better understood. Studies will need to be conducted over a wider range of atmospheric conditions and chemical composition to create a working definition of PAM.

The PAM chamber has the potential to be a powerful tool for experimental studies in the laboratory and large environmental chambers. The PAM chamber can be coupled to a wide range of gas and particle measurement tools. It provides an extreme, well-characterized oxidation environment – essentially a low-temperature flame - that enables tests of SOA formation and aging in large chambers and the atmosphere.

PAM measurements can be an inexpensive indicator of the presence of aerosol precursor gases in monitoring networks and sites where measurements of speciated aerosol precursor gases are not feasible on a routine basis, where resources for environmental monitoring instruments are scarce, or where particulate pollution problems are fierce. Also, the simultaneous deployment of the PAM chamber, aerosol mass and chemical measurements, and measurement of all known precursor inorganic and organic atmospheric constituents in a field study can be used to test any unmeasured VOCs that can be oxidized to form SOA. Furthermore, the in-situ measurement of PAM in monitoring networks can be used to track the transport of precursor gases in air masses.

References

Alfarra, R., Ph. D. Thesis, Insights into atmospheric organic aerosols using an Aerosol Mass Spectrometer, University of Manchester, 2004.

Alfarra, M.R., Paulsen, D., Gysel, M., Garforth, A.A., Dommen, J., Prévôt, A.S.H., Worsnop, D.R., Baltensperger, U., Coe, H.: A mass spectrometric study of secondary organic aerosols formed from the photooxidation of anthropogenic and biogenic precursors in a reaction chamber. Atmos. Chem. Phys., 6, 5279-5293, 2006.

Bahreini, R., Keywood, M.D., Ng, N.L., Varutbangkul, S., Gao, S., Flagan, R.C., Seinfeld, J.H., Worsnop, D.R., Jimenez, J.L.: Measurement of secondary organic aerosol from oxidation of cycloalkenes, terpenes, and m-xylene using an Aerodyne Aerosol Mass Spectrometer. Environ. Sci. Technol., 39, 5674-5688. 2005.

Canagaratna, M.R., Jayne, J.T., Jimenez, J.L., Allan, J.D., Alfarra, M.R., Zhang, Q., Onasch, T.B., Drewnick, R., Coe, H., Middlebrook, A., Delia, A., Williams, L.R., Trimborn, A.M., Northway, M.J., DeCarlo, P.F., Kolb, C.E., Davidovits, P., Worsnop, D.R.: Chemical and microphysical characterization of ambient aerosols with the Aerodyne Aerosol Mass Spectrometer. Mass Spectrometry Review, 26, 185-222, 2007.

Chan, A.W.H., Kroll, J.H., Ng, N.L., Seinfeld, J.H.: Kinetic modeling of secondary organic aerosol formation: effect of particle- and gas-phase reactions of semivolatile products. Atmos.Chem. Phys. Discuss., 7, 7051-7085, 2007.

Cocker III, D.R., Flagan, R.C., and Seinfeld, J.H.,: State-of-the-Art chamber facility for studying atmospheric aerosol chemistry, Environ. Sci. Technol., 35, 2594-2601, 2001.

Demerjian, K.L.,: A review of the national monitoring networks in North America, Atmos. Environ., 34, 1861-1884, 2000.

Drewnick, F., Schwab, J. J., Jayne, J. T., Canagaratna, M. R., Worsnop, D. R., and Demerjian, K. L.,: Measurement of ambient aerosol composition during the PMTACS-NY 2001 using an Aerosol Mass Spectrometer. Part I: Mass concentrations, Aerosol. Sci. Tech., 38, 92-103, 2004b.

Faloona, I.C., Tan, D., Lesher, R.L., Hazen, N.L., Frame, C.L., Simpas, J.B., Harder, H., Martinez, M., Di Carlo, P., Ren, X., and Brune, W.H.: A laser-induced

fluorescence instrument for detecting tropospheric OH and HO_2: Characteristics and calibration, J. Atmos. Chem., 139-167, 2004.

Gao, S., Keywood, M., Varutbangkul, V., Bahreini, R., Flagan, R.C., and Seinfeld, J.H.: Low-molecular-weight and oligomeric components in secondary organic aerosol from the ozonolysis of cycloalkenes and alpha-pinene, J. Phys. Chem. A108, 10147-10164, 2004.

Griffin, R.J., Cocker III, D.R., Flagan, R.C., and Seinfeld, J.H.: Organic aerosol formation of oxidation of biogenic hydrocarbons, J. Geophys. Res., 104, 3555-3567, 1999.

Huebert, B., Bertram, T., Kline, J., Howell, S., Eatough, D., and Blomquist, d.: Measurements of organic and elemental carbon in Asian outflow during ACE-Asia from the NSF/NCAR C-130, J. Geophy. Res., 109(D19), D19S11, doi:10.1029/2004JD004700, 2004.

Intergovernmental Panel on Climate Change (IPCC), Working Group I, Climate change: The scientific basis, Cambridge Univ. Press, New York, 2001.

Jaecker-Voirol, A. and Mirabel, P.: Nucleation rate in a binary mixture of sulfuric acid and water vapor, J.Phys. Chem., 92, 3518-3521, 1988.

Jaecker-Voirol, A., Ponche, J.L., and Mirabel, P.: Vapor pressures in the ternary system water-nitric acid-sulfuric-acid at low temperatures, J. Geophys. Res., 95, 11857-11863, 1990.

Jang, M., Czoschke, N.M., Lee, S., and Kamens, R.M.: Heterogeneous atmospheric aerosol production by acid-catalyzed particle-phase reactions, Science, 298, 814-817, 2002.

Jayne, J.T., Leard, D.C., Zhang, X., Davidovits, P., Smith, K. A., Kolb, C.E., Worsnop, D.R.: Development of and Aerosol Mass Spectrometer for size and composition analysis of submicron particles. Aerosol. Sci. Tech., 33, 49-70, 2000.

Jimenez, J.L., Jayne, J.T., Shi, Q., Kolb, C.E., Worsnop, D.R., Yourshaw, I., Seinfeld, J.H., Flagan, R.C., Zhang, X., Smith, K.A., Morris, J.W., Davidovitx, P.: Ambient aerosol sampling using the Aerodyne Aerosol Mass Spectrometer, J. Geophys. Res., 108(D7), 8425, doi:10.1029/2001JD001213, 2003.

Jonsson, A.M., Hallquist, M., and Ljungstrom, E.: Impact of humidity on the ozone initiated oxidation of Limonene, Δ^3-Carene, and α-Pinene, Environ. Sci. Technol., 40, 188-194, 2006.

Kamens, R., Jang, M., Chien, C., and Leach, K.: Aerosol formation from the reaction of α-Pinene and ozone using a gas-phase kinetics-aerosol partitioning model, Environ. Sci. Technol., 33, 1430-1438, 1999.

Kamens, R.M. and Jaoui, M.: Modeling aerosol formation from α-pinene + NO_x in the presence of natural sunlight using gas-phase kinetics and gas-particle partitioning theory, Environ. Sci. Technol., 35, 1394-1405, 2001.

Keywood M.D., Varutbangkul, V., Bahreini, R., Flagan, C., and Seinfeld, J.H.: Secondary organic aerosol formation from the ozonolysis of cycloalkenes and related compounds, Environ. Sci. Technol., 38, 4157-4164, 2004.

Kroll, J.H., Ng, N.L., Murphy, S., Flagan, R.C., Seinfeld, J.H.: Secondary organic aerosol formation from isoprene photooxidation. Environ.Sci.Technol., 40, 1869-1877, 2006.

Krewski, D., Burnett, R.T., Goldberg, M.S., Hoover, K., Siemiatycki, J., Jerrett, M., Abrahamowicz, M., White, W.H.: Reanalysis of the Harvard six-cites study and the American Cancer Society study of particulate air pollution and Mortality, Part Π: Sensitivity analysis. Cambridge, Massachusetts, Health Effects Institute. A Special Report of the Institute's Particle Epidemiology Reanalysis Project. 129-130, 2000.

Lall, R., Kendall, M., Ito, K., Thurston, G.D.: Estimation of historical annual PM2.5 exposures for health effects assessment. Atmos. Environ., 38, 5217-5226, 2004.

Lanz, V.A., Alfarra, M.R., Baltensperger, U., Buchmann, B., Hueglin, C., Prévôt, A.: Source apportionment of submicron organic aerosols at an urban site by factor analytical modeling of aerosol mass spectra, Atmos.Chem. Phys., 7, 1503-1522, 2007.

Lee, A., Goldstein, A.H., Kroll, J.H., Ng, N.L., Varutbangkul, V., Flagan, R.C., and Seinfeld, J.H.: Gas-phase products and secondary aerosol yields from the photooxidation of 16 different terpenes, J. Geophys. Res., 111, D17305, doi:10.1029/2006JD007050, 2006.

Long, R.W., Eatough, N.L., Eatough, D.J., Meyer, M.B., and Wilson, W.E.: Continuous determination of fine particulate matter mass in the Salt Lake City Environmental Monitoring project: a comparison of real-time and conventional TEOM monitor results, J. Air. Waste. Manage., 55(12), 1839-1846, 2005.

Marcolli, C., Canagaratna, M.R., Worsnop, D.R., Bahreini,R., Gouw, J.A., Warneke, C., Goldan, P.D., Kuster, W.C., Williams, E.J., Lerner, B.M., Roberts, J.M., Meagher, J.F., Fehsenfeld, F.C., Marchewka, M.L., Bertman, S.B., Middlebrook, A.M.: Cluster analysis of the organic peaks in bulk mass spectra obtained during

the 2002 New England Air Quality Study with an Aerodyne Aerosol Mass Spectrometer, Atmos. Chem. Phys. Discuss., 6, 4601-4641, 2006.

Martín-Reviejo, M. and Wirtz, K.: Is benzene a precursor for secondary organic aerosol? Environ. Sci. Technol., 39, 1045-1054, 2005.

The Master Chemical Mechanism (MCM), http://mcm.leeds.ac.uk/MCM/browse.htt, 2004.

Murphy, D.M., Thomson, D. S., M. J. and Mahoney, M. J.: In situ measurements of organics, meteoritic material, mercury, and other elements in aerosols at 5 to 19 Kilometers, Science, 282, 1664-1669, 1998.

The National Institue of Standards and Technology (NIST) Chemical Kinetics Standard Reference Database 17, Version 7.0 (Web Version), Release 1.4, (http://www.nist.gov/srd/chemkin.htm), 2000.

Ng., N.G., Kroll, J.H., Keywood, M.D., Bahreini, R., Varutbangkul, V., Flagan, R.C., and Seinfeld, J.H.: Contribution of first-versus second-generation products to secondary organic aerosols formed in the oxidation of biogenic hydrocarbons, Environ. Sci. Technol., 40, 2283-2297, 2006.

Ng., N.L., Kroll, J.H., Chan, A.W.H., Chhabra, P.S., Flagan, R.C., and Seinfeld, J.H.: Secondary organic aerosol formation from m-xylene, toluene, and benzene, Atmos. Chem. Phys. Diss., 7, 4085-4126, 2007.

Northcross, A.L. and Jang, M.: Heterogeneous SOA yield from ozonolysis of monoterpenes in the presence of inorganic acid, Atmos. Environ., 41, 1483-1493, 2006.

Odum J., Hoffmann T., Bowman F., Collins D., Flagan R., and Seinfeld J.H.: Gas/particle partitioning and secondary organic aerosol yields, Environ. Sci. Technol., 30, 2580-2585, 1996.

Odum, J.R., Jungkamp, T.P.W., Griffin, R.J., Flagan, R.C., and Seinfeld, JH.: The atmospheric aerosol-forming potential of whole gasoline vapor, Science, 276, 96-99, 1997.

Pankow, J.F., Seinfeld, J.F., Asher, W.E., and Erdakos, G.B.: Modeling the formation of Secondary organic aerosol. 1. Application of theoretical principles to measurements obtained in the α-pinene/, β-pinene/, sabinene/, Δ^3-carene/, and cyclohexene/ozone systems, Environ. Sci. Technol., 35, 1164-1172, 2001.

Presto, A.A., Huff Hartz K.E., and Donahue N.M.: Secondary organic aerosol production from terpene ozonolysis. 1. Effect of UV radiation, Environ. Sci. Technol., 39, 7036-7045, 2005a.

Presto, A.A., Huff Hartz K.E., and Donahue N.M.: Secondary organic aerosol production from terpene ozonolysis. 2. Effect of NO_x concentration, Environ. Sci. Technol., 39,7046-7054, 2005b.

Ren, X., Brune, W.H., Oliger, A., Metcalf, A.R., Simpas, J.B., Shirley, T., Schwab, J.J., Bai, C., Roychowdhury, U., Li, Y., Cai, C., Demerjian, K., He, Y., Zhou, X., Gao, H., and Hou, J.: OH, HO_2, and OH reactivity during the PMTACS-NY Whiteface Mountain 2002 campaign: Observations and model comparison, J. Geophys. Res., 111, D10S03, doi:10.1029/2005JD006126, 2006.

Robinson, A.L., Donahue, N.M., Shrivastava, M.K., Weitkamp, E.A., Sage, A.M., Grieshop, A.P., Lane, T.E., Pierce, J.R., Pandis, S.N.: Rethinking organic aerosols: semivolatile emissions and photochemical aging, Science, 315, 1259-262, 2007.

Root, M.J.: Determining the major oxidants in an environmental chamber. M.S. Thesis, The Pennsylvania State University, 2007.

Rudich, Y., Donahue, N.M., Mentel, T.F.: Aging of organic aerosol: Bridging the gab between laboratory and field studies, Annu. Rev. Phys. Chem. 58, 321-352, 2007.

Salcedo, D, Onasch, T.B., Dzepina, K., Canagaratna, M.R., Zhang, Q., Huffman, J.A., DeCarlo, P.F., Jayne, J.T., Mortimer, P., Worsnop, D.R., Kolb, C.E., Johnson, K.S., Zuberi, B., Marr, L.C., Volkamer, R., Molina, L.T., Molina, M.J., Cardenas, B., Bernabé, R.M., Márquez, C., Gaffney, J.S., Marley, N.A., Laskin, A., Shutthanandan, V., Xie, Y., Brune, W., Lesher, R., Shirley, T., and Jimenez, J.L.: Characterization of ambient aerosols in Mexico City during the MCMA-2003 campaign with Aerosol Mass Spectrometry: results from the CENICA Supersite, Atmos. Chem. Phys., 6, 925-946, 2006.

Schwab, J.J., Hogrefe, O., Demerjian, K.L., and Ambs, J.L.: Laboratory characterization of modified tapered element oscillating microbalance samplers, J. Air. Waste. Manage., 54(10), 1254-1263, 2004.

Schwab, J.J., Felton, H.D., Rattigan, O.V., and Demerjian, K.L.: New York State urban and rural measurements of continuous PM2.5 mass by FDMS, TEOM, and BAM, J. Air. Waste. Manage., 56(4), 372-383, 2006.

Seinfeld,. J.H. and Pandis, S.N.: Atmospheric chemistry and physics, John Wiley and Sons, Inc., New York, 997--1000, 1139-1143,1998.

Seinfeld, J.H., Erdakos, G.B., Asher, W.E., and Pankow, J.F.: Modeling the formation of secondary organic aerosol (SOA). 2. The predicted effect of relative humidity on aerosol formation in the α-pinene, β-pinene, sabinene, Δ^3-carene, and cyclohexene-ozone systems, Environ. Sci. Technol., 35, 1806-1817, 2001.

Seinfeld, J.H., and Pankow, J.F.: Organic atmospheric particulate material, Annu. Rev. Phys. Chem., 54, 121-140, 2003.

Shilling, J.E., King, S.M., Mochida, M., Worsnop, D.R., Martin, S.T.: Mass spectral evidence that small changes in composition caused by oxidative aging processes alter aerosol CCN properties. J. Phys. Chem. A, 111, 3358-3368, 2007.

Song, C., Na, K., and Cocker III, D.R.: Impact of the hydrocarbon to NOx ratio on secondary organic aerosol formation, Environ. Sci. Technol., 39, 3143-3149, 2005.

Surratt, J.D., Murphy, S.M., Kroll, J.H., Ng, N.L., Hildebrandt, L., Sorooshian, A., Szmigielski, R., Vermeylen, R., Maenhaut, W., Claeys, M., Flagan, R.C., Seinfeld, J.H.: Chemical composition of secondary organic aerosol formed from the photooxidation of isoprene. J. Phys. Chem. A., 110, 9665-9690, 2006.

Takekawa, H., Minoura, H., and Yamazaki, S.: Temperature dependence of secondary organic aerosol formation by photo-oxidation of hydrocarbons, Atmos. Environ., 37, 3413-3424, 2003.

Teom 1400A monitor, Technical note 4. Low temperature operation of the TEOM series 1400-PM 10 moitor, http://www.rpco.com/products/ambprod/amb1400/index.htm, 1992.

Varutbangkul, V., Brechtel, F.J., Bahreini, R., Ng, N.L., Keywood, M.D., Kroll, J.H., Flagan, R.C., Seinfeld, J.H., Lee, A., and Goldstein, A.H.: Hygroscopicity of secondary organic aerosols formed by oxidation of cycloalkenes, monoterpenes, sesquiterpenes, and related compounds, Atmos. Chem. Phys. Disc., 6, 1121-1177, 2006.

Vehkamaki, H., Kulmala, M., Napari, I., Lehtinen, K. E. J., Timmreck, C., Noppel, M., and and Laaksonen A.: An improved parameterization for sulfuric acid-water nucleation rates for tropospheric and stratospheric conditions, J. Geophys. Res., 107(D22), doi:10.1029/2002JD002184, 2002.

Volkamer, R., Jimenz, J.L., Martini, F.S., Dzepina, K., Zhang, Q., Salcedo, D., Molina, L.T., Worsnop, D.R., and Molina, M.J.: Secondary organic aerosol formation from anthropogenic air pollution: Rapid and higher than expected, J. Geophys. Res., 33, L17811, doi: 10.1029/2006GL026899, 2006.

Wilson. W.E., Grover, B.D., Long, R.W., Eatough, N.L., and Eatough, D.J.: The measurement of fine particulate semivolatile material in urban aerosols, J. Air. Waste. Manage., 56(4), 384-397, 2006.

Zhang, Q., Alfarra, M.R., Worsnop, D.R., Allan, J.D., Coe, H., Canagaratna, M.R., Jimenez, J.L.: Deconvolution and quantification of hydrocarbon-like and

oxygenated organic aerosols based on Aerosol Mass Spectrometer, Environ. Sci. Technol., 39, 4938-4952, 2005.

VITA

Eunha Kang

Education

2007 Ph. D. Department of Meteorology, Pennsylvania State University, University Park, PA (GPA 3.6/4.0)

2001 M.S. in Environmental Science and Engineering, GIST (Gwangju Institute of Science and Technology), Republic of Korea (GPA 3.8/4.5)

1999 B.Eng. in Environmental Engineering, Chungnam National University, South Korea (GPA 4.0/4.5)

Experience

8/2002 – Present Graduate Research Assistant, Pennsylvania State University, University Park, PA

3/1999 –5/2001 Graduate Research Assistant, GIST (Gwangju Institute of Science & Technology), Republic of Korea

Awards and Honors

- Highest honor in the Environmental Engineering in the Chungnam National University, Republic of Korea
- The certified engineer in Atmospheric Environmental Engineering, Republic of Korea

Grants and Fellowship

- Jungsu fellowship for high honor in Chungnam National University, Republic of Korea (1996~ 1999)

Journal Publications

Kang E., Root M. and Brune W. Introducing the concept Potential Aerosol Mass (PAM) (PAM), Atmos. Chem. Phys. 6, 1--48, 2007.

Kang E., Root M., Toohey D. and Brune W. The formation and aging of Secondary Organic Aerosol (SOA) in a highly oxidizing environment, *in preparation*